

AD-A162 904

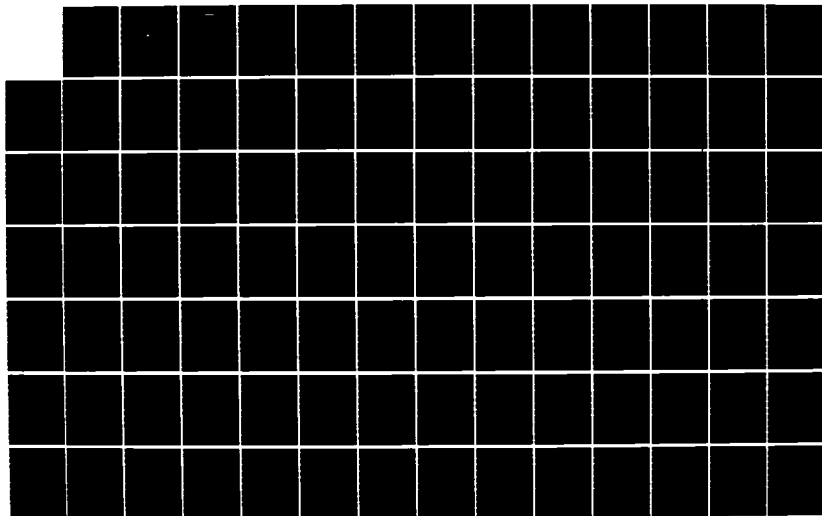
UNDERWATER ACOUSTIC MODEL-BASED SIGNAL PROCESSING  
APPLIED TO THE DETECTIO. (U) NAVAL POSTGRADUATE SCHOOL  
MONTEREY CA R J BLOUNT SEP 85

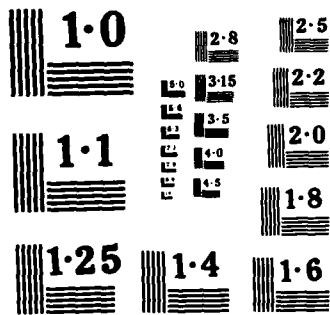
1/2

UNCLASSIFIED

F/G 17/1

NL





NATIONAL BUREAU OF STANDARDS  
MICROCOPY RESOLUTION TEST CHART

(2)

AD-A162 904

# NAVAL POSTGRADUATE SCHOOL

Monterey, California



DTIC  
ELECTE  
NOV 12 1985  
S B D

## THESIS

UNDERWATER ACOUSTIC MODEL-BASED SIGNAL  
PROCESSING APPLIED TO THE DETECTION OF  
SIGNALS FROM A PLANAR ARRAY OF POINT  
SOURCE ELEMENTS

by

Richard J. Blount, Jr.

September 1985

Thesis Advisor:

Lawrence J. Ziomek

MMR FILE COPY

Approved for public release; distribution is unlimited

85 11 12 115

UNCLASSIFIED

SECURITY CLASSIFICATION OF THIS PAGE (When Data Entered)

AD-A162 904

| REPORT DOCUMENTATION PAGE   |                       | READ INSTRUCTIONS<br>BEFORE COMPLETING FORM                             |  |
|---|-----------------------|---|--|
| 1. REPORT NUMBER  | 2. GOVT ACCESSION NO. | 3. RECIPIENT'S CATALOG NUMBER   |  |
| 4. TITLE (and Subtitle)<br>Underwater Acoustic Model-based Signal Processing Applied to the Detection of Signals from a Planar Array of Point Source Elements   |                       | 5. TYPE OF REPORT & PERIOD COVERED<br>Master's Thesis<br>September 1985 |  |
| 7. AUTHOR(s)<br>Richard J. Blount, Jr.  |                       | 6. PERFORMING ORG. REPORT NUMBER  |  |
| 9. PERFORMING ORGANIZATION NAME AND ADDRESS<br>Naval Postgraduate School<br>Monterey, California 93943-5100   |                       | 8. CONTRACT OR GRANT NUMBER(s)  |  |
| 11. CONTROLLING OFFICE NAME AND ADDRESS<br>Naval Postgraduate School<br>Monterey, California 93943-5100   |                       | 10. PROGRAM ELEMENT, PROJECT, TASK AREA & WORK UNIT NUMBERS             |  |
| 14. MONITORING AGENCY NAME & ADDRESS (if different from Controlling Office)   |                       | 12. REPORT DATE<br>September 1985                                       |  |
|   |                       | 13. NUMBER OF PAGES<br>137  |  |
|   |                       | 15. SECURITY CLASS. (of this report)<br>Unclassified                    |  |
|   |                       | 15a. DECLASSIFICATION/DOWNGRADING SCHEDULE                              |  |
| 16. DISTRIBUTION STATEMENT (of this Report)<br>Approved for public release; distribution is unlimited   |                       |   |  |
| 17. DISTRIBUTION STATEMENT (of the abstract entered in Block 20, if different from Report)  |                       |   |  |
| 18. SUPPLEMENTARY NOTES   |                       |   |  |
| 19. KEY WORDS (Continue on reverse side if necessary and identify by block number)<br>SONAR; Model-Based; Signal Processing; Planar Array; Correlator Receivers   |                       |   |  |
| 20. ABSTRACT (Continue on reverse side if necessary and identify by block number)<br>A computer simulation of a correlator receiver was developed and exercised to study the impact of a model-based signal processing algorithm on the detection of transmitted CW and LFM pulse acoustic signals incident on a planar array of electro-acoustic transducers. The model of the ocean communication channel incorporates a space-variant sound speed profile. The transducer output electrical signals are cophased by an FFT |                       |   |  |

DD FORM 1473  
1 JAN 73

EDITION OF 1 NOV 68 IS OBSOLETE  
S N 0102-LF-014-6601

1

UNCLASSIFIED

SECURITY CLASSIFICATION OF THIS PAGE (When Data Entered)

#20 - ABSTRACT - CONTINUED

beamformer via phase weighting, and summed to form a total array output signal. The total array output signal is correlated with a delayed replica of the transmit waveform and compared to a Neyman-Pearson threshold. Receiver performance is measured using a Monte Carlo technique to estimate the probability of detection for a fixed probability of false alarm versus the signal-to-noise ratio at the input of a single transducer. White, zero-mean, Gaussian transducer noise is assumed to facilitate comparison between theoretical and simulated performance. Results indicate that model-based signal processing provides significant improvement of receiver performance.

|                    |              |                                     |
|--------------------|--------------|-------------------------------------|
|                    |              | <input checked="" type="checkbox"/> |
|                    |              | <input type="checkbox"/>            |
|                    |              | <input type="checkbox"/>            |
| Availability Codes |              |                                     |
| Dist               | Avail and/or |                                     |
|                    | Special      |                                     |
| A-1                |              |                                     |



Approved for public release; distribution is unlimited.

Underwater Acoustic Model-based Signal Processing  
Applied to the Detection of Signals from a  
Planar Array of Point Source Elements

by

Richard J. Blount, Jr.  
Lieutenant, United States Coast Guard  
B.S., DeVry Institute of Technology, 1979

Submitted in partial fulfillment of the  
requirements for the degree of

MASTER OF SCIENCE IN ELECTRICAL ENGINEERING

from the

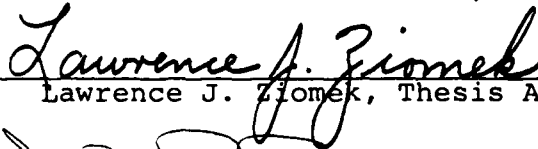
NAVAL POSTGRADUATE SCHOOL  
September 1985

Author:



Richard J. Blount, Jr.

Approved by:



Lawrence J. Ziomek, Thesis Advisor



J. P. Powers, Second Reader



Harriett B. Rigas, Chairman, Department of  
Electrical and Computer Engineering



John N. Dyer  
Dean of Science and Engineering

### ABSTRACT

A computer simulation of a correlator receiver was developed and exercised to study the impact of a model-based signal processing algorithm on the detection of transmitted CW and LFM pulse acoustic signals incident on a planar array of electroacoustic transducers. The model of the ocean communication channel incorporates a space-variant sound speed profile. The transducer output electrical signals are cophased by an FFT beamformer via phase weighting, and summed to form a total array output signal. The total array output signal is correlated with a delayed replica of the transmit waveform and compared to a Neyman-Pearson threshold. Receiver performance is measured using a Monte Carlo technique to estimate the probability of detection for a fixed probability of false alarm versus the signal-to-noise ratio at the input of a single transducer. White, zero-mean, Gaussian transducer noise is assumed to facilitate comparison between theoretical and simulated performance. Results indicate that model-based signal processing provides significant improvement of receiver performance.

TABLE OF CONTENTS

|      |  |    |
|------|--|----|
| I.   | INTRODUCTION -----   | 11 |
| II.  | THEORY OF THE RECEIVER MODEL -----                               | 15 |
|      | A. OVERVIEW OF THE COMMUNICATION SYSTEM -----                    | 15 |
|      | B. FUNCTIONAL DESCRIPTION OF THE RECEIVER -----                  | 17 |
|      | C. STATISTICAL DESCRIPTION OF THE RECEIVER -----                 | 23 |
|      | 1. Array Element Output Signal Description -                     | 24 |
|      | 2. Generation of Complex Weight Phase<br>Factors -----           | 28 |
|      | 3. Array Processor Output Signal<br>Statistics -----             | 32 |
|      | 4. Hypothesis Testing and the Neyman-<br>Pearson Criterion ----- | 39 |
| III. | COMPUTER SIMULATION OF THE RECEIVER -----                        | 50 |
|      | A. TOP LEVEL PROGRAM DESCRIPTION -----                           | 50 |
|      | 1. Subprogram READY -----  | 65 |
|      | 2. Subprogram SGNLGN -----                                       | 67 |
|      | 3. Subprogram AMPWGT -----                                       | 70 |
|      | 4. Subprogram PHSWGT -----                                       | 70 |
|      | 5. Subprogram ARYPRO -----                                       | 74 |
|      | 6. Subprogram AWGN -----   | 77 |
|      | 7. Subprogram INTGRT -----                                       | 79 |
|      | 8. Subprogram WRITBL -----                                       | 80 |
|      | 9. Subprogram PDPLOT -----                                       | 81 |
|      | B. MODEL VERIFICATION -----                                      | 83 |



|     |   |     |
|-----|---|-----|
| 1.  | Characterization of the Noise Source ---- | 84  |
| 2.  | Verification of the Output Data -----     | 90  |
| IV. | PRESENTATION OF RESULTS -----             | 94  |
| A.  | TRANSMIT WAVEFORMS -----                  | 94  |
| B.  | CASE TEST -----                           | 98  |
| C.  | CASE HMGl -----                           | 107 |
| D.  | CASE INHMGl -----                         | 118 |
| V.  | CONCLUSIONS AND RECOMMENDATIONS -----     | 134 |
|     | LIST OF REFERENCES -----                  | 136 |
|     | INITIAL DISTRIBUTION LIST -----           | 137 |

LIST OF FIGURES

|     |  |    |
|-----|--|----|
| 1.  | System Geometry -----  | 16 |
| 2.  | Ray Path Bending Due to Inhomogeneous Medium -----                   | 17 |
| 3.  | Receiver Block Diagram -----   | 19 |
| 4.  | Planar Array Geometry -----  | 19 |
| 5.  | Array Element Quadrature Demodulator -----                           | 20 |
| 6.  | Array Processor Block Diagram -----                                  | 21 |
| 7.  | Correlator/Matched Filter Detector -----                             | 23 |
| 8.  | Density Functions of the Magnitude-Square<br>Correlator Output ----- | 47 |
| 9.  | Program RCVR Flowchart -----   | 51 |
| 10. | Subprogram READY Flowchart -----                                     | 66 |
| 11. | Subprogram SGNLGN Flowchart -----                                    | 68 |
| 12. | Subprogram AMPWGT Flowchart -----                                    | 71 |
| 13. | Subprogram PHSWGT Flowchart -----                                    | 72 |
| 14. | Subprogram ARYPRO Flowchart -----                                    | 75 |
| 15. | Subprogram AWGN Flowchart -----                                      | 78 |
| 16. | Subprogram INTGRT Flowchart -----                                    | 79 |
| 17. | Subprogram WRITBL Flowchart -----                                    | 80 |
| 18. | Subprogram PDPLOT Flowchart -----                                    | 82 |
| 19. | Histogram of I-Channel Noise -----                                   | 86 |
| 20. | Histogram of Q-Channel Noise -----                                   | 87 |
| 21. | Autocovariance of I-Channel Noise -----                              | 88 |
| 22. | Autocovariance of Q-Channel Noise -----                              | 89 |
| 23. | Estimated Power Spectral Density of<br>I-Channel Noise -----         | 91 |

|     |  |     |
|-----|--|-----|
| 24. | Estimated Power Spectral Density of<br>Q-Channel Noise -----                                 | 92  |
| 25. | Receiver Performance for case TEST, CW Pulse,<br>Pfa = 0.1, Geometry Phase Weighting -----   | 101 |
| 26. | Receiver Performance for case TEST, CW Pulse,<br>Pfa = 0.01, Geometry Phase Weighting -----  | 102 |
| 27. | Receiver Performance for case TEST, LFM Pulse,<br>Pfa = 0.1, Geometry Phase Weighting -----  | 103 |
| 28. | Receiver Performance for case TEST, LFM Pulse,<br>Pfa = 0.01, Geometry Phase Weighting ----- | 104 |
| 29. | Receiver Performance for case HMGL, CW Pulse,<br>Pfa = 0.01, No Phase Weighting -----        | 109 |
| 30. | Receiver Performance for case HMGL, CW Pulse,<br>Pfa = 0.1, Geometry Phase Weighting -----   | 110 |
| 31. | Receiver Performance for case HMGL, CW Pulse,<br>Pfa = 0.01, No Phase Weighting -----        | 111 |
| 32. | Receiver Performance for case HMGL, CW Pulse,<br>Pfa = 0.01, Geometry Phase Weighting -----  | 112 |
| 33. | Receiver Performance for case HMGL, LFM Pulse,<br>Pfa = 0.1, No Phase Weighting -----        | 113 |
| 34. | Receiver Performance for case HMGL, LFM Pulse,<br>Pfa = 0.1, Geometry Phase Weighting -----  | 114 |
| 35. | Receiver Performance for case HMGL, LFM Pulse,<br>Pfa = 0.01, No Phase Weighting -----       | 115 |
| 36. | Receiver Performance for case HMGL, LFM Pulse,<br>Pfa = 0.01, Geometry Phase Weighting ----- | 116 |
| 37. | Receiver Performance for case INHMGL, CW Pulse,<br>Pfa = 0.1, No Phase Weighting -----       | 120 |
| 38. | Receiver Performance for case INHMGL, CW Pulse,<br>Pfa = 0.1, Geometry Phase Weighting ----- | 121 |
| 39. | Receiver Performance for case INHMGL, CW Pulse,<br>Pfa = 0.1, Medium Phase Weighting -----   | 122 |
| 40. | Receiver Performance for case INHMGL, CW Pulse,<br>Pfa = 0.01, No Phase Weighting -----      | 123 |

|     |  |     |
|-----|--|-----|
| 41. | Receiver Performance for case INHMGl, CW Pulse,<br>Pfa = 0.01, Geometry Phase Weighting -----  | 124 |
| 42. | Receiver Performance for case INHMGl, CW Pulse,<br>Pfa = 0.01, Medium Phase Weighting -----    | 125 |
| 43. | Receiver Performance for case INHMGl, LFM Pulse,<br>Pfa = 0.1, No Phase Weighting -----        | 126 |
| 44. | Receiver Performance for case INHMGl, LFM Pulse,<br>Pfa = 0.1, Geometry Phase Weighting -----  | 127 |
| 45. | Receiver Performance for case INHMGl, LFM Pulse,<br>Pfa = 0.1, Medium Phase Weighting -----    | 128 |
| 46. | Receiver Performance for case INHMGl, LFM Pulse,<br>Pfa = 0.01, No Phase Weighting -----       | 129 |
| 47. | Receiver Performance for case INHMGl, LFM Pulse,<br>Pfa = 0.01, Geometry Phase Weighting ----- | 130 |
| 48. | Receiver Performance for case INHMGl, LFM Pulse,<br>Pfa = 0.01, Medium Phase Weighting -----   | 131 |

ACKNOWLEDGMENT

The author would like to thank Professor L.J. Ziomek for his assistance, patience and encouragement during the course of this research.

## I. INTRODUCTION

Model-based signal processing is described by Mendel [Ref. 1] as an approach that exploits knowledge of the underlying physics of a problem to develop signal processing algorithms. Use of the approach implies that some a priori knowledge exists regarding the problem under consideration. In the case of an underwater acoustic communication problem, such a model has been developed by Ziomek [Ref. 2].

Ziomek derived a time-invariant, space-variant transfer function of the ocean volume based on the WKB approximation, which is an approximate solution of the linear, inhomogeneous, scalar wave equation describing the propagation of small-amplitude acoustic pressure waves when the speed of sound is a function of depth. Based on the transfer function of the ocean volume, Ziomek [Ref. 2:pp. 257-261] also derived an equation describing the output electrical signal at each element of a planar array of point sources. The output signal is described in terms of the frequency spectrum of the transmitted electrical signal, the transmit and receive planar arrays, and the random ocean medium transfer function. Vos [Ref. 3] used these results to develop a computer program that generates time-samples of a real baseband output electrical signal at each element in a receive planar array as a function of a variable ocean medium sound speed profile,

planar array size, array far-field beam patterns and functional form of the transmit signal. Ziomek has since modified this program to generate time-samples of the complex envelope of real bandpass output electrical signals.

The research documented in this thesis has the following objectives:

- develop a computer simulation of a correlator receiver which processes the output electrical signals generated by the computer program developed by Ziomek and Vos;
- apply the concept of model-based signal processing to the development of the signal processing algorithm used by the receiver;
- determine the effectiveness of the approach in the detection of signals from a planar array of point source elements.

Since the effects of the ocean medium on the signals processed by the receiver are embodied in the random ocean medium transfer function, the basic question to be addressed may be stated as follows. Can a priori knowledge of the ocean medium, based on physical principles of acoustic wave propagation, be used to improve the detection of signals in a receiver, and to what degree?

Ziomek's use of linear systems theory to develop a transfer function model of the ocean medium immediately suggests the use of a compensating filter at the array output to remove the undesirable time delays due to system geometry and wave propagation effects. This filter would ideally cophase the signals at each element in the planar array, resulting in maximum signal output when the signals

are added together. This filter is implemented in the frequency domain through the use of Discrete Fourier Transforms (DFT), and the approach is exactly analogous to the FFT beamforming procedure discussed by Ziomek [Ref. 2: pp. 153-176].

In the frequency domain, the time delays due to system geometry and wave propagation effects are represented as phase shifts which may be eliminated if known a priori. The concept of model-based signal processing is applied here to obtain the proper compensating phase shift for the known system geometry and wave propagation conditions.

Section II describes the theory used to develop the receiver model. The system context within which the receiver operates is described and related to previous investigations. A functional description of the receiver is shown, and each of the major functional blocks is explained in some detail. Finally, a statistical description of the receiver's performance is developed.

The computer implementation of the receiver structure is described in Section III. The logical flow of the computer program is discussed and related to the receiver description. The use of multiple trials to estimate the probability of detection is explained. Each of the major subprograms is characterized in terms of function and implementation. Verification of the computer simulation is discussed last.



Section IV presents the data obtained from the simulation when a rectangular-envelope, continuous wave (CW) pulse or a rectangular-envelope, linear-frequency-modulated, (LFM) carrier is transmitted. Receiver performance is described by plotting the probability of detection ( $P_d$ ), for a given probability of false alarm ( $P_{fa}$ ), as a function of the input signal-to-noise ratio (SNR) at each element in the receive array. Plots are provided for different values of  $P_{fa}$ , and show the relative improvement in receiver performance as various medium and wave propagation effects are compensated for by the model-based, signal processing algorithm. In each plot, the receiver performance predicted by theory when all array element output signals are precisely cophased, and the array element input noise is zero-mean, uncorrelated and Gaussian is shown as a dashed line. The dashed line is plotted from data obtained from a closed form expression relating  $P_d$  to  $P_{fa}$  as a function of array element input SNR, and is superimposed on the output plots to provide a baseline for judging the validity of the receiver simulation output data.

Conclusions and recommendations are discussed in Section V.

## II. THEORY OF THE RECEIVER MODEL

A receiver operates in the context of a total communication system consisting of a signal source (transmitter), a signal propagation medium (channel) and a signal sink (receiver). It is the model of the communication channel that is of initial interest since the signal processing algorithm will depend in large part on the physics describing the propagation of the signal through the channel.

### A. OVERVIEW OF THE COMMUNICATION SYSTEM

Ziomek's model (Ref. 2] of the ocean medium is described in general as a time-variant, space-variant, random filter (transfer function) in which the index of refraction, or equivalently, the speed of sound, is a function of depth, and includes both a deterministic and a random component. However, in describing the electrical output signals from the receive aperture, the model becomes more restrictive in the sense that the channel is considered to be time-invariant, but still space-variant. Furthermore, the transmit and receive apertures are taken to be rectangular, planar arrays whose elements consist of complex weighted point sources. Complex weighting of the array elements provides the means for amplitude shading and beam steering both the transmit and receive array patterns. The complex weights are ideal

for removing the undesired effects of the channel on the output electrical signals from the receive array elements, and become the tool for applying the model-based, signal processing concept. Figure 1 depicts the geometry of the transmit and receive arrays in the transmission medium.

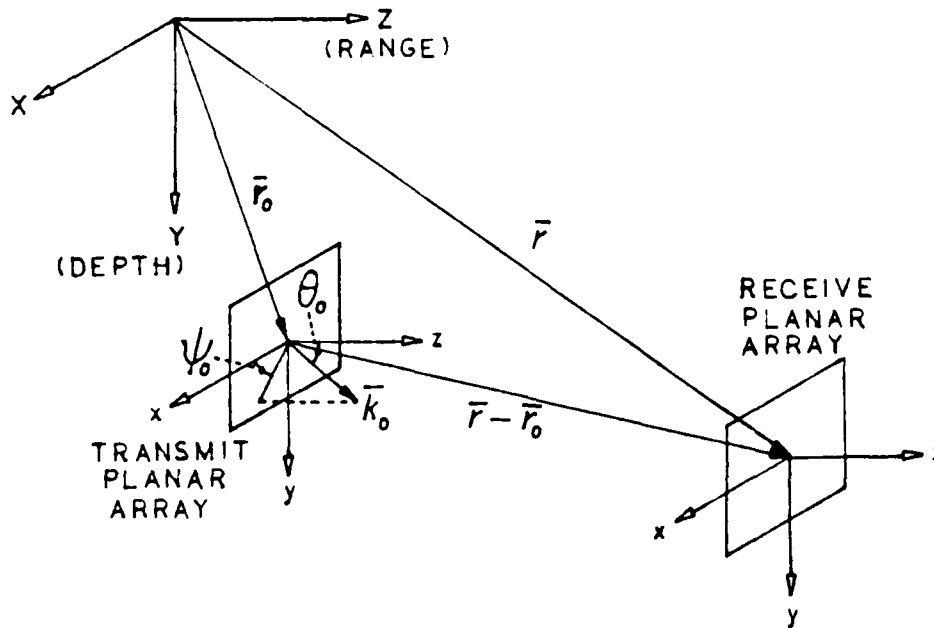


Figure 1. System Geometry

Ziomek goes further than simply considering system geometry in generating the output signals at the receive array. The spatial variance of the transfer function permits modeling of propagation effects due to the dependence of the index of refraction on depth. Figure 2 shows the ray-bending effects of propagation through such an

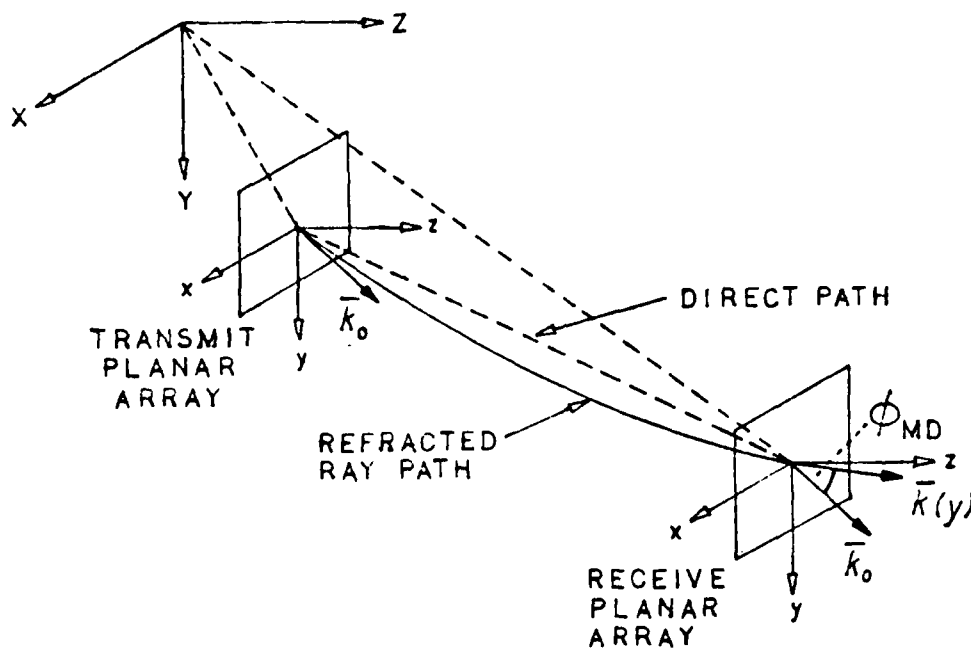


Figure 2. Ray Path Bending Due to Inhomogeneous Medium

inhomogeneous medium. The phase shifts due to system geometry and propagation effects may be considered together or separately in the generation of the output electrical signal data in the computer simulation due to Vos [Ref. 3]. It is this output electrical signal data which is used as the input signal to the receiver.

#### B. FUNCTIONAL DESCRIPTION OF THE RECEIVER

The output electrical signal data processed by the receiver are time samples of the complex envelope of the bandpass electrical signal at the output of each element in the receive array. This implies that the bandpass acoustic signal incident on the receive array has been converted to

an output electrical signal by each transducer element in the array. Each real, bandpass electrical signal then passes through a quadrature demodulator to become an equivalent baseband, complex envelope signal, which is time-sampled and converted from analog to digital form. The complex envelope is represented by the I-channel (in-phase) and Q-channel (quadrature-phase) components generated by the quadrature demodulator. Time-sampling is done in a manner that satisfies the Nyquist criterion for the baseband information contained in the I and Q channels. Thus, many of the components associated with a receiving system are already contained within the simulation that generates the planar array output signal data. The receiver simulation assumes these components exist, and essentially provides signal processing of the complex envelope of the output bandpass electrical signals. The major functional blocks of the receiver include:

- an array signal processor,
- a correlator implementation of a matched filter receiver,
- a magnitude-square operation, and
- a threshold decision operation.

Figure 3 shows the functional block diagram for the receiver model. The magnitude-square and the threshold decision operations are considered to be part of the correlator (matched filter) detector function block shown in Figure 3.

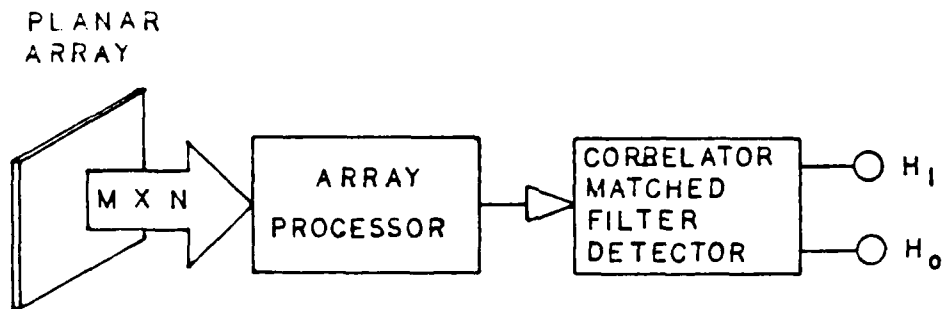


Figure 3. Receiver Block Diagram

The receive array is assumed to be a rectangular planar array of  $M \times N$  elements where both  $M$  and  $N$  are odd numbers. Each element is assumed to be an omnidirectional point source. The geometry of the planar array and associated mathematical notation is shown in Figure 4.

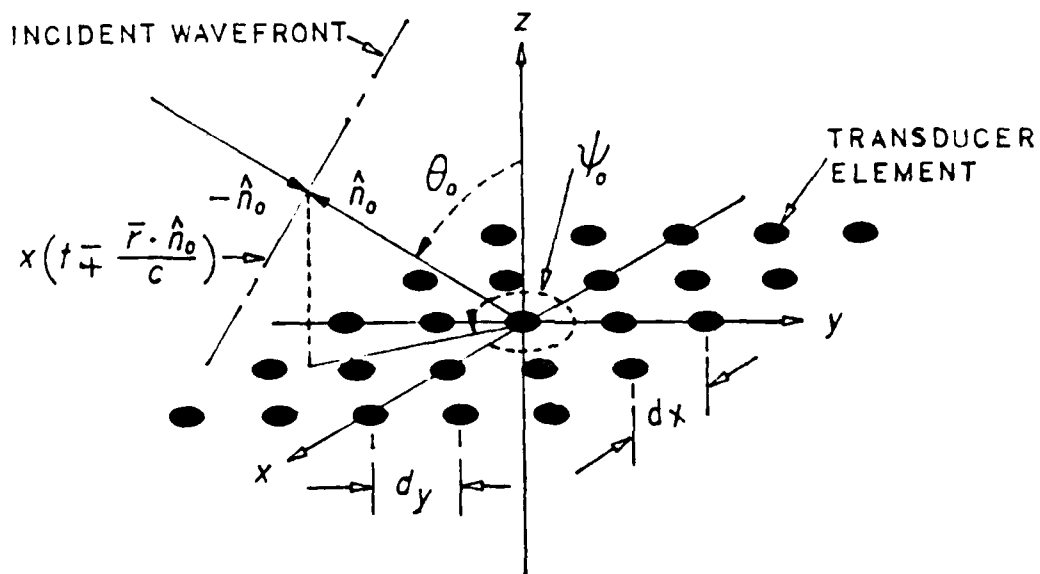


Figure 4. Planar Array Geometry

The function of each quadrature demodulator is to convert the amplitude and angle-modulated, bandpass, electrical signal at each transducer output into its baseband, complex envelope. Thus, the low-pass complex envelope may be sampled at a much lower rate. Note that the use of a quadrature demodulator does imply that the carrier frequency of the transmitted signal is known. It should be emphasized that the output electrical signal at each element in the receive array is passed through its own quadrature demodulator before array processing begins. The quadrature demodulator is shown schematically in Figure 5, where the complex envelope of  $y(t)$ , denoted  $\tilde{y}(t)$ , is given by,

$$\tilde{y}(t) = y_c(t) + j y_s(t) \quad (2.1)$$

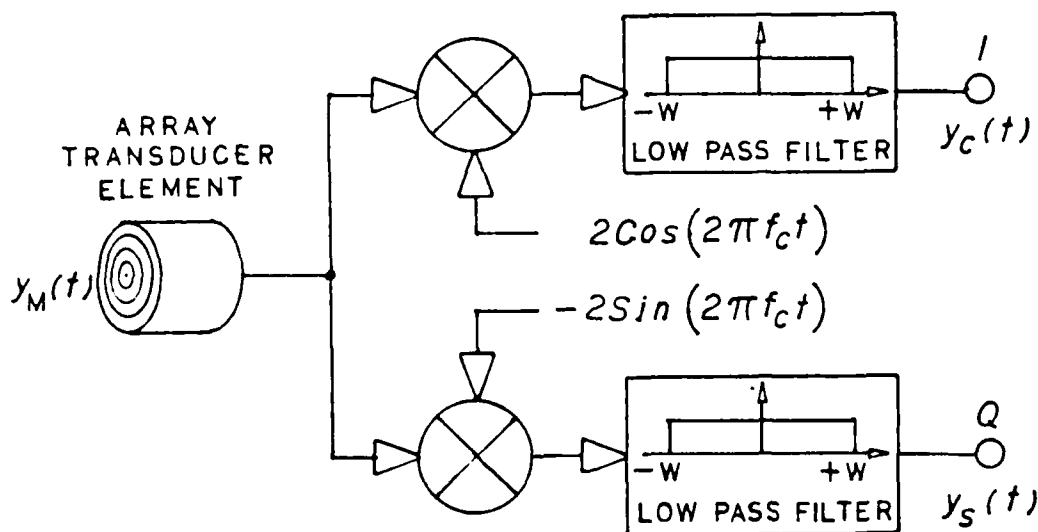


Figure 5. Array Element Quadrature Demodulator

where:

$\tilde{y}_c(t)$ : is the I-channel (in-phase) component of  $y(t)$ , and

$\tilde{y}_s(t)$ : is the Q-channel (quadrature-phase) component of  $y(t)$ .

The array signal processor, shown schematically in Figure 6, is a FFT beamformer. The function of the array processor is to maximize the total output signal when the signals from each element in the array are summed.

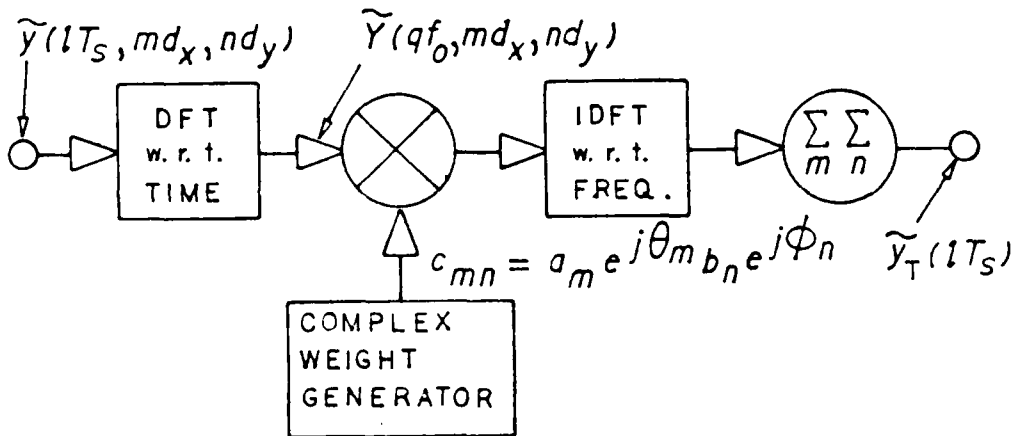


Figure 6. Array Processor Block Diagram

The array processor is essentially a filter that compensates for system geometry and wave propagation effects on the signal transmitted through the channel. The array processor is implemented in the frequency domain where



filtering can be obtained by multiplication of each spectral component of the complex envelope by a complex weighting coefficient. The complex coefficients are computed from a knowledge of the channel model, thus the application of model-based signal processing. After applying the complex weights, the Inverse DFT is computed to recover cophased, time domain, complex envelope signals from each array element. By summing these cophased signals over all  $M \times N$  array elements, a constructive interference effect is achieved, and the total output signal is maximized.

The matched filter portion of the receiver is implemented by correlating the total time-sampled output signal and noise from the array,  $\tilde{r}(\ell T_s)$ . Where,

$$\tilde{r}(\ell T_s) = \tilde{y}_T(\ell T_s) + \tilde{n}_T(\ell T_s) \quad (2.2)$$

with a time and frequency shifted replica of the complex envelope of the transmitted waveform,  $\tilde{x}(t)$ . Since the phase of the received signal is, in general, unknown, the magnitude-square of the correlator output is taken as the input to the threshold detector. This input is compared to a preset threshold level  $\gamma$  to determine the presence of a signal. The preset threshold  $\gamma$  is computed from a Neyman-Pearson criterion. The schematic of the correlator/matched filter detector is shown in Figure 7, and has been shown by Van Trees [Ref. 4:pp. 244-247] to be the optimum receiver

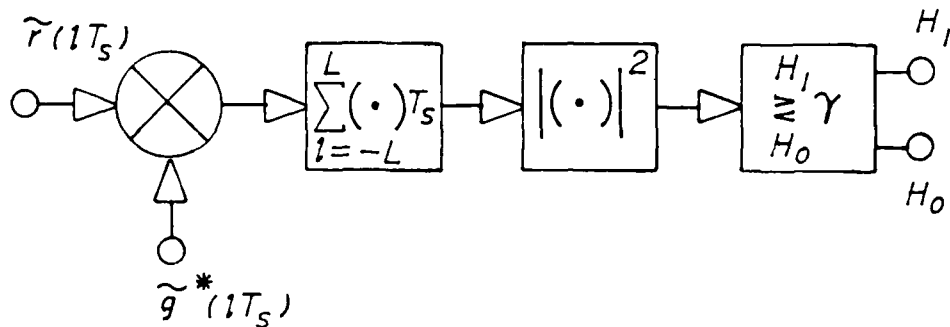


Figure 7. Correlator/Matched Filter Detector

for the detection of a bandpass signal, with random amplitude and phase, in the presence of white, Gaussian noise.

#### C. STATISTICAL DESCRIPTION OF THE RECEIVER

The output electrical signal data embodies several assumptions and restrictions that must be restated before further development of the receiver model. The signal data is assumed to be generated by a real, bandpass, acoustic field,  $y_M(t, \underline{r})$ , incident upon an array of electroacoustic transducers. The acoustic wave,  $y_M(t, \underline{r})$ , is propagating in the  $\hat{n}_0$  direction with velocity  $c$ , or

$$y_M(t, \underline{r}) = x\left(t \mp [\underline{r} \cdot \hat{n}_0]/c\right) \quad (2.3)$$

where:

$$\underline{r} = x\hat{x} + y\hat{y} + z\hat{z} \quad (2.4)$$

$$\hat{n}_o = u_o\hat{x} + v_o\hat{y} + w_o\hat{z} \quad (2.5)$$

$$u_o = \sin \theta_o \cos \psi_o \quad (2.6)$$

$$v_o = \sin \theta_o \sin \psi_o \quad (2.7)$$

and

$$w_o = \cos \theta_o \quad (2.8)$$

Note that  $x(t)$  may be an arbitrary function of time.

#### 1. Array Element Output Signal Description

The acoustic field, incident upon an element in the array, is converted to an output electrical signal by the transducer, and is transformed into a baseband complex envelope at the output of the quadrature demodulator. After time sampling at a rate  $f_s = 1/T_s$  (in samples per second), spatial sampling over the receive planar aperture in increments of  $d_x$  and  $d_y$ , and assuming linearity in the transducer operation, the complex envelope of the output electrical signal at the  $m^{\text{th}}, n^{\text{th}}$  element of the planar array lying in the XY-plane may be written as,

$$\tilde{y}(\ell T_s, m d_x, n d_y) = \tilde{x}(\ell T_s + [u_o m d_x + v_o n d_y]/c) \quad (2.9)$$

For example, if the real, bandpass output electrical signal  $y(t)$  is an amplitude and angle modulated cosine wave of the form

$$y(t) = a(t)\cos[2\pi f_c t + \theta(t)] \quad (2.10)$$

after quadrature demodulation, the complex envelope of  $y(t)$  may be represented as

$$\tilde{y}(t) = y_c(t) + jy_s(t) \quad (2.11)$$

where:

$$y_c(t) = a(t)\cos \theta(t) \quad (2.12)$$

and

$$y_s(t) = a(t)\sin \theta(t) \quad (2.13)$$

or, in magnitude-phase form

$$a(t) = \sqrt{y_c^2(t) + y_s^2(t)} \quad (2.14)$$

and

$$\theta(t) = \text{Tan}^{-1}[y_s(t)/y_c(t)] \quad (2.15)$$

It is also possible to show that the envelope function,  $E(t)$ , of the real, bandpass signal  $y(t)$  is

$$E(t) = |a(t)| \quad (2.16)$$

The main advantage of working with the complex envelope form of the real bandpass signal is that the baseband complex envelope may be sampled at a rate  $f_s$  (in samples per second) determined by the bandwidth of the baseband modulating waveform, independent of the carrier frequency.

It is further assumed that the complex envelope of the transmitted waveform  $\tilde{x}(t)$  can be represented exactly, over an interval of  $T_0$  seconds, by a finite, complex, Fourier series such as,

$$\tilde{x}(t) = \sum_{q=-K}^K c_q \exp [+j2\pi q f_0 t] \quad (2.17)$$

where the complex Fourier coefficient  $c_q$  can be written as,

$$c_q = a_q \exp [+j\theta_q] \quad (2.18)$$

where:

$f_0$ : is the fundamental frequency in Hertz of the signal  $\tilde{x}(t)$  with period  $T_0 = 1/f_0$  seconds, and

K: is the maximum number of harmonics used to represent the signal  $\tilde{x}(t)$ .

The complex Fourier coefficients  $c_q$  can then be determined directly from the DFT with respect to time of  $\tilde{x}(\ell T_s)$ , or

$$c_q = \frac{1}{L} \sum_{\ell=-L'}^{L'} \tilde{x}(\ell T_s) W_L^{q\ell} \quad (2.19)$$

where:

$$W_L \triangleq \exp[+j2\pi/L] \quad (2.20)$$

$$L' \triangleq (L-1)/2 \quad (2.21)$$

and:

L: is the total number of time samples taken during the time interval  $T_0$  seconds where L is a non-negative, odd integer,

$T_0$ : is the fundamental period or data record length in seconds, and

$T_s$ : is the sampling period in seconds (note  $f_s = 1/T_s$ ).

To satisfy the Nyquist sampling theorem, it can be shown [Ref. 2:pp. 164-165] that,

$$L \geq 2K + 1 \quad (2.22)$$

and,

$$T_s \leq T_o/L \quad (2.23)$$

## 2. Generation of Complex Weight Phase Factors

With these assumptions it can be shown [Ref. 2:pp. 165-166] that the normalized DFT with respect to time of the complex envelope of the output electrical signal  $\tilde{y}(\ell T_s, m d_x, n d_y)$  can be expressed as,

$$\begin{aligned} \tilde{y}_{SN}(q f_o, m d_x, n d_y) &= c_q \exp[+j\theta_m] \exp[\mp j 2\pi f u_o m d_x / c] \\ &\cdot x \exp[+j\phi_n] \exp[\mp j 2\pi f v_o n d_y / c] \end{aligned} \quad (2.24)$$

where:

$$f = f_c + q f_o ; \quad -K, \dots, q, \dots, K \quad (2.25)$$

and:

- $f_c$ : is the carrier frequency,
- $c$ : is the constant speed of sound in homogeneous ocean medium at the receive array,
- $u_o$ : is the direction cosine of the wave propagation vector along the x-axis, equation (2.6), and
- $v_o$ : is the direction cosine of the wave propagation vector along the y-axis. See equation (2.7).

Phase factors  $\theta_m$  and  $\phi_n$  are due to the separable complex weight,  $c_{mn}$ . That is,

$$c_{mn} = c_m d_n = a_m \exp[+j\theta_m] b_n \exp[+j\phi_n] \quad (2.26)$$

Notice that by a proper choice of  $\theta_m$  and  $\phi_n$  in equation (2.24) where,

$$\theta_m = \pm j 2\pi f u_o m d_x / c \quad (2.27)$$

and

$$\phi_n = \pm j 2\pi f v_o n d_y / c \quad (2.28)$$

the phase shifts due to system geometry may be completely cancelled leaving only the complex Fourier coefficients  $c_q$  at each element in the planar array. It should be noted that the phase correction factors are functions of both the array element position ( $md_x$  or  $nd_y$ ), and the frequency  $f$  of each spectral component of the input bandpass signal spectrum. That is, the frequency is given by equation (2.25).

Once the phase shifts due to geometry are eliminated, taking the inverse DFT with respect to frequency of the spectrum of the output electrical signal  $\tilde{Y}(qf_o, md_x, nd_y)$  will yield cophased time signals at each element. Summing all the cophased signals will result in a maximum total



output signal  $\tilde{Y}_T(\ell T_S)$  from the array processor. That is,

$$\tilde{Y}_T(\ell T_S) = \sum_{m=-M'}^{M'} \sum_{n=-N'}^{N'} \tilde{Y}(\ell T_S, m d_x, n d_y) \quad (2.29)$$

where:

$$M' = (M-1)/2 \quad (2.30)$$

and

$$N' = (N-1)/2 \quad (2.31)$$

This approach is extended to compensate for the deterministic signal phase shifts caused by transmission through an inhomogeneous ocean medium. Since the variation in the speed of sound  $c(y)$  is assumed to be a function of  $y$  (depth) alone, the calculation involves only the  $\phi_n$  phase factor of the complex weight. Ziomek<sup>1</sup> has shown that for a sound-speed profile  $c(y)$  with a constant gradient  $g$ , a closed form expression for the deterministic component of phase shift is,

$$\phi_{MD} = + \frac{k_o}{2v_o} \left\{ \frac{c_o}{g} [n_D(y) - 1] + \Delta y_n \right\} \quad (2.32)$$

---

<sup>1</sup>Extension of work by Ziomek based on expression for  $\theta_{MD}$  [Ref. 2:pp. 263-268].

where:

$$n_D(y) = c_0/c_D(y) \quad (2.33)$$

$$c_D(y) = c_0 + g\Delta y_n \quad (2.34)$$

$$\Delta y_n = (y_r - y_0) + nd_y \quad (2.35)$$

$$k_0 = 2\pi f_0/c \quad (2.36)$$

- $n_D(y)$ : is the space-variant (with depth only) index of refraction,
- $c_D(y)$ : is the speed of sound at depth  $y$ ,
- $c_0$  : is the speed of sound at the transmit array,
- $k_0$  : is the wave propagation constant at the transmit array,
- $g$  : is the gradient (slope) of the sound speed profile,
- $y_0$  : is the depth of the center element of the transmit array, and
- $y_r$  : is the depth of the center element of the receive array.

The negative of the deterministic medium phase factor, equation (2.32), is simply added to the system geometry phase factor, equation (2.28), to obtain the total complex weight phase factor in the  $y$  direction.

### 3. Array Processor Output Signal Statistics

Development of a receiver model also requires a specification of the noise environment in which the receiver operates. Any realistic model for the noise environment is extremely complex. However in order to form tractable theoretical results that can be reasonably approximated in a computer simulation, zero-mean, additive, white, Gaussian noise (AWGN) is assumed at the output of each array element. Remember that the array element output is also the input to the quadrature demodulator.

The AWGN model permits derivation of a closed form expression relating Pd, Pfa and array input Signal-to-Noise Ratio (SNR). This type of noise process can also be reasonably approximated by using computer generated pseudo-random number sequences from a standard Gaussian random number generator. By comparing the theoretically predicted receiver performance with the results of the simulation, verification of the computer implementation of the receiver can be achieved. Once verified, the computer simulation can test more realistic noise models with some confidence in the resulting data.

The input SNR at a single element in the array is defined as,

$$\text{SNR}_i \triangleq \frac{E\{|\tilde{y}(\ell T_s, m d_x, n d_y)|^2\}}{E\{|\tilde{n}(\ell T_s, m d_x, n d_y)|^2\}} \quad (2.37)$$

where  $E\{ \}$  denotes the expected value of the quantity within the curly braces.

If the random input signal  $\tilde{y}(\ell T_s, m d_x, n d_y)$  is ergodic, then the mean-square value of the signal can be found by computing the time-average instead of the ensemble average, that is,

$$E\{ |\tilde{y}(\ell T_s, m d_x, n d_y)|^2 \} = \langle |\tilde{y}(\ell T_s, m d_x, n d_y)|^2 \rangle \quad (2.38)$$

where  $\langle (\cdot) \rangle$  denotes the time-average of the quantity within the parenthesis, or

$$\langle (\cdot) \rangle = \frac{1}{T_0} \int_{-T_0/2}^{T_0/2} (\cdot) dt \quad (2.39)$$

The integral in equation (2.39) can be approximated for computer simulation purposes by,

$$\langle (\cdot) \rangle \doteq \frac{1}{T_0} \sum_{l=-L'}^{L'} (\cdot) T_s \quad (2.40)$$

where the infinitesimal  $dt$  is approximated by,

$$dt \doteq T_s \quad (2.41)$$

Because of the assumption regarding the use of a finite Fourier series to represent the original transmitted waveform, the input signal power at a single element in the receive array can be computed from the sum of the magnitude-square of the complex Fourier coefficients [Ref. 5:pp. 44-45], that is,

$$\langle |\tilde{y}(\ell T_s, md_x, nd_y)|^2 \rangle = \sum_{q=-K}^K |c_q|^2 \quad (2.42)$$

These coefficients are easily obtained for each array element by computing the DFT with respect to time of the complex envelope of the output electrical signal data at each element, or

$$c_q = \frac{1}{L} \sum_{\ell=-L'}^{L'} \tilde{y}(\ell T_s, md_x, nd_y) W_L^{q\ell} \quad (2.43)$$

The mean-square value of the zero mean noise signal at the array element input is equal to the variance  $\sigma_{mn}^2$  of the noise input, or

$$E\{|\tilde{n}(\ell T_s, md_x, nd_y)|^2\} = \sigma_{mn}^2 \quad (2.44)$$

Substituting equations (2.42) and (2.44) into equation (2.37), the expression for input SNR at element (m,n) may be written

as,

$$\text{SNR}_i = \sum_{q=-K}^K |c_q|^2 / \sigma_{mn}^2 \quad (2.45)$$

or, by rearranging the variance, equation (2.45) becomes

$$\sigma_{mn}^2 = \sum_{q=-K}^K |c_q|^2 / \text{SNR}_i \quad (2.46)$$

The measured input signal power at an array element and a desired input SNR parameter value  $\text{SNR}_i$  can be used to obtain the noise power (variance) required to scale the output from the random number generator. The ability to set a desired input SNR value is necessary in order to test receiver performance.

Because the DFT and IDFT are linear operations, the noise statistics at the output of the array processor are still Gaussian, and uncorrelated in both spatial and temporal coordinates. The total noise signal  $\tilde{n}_T(\ell T_S)$  at the output of the array processor may be written as,

$$\tilde{n}_T(\ell T_S) = \sum_{m=-M'}^{M'} \sum_{n=-N'}^{N'} \tilde{n}(\ell T_S, m d_x, n d_y) \quad (2.47)$$

The variance of the total noise  $\sigma_T^2$  is equal to the mean square value of the total noise signal from the array

processor, and is also equal to the sum of the variances of the noise signals at each element since the noise process at one element is by assumption independent of the noise process at any other element in the array. The variance of the total noise signal is then

$$E\{|\tilde{n}_T(\lambda T_S)|^2\} = \sum_{m=-M'}^{M'} \sum_{n=-N'}^{N'} \sigma_{mn}^2 \quad (2.48)$$

If the variance  $\sigma_{mn}^2$  at each element is the same for all elements in the array, or

$$\sigma_{mn}^2 = \sigma^2 \quad (2.49)$$

then, the variance of the total noise  $\sigma_T^2$  can be written in terms of the variance of the noise at each element in the array by substituting equation (2.49) into equation (2.48) to obtain,

$$\sigma_T^2 = MN\sigma^2 \quad (2.50)$$

or, in terms of mean square values,

$$E\{|\tilde{n}_T(\lambda T_S)|^2\} = MNE\{|\tilde{n}(\lambda T_S)|^2\} \quad (2.51)$$

where  $E\{|\tilde{n}(\ell T_s)|^2\}$  is the noise power at an array element when the noise power is considered to be the same for all array elements  $(m,n)$ .

Both the output signal and output noise components at all elements in the array are baseband complex envelope signals with I and Q channel components. The bandwidth of the noise signal is set by the bandwidth of the low-pass filter in the quadrature demodulator to  $W$  Hertz. For the purpose of the simulation,  $W$  is always adjusted to include the highest harmonic of the complex envelope signal, that is,

$$W = Kf_o \quad (2.52)$$

Knowing the bandwidth  $W$  and using the AWGN assumptions, the noise power spectral density  $N_o$  at each element can be related to the variance of the noise process at each element by,

$$N_o = \sigma_{mn}^2 / (2Kf_o) \quad (2.53)$$

The SNR at the output of the array processor  $SNR_A$  is defined as the ratio of the total signal power to the total noise power, or

$$SNR_A \triangleq \frac{E\{|\tilde{y}_T(\ell T_s)|^2\}}{E\{|\tilde{n}_T(\ell T_s)|^2\}} \quad (2.54)$$



where,

$$E\{|\tilde{y}_T(\ell T_S)|^2\} = E\left\{\left|\sum_{m=-M'}^{M'} \sum_{n=-N'}^{N'} \tilde{y}(\ell T_S, m d_x, n d_y)\right|^2\right\} \quad (2.55)$$

For the case of perfectly cophased signals with identical signal power at each element, the right-hand side of equation (2.55) reduces to

$$E\{|\tilde{y}_T(\ell T_S)|^2\} = (MN)^2 E\{|\tilde{y}(\ell T_S)|^2\} \quad (2.56)$$

where  $E\{|\tilde{y}(\ell T_S)|^2\}$  is equivalent to the time-average power at each element in the array, and  $E\{|\tilde{y}_T(\ell T_S)|^2\}$  is equivalent to the time-average power of the total output signal from the array processor. Using the uncorrelated and equal array element input power noise assumptions, the expression for  $SNR_A$  can be rewritten by substituting equations (2.51) and (2.56) into equation (2.54), or

$$SNR_A = MN \frac{E\{|\tilde{y}(\ell T_S)|^2\}}{E\{|\tilde{n}(\ell T_S)|^2\}} = MNSNR_i \quad (2.57)$$

Since the array gain (AG) is defined as,

$$AG \triangleq 10 \log_{10} [SNR_A/SNR_i] \quad (\text{dB}) \quad (2.58)$$

the array gain in this case becomes,

$$AG = 10 \log_{10} [MN] \quad (\text{dB}) \quad (2.59)$$

Note that for a  $5 \times 5$  element planar array,  $M \times N = 25$ , and the array gain is 13.979 dB.

#### 4. Hypothesis Testing and the Neyman-Pearson Criterion

The correlator/matched filter detector portion of the receiver, Figure 7, is modeled as a binary hypothesis testing problem using the Neyman-Pearson decision criterion. The two hypotheses,  $H_0$  and  $H_1$ , are defined as,

$$r(\ell T_S) = \begin{cases} Y_T(\ell T_S) + n_T(\ell T_S) & : H_1 \\ n_T(\ell T_S) & : H_0 \end{cases} \quad (2.60)$$

where, in terms of the transmitted waveform  $\tilde{x}(t)$ ,

$$Y_T(\ell T_S) = c \sum_{m=-M'}^{M'} \sum_{n=-N'}^{N'} \tilde{x} [(\ell T_S - \tau_{mn}), m d_x, n d_y] \cdot \exp [ +j2\pi\phi_A \ell T_S ] \quad (2.61)$$

and  $n_T(\ell T_S)$  is given by equation (2.47). If one assumes that all array element output signals are cophased and identical, equation (2.61) reduces to

$$\tilde{y}_T(\ell T_S) = c \sum_{mn} \tilde{x}(\ell T_S - \tau_A) \exp[+j2\pi\phi_A \ell T_S] \quad (2.62)$$

where:

$$c = a \exp [+j\theta] \quad (2.63)$$

and,

- $\tau_{mn}$ : is the actual time delay in seconds at each element in the array due to range separation between individual elements of the transmit and receive arrays,
- $\tau_A$ : is the actual time delay in seconds due to range separation between transmit and receive arrays when all signals are cophased,
- $\phi_A$ : is the actual doppler shift in Hertz due to relative motion between transmit and receive arrays,
- $a$ : is the amplitude attenuation factor that is, in general, a random variable,
- $\theta$ : is the generalized phase shift of the received signal with respect to the transmitted signal. (In general, it is also a random variable dependent on both spatial and temporal coordinates.), and
- $H_0$ : is the null or noise only (no signal) hypothesis.

Matched filtering is obtained by correlating the complex envelope of the total array output  $\tilde{r}(\ell T_S)$  with the complex conjugate of the processing waveform  $\tilde{g}(\ell T_S)$ . The functional form of  $\tilde{g}(\ell T_S)$  can be written as,

$$\tilde{g}(\ell T_S) = \tilde{x}(\ell T_S - \hat{\tau}) \exp[+j2\pi\hat{\phi}\ell T_S] \quad (2.64)$$

which is a time and frequency shifted replica of the transmitted signal  $\tilde{x}(t)$  where

- $\hat{\tau}$ : is the estimate of time delay at the receiver,  
and
- $\hat{\phi}$ : is the estimate of the doppler shift at the receiver.

For the purposes of this study, the estimates of time delay and doppler shift are assumed to be precisely correct, or

$$\tau = \hat{\tau} - \tau_A = 0.0 \quad (2.65)$$

and

$$\phi = \phi_A - \hat{\phi} = 0.0 \quad (2.66)$$

The correlation, or inner product  $\tilde{\ell}$  between two functions  $\tilde{r}(t)$  and  $\tilde{g}(t)$ , is given by

$$\tilde{\ell} = \langle \tilde{r}(t), \tilde{g}(t) \rangle \triangleq \int_{-\infty}^{+\infty} \tilde{r}(t) \tilde{g}^*(t) dt \quad (2.67)$$

which is approximated in the simulation using the trapezoidal rule approximation to the integral, that is,

$$\tilde{\ell} = \sum_{\ell=-L'}^{L'-1} \frac{\tilde{r}(\ell T_s) \tilde{g}^*(\ell T_s) + \tilde{r}[(\ell+1)T_s] \tilde{g}^*[(\ell+1)T_s]}{2} T_s \quad (2.68)$$

The magnitude-square of the correlator output is taken for two reasons. First, the phase of the carrier frequency waveform is, in general, unknown. As the phase of the received carrier varies with respect to the phase of the quadrature demodulator local oscillator (LO) signal, the output of the quadrature demodulator would vary from a maximum negative to a maximum positive value depending on the phase difference between the carrier and the LO which usually is taken to be a uniformly distributed random variable between 0 and  $2\pi$  radians. The change in polarity of the quadrature demodulator output would propagate through to the output of the integrator in the correlator/matched filter detector, Figure 7. Taking the magnitude of the integrator output ensures that the input to the threshold comparator will always be non-negative regardless of the phase difference between the carrier and LO waveforms. Second, when the array element noise statistics are assumed to be Gaussian, the square of the magnitude of the integrator output yields an input to the threshold comparator which can be described statistically by exponential density functions for both  $H_1$  and  $H_0$  signal hypotheses. As will be shown in the following derivations, the exponential density functions can be easily integrated to obtain a closed form expression for  $P_d$  and  $P_{fa}$  in terms of the SNR at the input to the threshold comparator. The output of the magnitude-square operation is the sufficient statistic

on which the binary decision is made. That is, choose  $H_1$  if,

$$|\tilde{\ell}|^2 > \gamma \quad (2.69)$$

or choose  $H_0$  if,

$$|\tilde{\ell}|^2 < \gamma \quad (2.70)$$

Assuming that the total noise  $n_T(t)$  is a baseband Gaussian process of bandwidth  $W$ , the conditional probability density functions (pdf's) of the magnitude-square of the correlator output with and without a signal present can be shown to be exponential.<sup>2</sup> The conditional pdf's are given by

$$p(|\tilde{\ell}|^2 | H_0) = 1/(2\sigma_0^2) \exp[-|\tilde{\ell}|^2/(2\sigma_0^2)] \quad (2.71)$$

and,

$$p(|\tilde{\ell}|^2 | H_1) = 1/(2\sigma_1^2) \exp[-|\tilde{\ell}|^2/(2\sigma_1^2)] \quad (2.72)$$

For zero mean, AWGN, and cophased, equal energy (power) signals at each array element output, the variances of

---

<sup>2</sup>Derivations for the pdf's, expressions for  $P_d$ ,  $P_{fa}$  and the decision threshold  $\gamma$  were provided by Prof. L. J. Ziomek in private communication.

the magnitude-square of the correlator output can be shown to be

$$\sigma_0^2 = E\{|\tilde{\ell}_N|^2\}/2 = M N N_0 E_{\tilde{x}}/2 \quad (2.73)$$

and

$$\begin{aligned} \sigma_1^2 &= E\{|\tilde{\ell}_S|^2 + |\tilde{\ell}_N|^2\}/2 \\ &= [(MN)^2 E\{a^2\} |X(\tau, \phi)|^2 + M N N_0 E_{\tilde{x}}]/2 \end{aligned} \quad (2.74)$$

where:

- $|\tilde{\ell}_N|^2$ : is the magnitude-square of the correlator output when the input to the receive array is noise alone,
- $|\tilde{\ell}_S|^2$ : is the magnitude square of the correlator output when the input to receive array consists of signal alone,
- $N_0$ : is the power spectral density level of the noise signal at each array element output,
- $E_{\tilde{x}}$ : is the energy in the transmitted signal which for simulation purposes is defined to be equal to the energy  $E_{\tilde{g}}$  in the local processing waveform  $\tilde{g}(t)$ ,
- $E\{a^2\}$ : is the mean-square value of the amplitude attenuation factor (note:  $E\{a^2\} = a^2$  only when deterministic effects are considered), and
- $|X(\tau, \phi)|^2$ : is the magnitude-square of the auto-ambiguity function. Note that  $|X(\tau, \phi)|^2 = E_{\tilde{x}}^2 |X_N(\tau, \phi)|^2$ , or in our case where  $\tau = 0$  and  $\phi = 0$ ,  $|X(0, 0)|^2 = E_{\tilde{x}}^2$  since  $|X_N(0, 0)|^2 = 1$ . [Ref. 2, pp. 190-191]

To calculate the threshold  $\gamma$  for a desired Pfa and input SNR, the integral of the pdf for the null, or  $H_0$  hypothesis, is set equal to the desired Pfa, and the resulting equation is solved for the threshold. The magnitude-square operation results in particularly simple threshold equation when the input noise is assumed to be white, zero mean, and Gaussian. Computing the Pfa yields

$$\begin{aligned}
 Pfa &= \int_{\gamma}^{+\infty} p(|\tilde{\ell}|^2 | H_0) d|\tilde{\ell}|^2 \\
 &= \exp[-\gamma / (2\sigma_0^2)] \\
 &= \exp[-\gamma / (MNN_0 E_{\tilde{x}})] \quad (2.75)
 \end{aligned}$$

By solving equation (2.75) for the threshold  $\gamma$ ,

$$\gamma = MNN_0 E_{\tilde{x}} \ln [1/Pfa] \quad (2.76)$$

Once the threshold is obtained, the correlator output pdf for the  $H_1$  hypothesis may be evaluated to obtain the Pd.

$$\begin{aligned}
 Pd &= \int_{\gamma}^{\infty} p(|\tilde{\ell}|^2 | H_1) d|\tilde{\ell}|^2 \\
 &= \exp[-\gamma / 2\sigma_1^2] \\
 &= \exp\{-\gamma / [(MN)^2 E\{a\}^2 |X(\tau, \phi)|^2 + MNN_0 E_{\tilde{x}}]\} \quad (2.77)
 \end{aligned}$$



Since in our problem  $\tau = 0$  and  $\phi = 0$ ,

$$|X(\tau, \phi)|^2 = |X(0, 0)|^2 = E_{\tilde{x}}^2 \quad (2.78)$$

and if we let

$$\text{SNR}_{|\tilde{\ell}|^2} = MN \left( \frac{E\{a^2\}E_{\tilde{x}}}{N_0} \right) \quad (2.79)$$

then,

$$P_d = \exp\{-\gamma/[MNN_0E_{\tilde{x}} \left( \frac{MNE\{a^2\}E_{\tilde{x}}}{N_0} + 1 \right)]\} \quad (2.80)$$

and

$$P_d = \exp\{-\gamma/[MNN_0E_{\tilde{x}}(\text{SNR}_{|\tilde{\ell}|^2} + 1)]\} \quad (2.81)$$

Substitution of equation (2.75) into equation (2.81) gives the desired closed form expression relating  $P_d$ ,  $P_{fa}$  and the SNR of the magnitude-square of the correlator output, that is,

$$P_d = P_{fa}^{1/[1+\text{SNR}_{|\tilde{\ell}|^2}]} \quad (2.82)$$

This result agrees in form with the result given in Van Trees [Ref. 4:pp. 246-247] for a similar single channel receiver model. Figure 8 graphically depicts the relationship

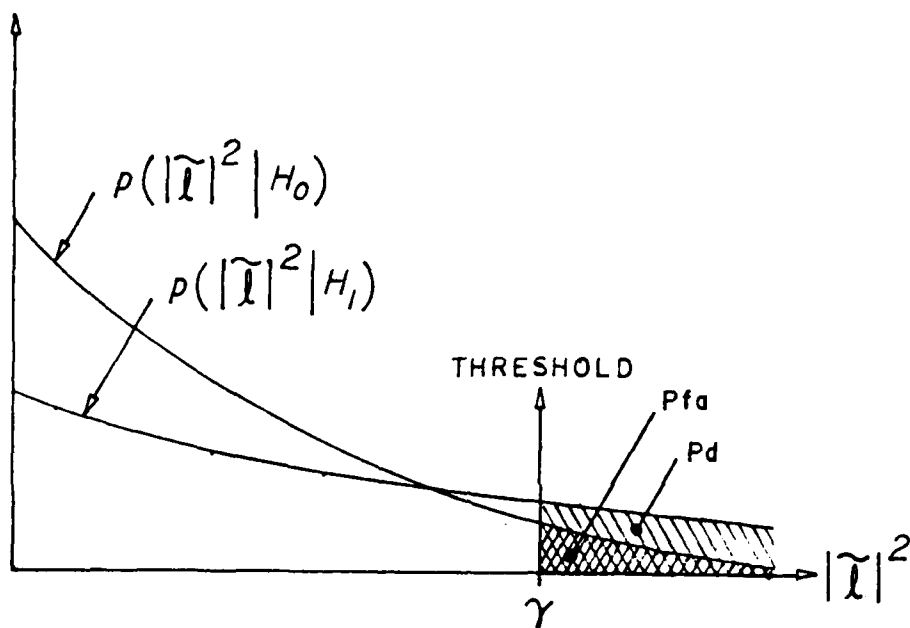


Figure 8. Density Functions of the Magnitude-Square Correlator Output

between the conditional pdf's, the decision threshold  $\gamma$ , the Pfa and the Pd.

The correlator output SNR, equation (2.79), can be related to the input SNR at a single element in the array through the array gain, and a factor resulting from the slightly different definitions of input SNR and correlator output SNR. In terms of array element input signal energy  $E_y$ , the input SNR given in equation (2.45) may be rewritten as,

$$\text{SNR}_i = \frac{(1/T_o) E_y}{\sigma_{mn}^2} = \frac{E\{a^2\} E_x}{T_o \sigma_{mn}^2} \quad (2.83)$$

where,

$$E_{\tilde{y}} = E\{a^2\}E_{\tilde{x}} \quad (2.84)$$

is the average received energy at a single element in the array due to the transmitted signal  $x(t)$ , and from equation (2.53)

$$\sigma_{mn}^2 = 2kf_o N_o = \frac{2kN_o}{T_o} \quad (2.85)$$

The magnitude-square correlator output SNR can be written as,

$$SNR_{|\tilde{\ell}|^2} \triangleq \frac{E\{|\tilde{\ell}_s|^2\}}{E\{|\tilde{\ell}_N|^2\}} \quad (2.86)$$

where,

$$E\{|\tilde{\ell}_s|^2\} = (MN)^2 E\{a^2\} E_{\tilde{x}}^2 \quad (2.87)$$

and,

$$E\{|\tilde{\ell}_N|^2\} = M N N_o E_{\tilde{x}} \quad (2.88)$$

Substitution of equations (2.87) and (2.88) into equation (2.86) gives

$$\text{SNR}_{|\tilde{x}|^2} = MN \frac{E\{a^2\}E_{\tilde{x}}}{N_o} \quad (2.89)$$

By substituting equation (2.85) into equation (2.83) and rearranging terms, equation (2.83) becomes

$$\text{SNR}_i = \frac{E\{a^2\}E_{\tilde{x}}}{2KN_o} \quad (2.90)$$

By rearranging terms in equation (2.90) and substituting the result into equation (2.89), the desired relationship expressing the magnitude-square correlator output SNR in terms of the array element input SNR at a single element in the array is obtained. That is,

$$\text{SNR}_{|\tilde{x}|^2} = MN2K\text{SNR}_i \quad (2.91)$$

Writing both sides of equation (2.91) in dB form yields,

$$\text{SNR}_{|\tilde{x}|^2} \text{ (dB)} = \underbrace{10 \log_{10}(MN)}_{\text{AG}} + 10 \log(2K) + \text{SNR}_i \text{ (dB)} \quad (2.92)$$

where AG is the array gain given in equation (2.59).

To summarize, Section II.C provides the equations needed to implement a computer simulation of the receiver structure described in Section II.B. The implementation of the computer simulation is the subject of Section III.

### III. COMPUTER SIMULATION OF THE RECEIVER

The computer program RCVR simulates receiver operation through straightforward application of the equations and the concepts developed in Section II. Written in FORTRAN, the computer program RCVR consists of a top level, or main program, and nine subprograms. The computer program will be explained from a functional viewpoint. That is, the algorithms used to implement the receiver simulation will be related to the theoretical development outlined in Section II, but translation of these algorithms into FORTRAN statements will not be discussed. The main program will be described first. The description of the main program will be followed by a detailed discussion of each subprogram. In addition to explaining the computer simulation, the methods used to validate the receiver simulation output data will be presented.

#### A. TOP LEVEL PROGRAM DESCRIPTION

The organization and logic flow of the top level, or main program, is shown in Figures 9a through 9e. The functions of the main program include:

- initializing the simulation run-time environment,
- invoking subprograms in the proper sequence to process the input signal data.
- providing control logic and noise generation algorithms needed to measure receiver performance, and

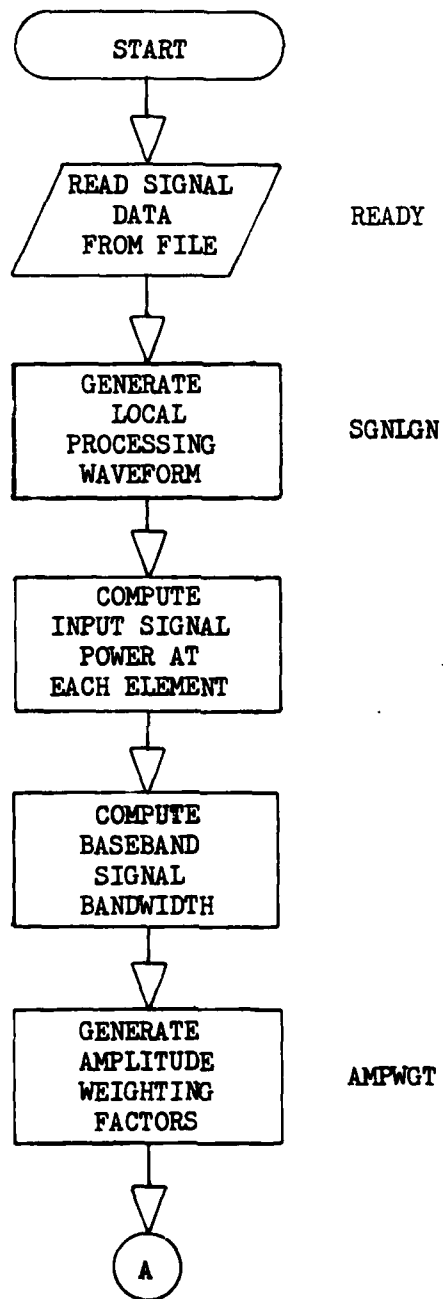


Figure 9a. Program RCVR Flowchart

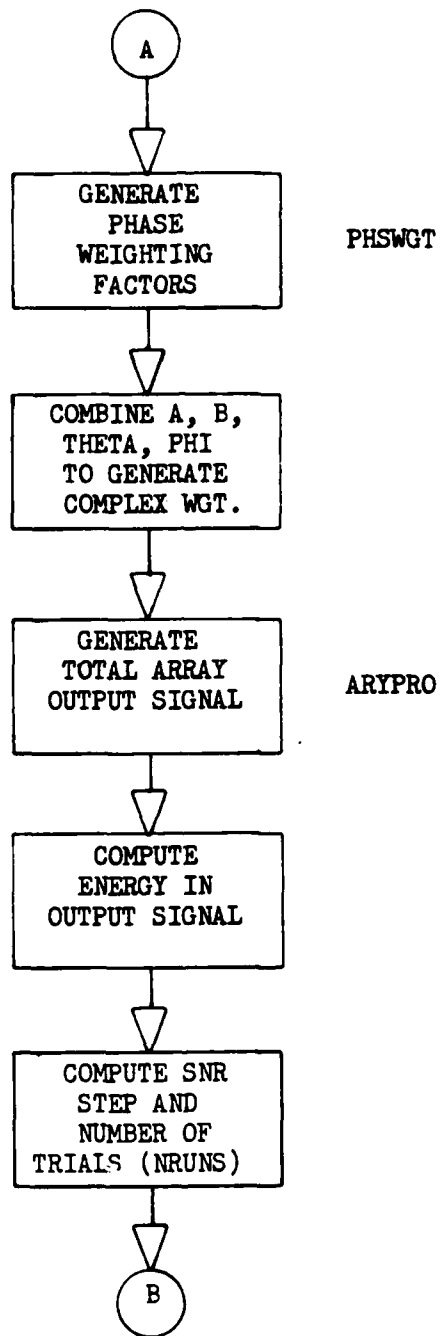


Figure 9b. Program RCVR Flowchart

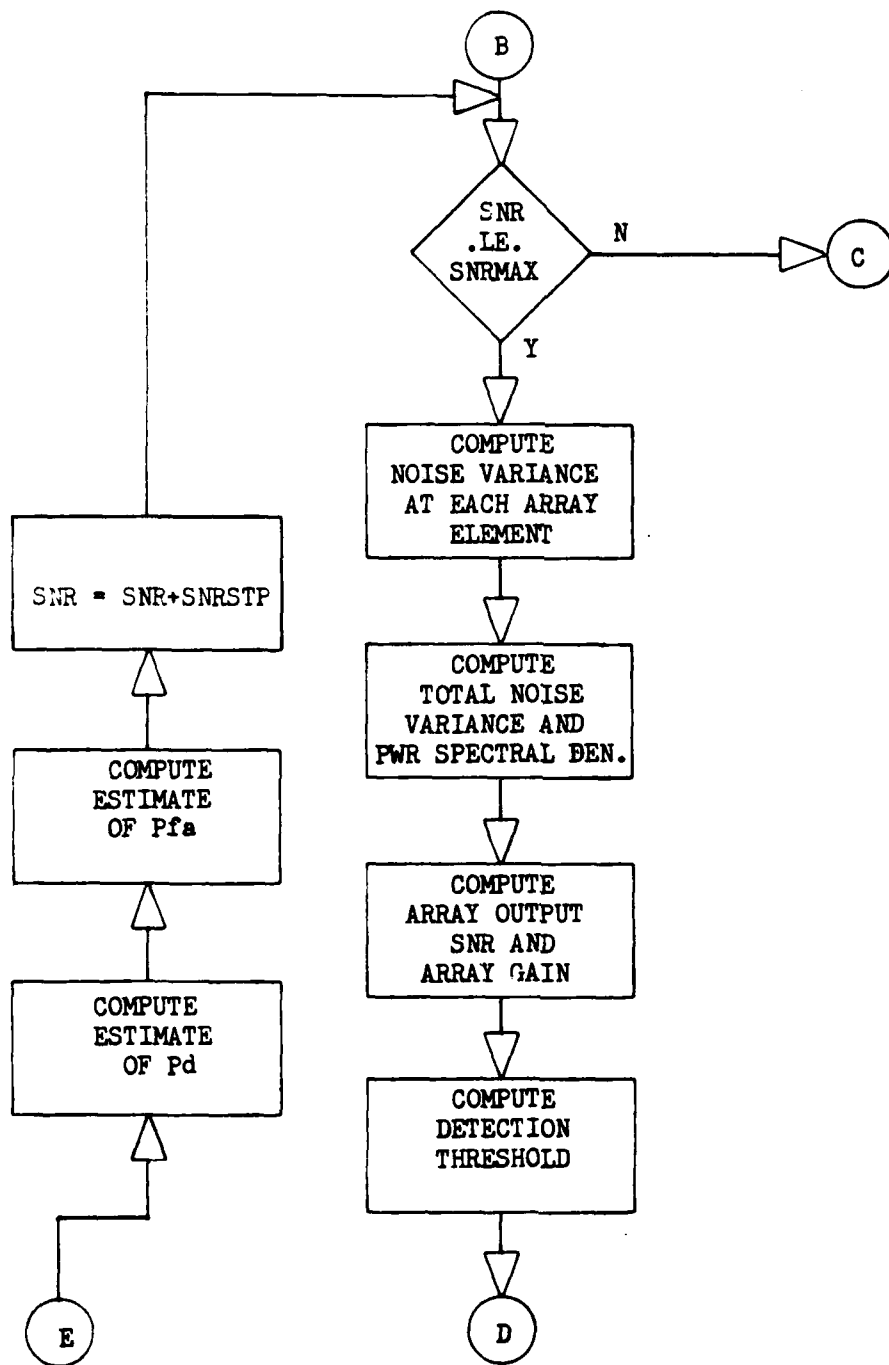


Figure 9c. Program RCVR Flowchart



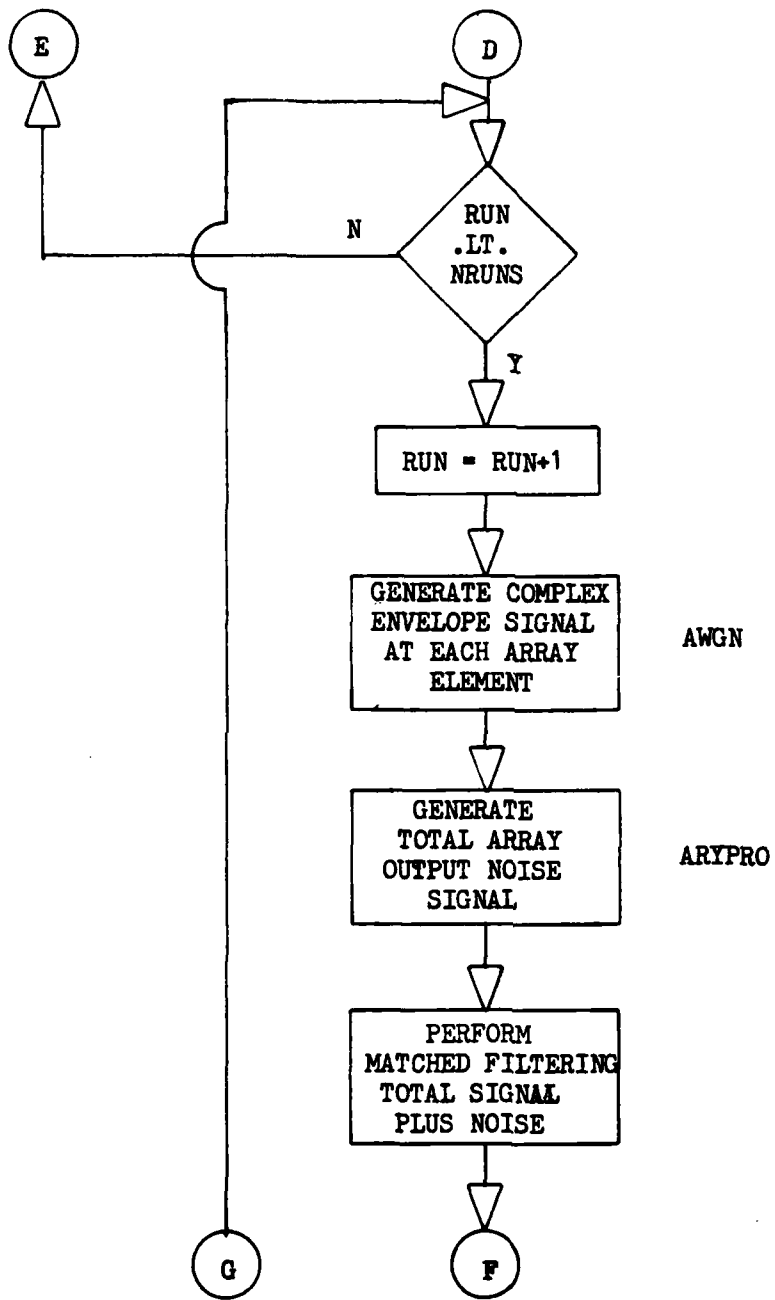


Figure 9d. Program RCVR Flowchart

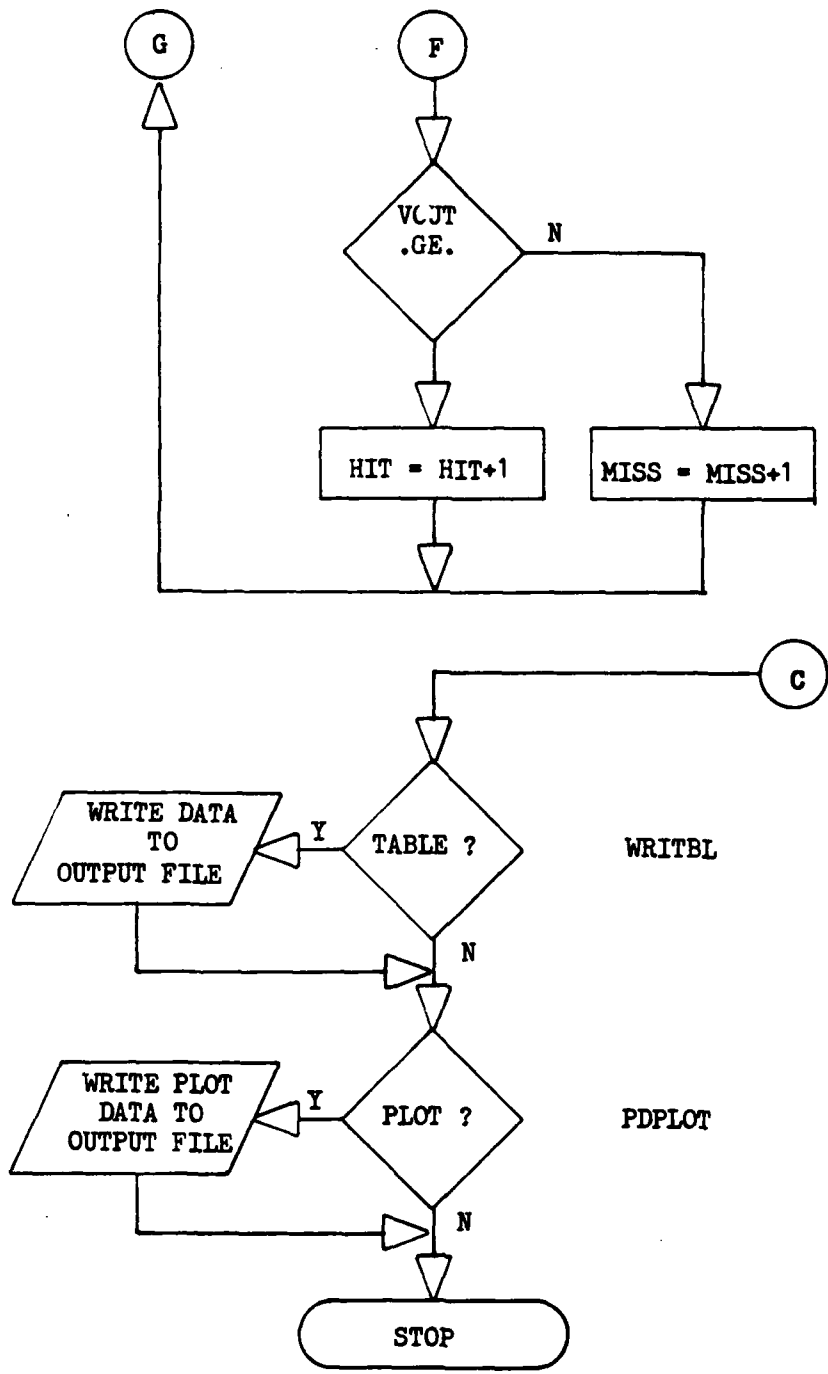


Figure 9e. Program RCVR Flowchart

- selecting the form of the simulation output data.

Initialization of the run-time environment involves reading input data from file to internal storage, generating the local processing waveform, measuring the time-average input signal power at each array element, computing the baseband signal bandwidth, and generating the complex weights used by the array processor. The input data is read by a call to the subprogram READY which returns a set of simulation parameters in COMMON storage and the complex envelope electrical signal data for each array element in matrix form. The local processing waveform is obtained by a call to the subprogram SGNLGN. The time-average signal power at each element (m,n) in the planar array is found by using the fact that the original transmit signal was synthesized from a finite Fourier series, and applying equation (2.43) to obtain the complex Fourier coefficients,  $c_q$ . Once the complex Fourier coefficients at each element in the planar array are obtained, the time-average power is computed using equation (2.42). The baseband signal bandwidth W is computed using equation (2.52). The separable complex weights,  $c_m$  and  $d_n$  in equation (2.26) are generated in two stages. First, the real amplitude factors,  $a_m$  and  $b_n$  in equation (2.26), are computed by a call to subprogram AMPWGT. Second, the real phase factors,  $\theta_m$  and  $\phi_n$  in equation (2.26), are obtained by a call to subprogram PHSWGT. The complex weights are then computed by combining the amplitude and phase factors as shown in equation (2.26).

The first signal processing step is to generate the total array output signal in the absence of additive noise by a call to subprogram ARYPRO. Subprogram ARYPRO which uses the complex weights  $c_m$  and  $d_n$  to cophase the planar array output signal returns a total array output signals. The total array output signal energy is computed using equation (2.40) for later use in calculating a SNR at the output of the array processor. The ratio of array output SNR to the input SNR defines the array gain, and provides a check on the validity of the data generated by the array processor algorithm.

Receiver performance is measured by computing a relative frequency estimate of the Pd over the specified range of array element input SNR values when the Pfa is a known, time-invariant parameter. Using the Pfa and a range of SNR values specified by the programmer in a receiver control data block, the main program establishes nine input SNR values for which the estimate of the Pd will be computed, and determines the number of trials, or runs, to be used in computing the estimate.

At point B in the flowchart of Figure 9c, the main program enters a loop that initializes the noise source, performs an array gain calculation, computes the detection threshold and then enters a second, inner loop where the correlation detection is done. After exiting the inner loop, the relative frequency estimate of the Pd is computed.

The outer loop increments through the input SNR values determined earlier, and exits the loop when the specified maximum input SNR value is reached.

The first step in initializing the noise generator is to determine the noise variance (power) at each array element. The power level, or variance, of the noise samples for a particular element in the array is a function of the time-average signal power at each element and the array element input SNR. The variance can be found using equation (2.46). By controlling the power level of the noise process at each array element, the receiver performance can be measured over a range of array element input SNR values regardless of the time-average signal power level at a particular array element.

The variance computed in this manner is the variance of the complex envelope baseband noise signal. The variance of the real baseband noise signal produced by the noise generator subprogram AWGN in the I or Q channel is one-half the variance of the complex noise signal since the complex envelope is the sum of the two independent I and Q channel noise signals. Therefore, the variance of the complex envelope of the noise is divided in half prior to being passed to the noise generating subprogram as a scale parameter.

The variance of the total complex envelope noise signal  $\sigma_T^2$  is obtained by summing all the noise variances of the array element complex envelope signals,  $\sigma_{mn}^2$ , as indicated

by equation (2.48). A power spectral density of the total noise signal is computed using equation (2.53) where  $\sigma_T^2$  is substituted for  $\sigma_{mn}^2$ .

The SNR at the array processor output is computed using equation (2.54) where the time-average power of the total array output signal is substituted for the mean square ensemble average, and the mean square ensemble average of the total noise is taken to be the same as the total noise signal variance. The array gain is computed using equation (2.58), and is held in internal storage for later output in tabular format.

The detection threshold  $\gamma$  is computed using equation (2.76) where the total noise power spectral density is substituted for the  $MNN_0$  factor and the energy of the local processing waveform  $E_g$  is used instead of the transmit signal energy  $E_x$ . For the purpose of this simulation however, the energy in the local processing waveform is the same as the energy in the transmit waveform. That is,  $E_g$  and  $E_x$  are equal.

The second, or inner loop, of the main program begins at point D in Figure 9c. Within the inner loop, the complex envelope noise signals are generated for all array elements, the total noise output signal is generated by the array processor subprogram ARYPRO, the total signal and total noise are summed and correlated with the local processing waveform, and the signal detection decision is made. The

inner loop terminates when the number of iterations through the loop equals the number of trials allowed to form the estimate of  $P_d$ .

The time-sampled, complex envelope array element noise data is obtained by repeated calls to the noise generator subprogram AWGN. Each call to AWGN returns a properly scaled pseudorandom number representing one sample of the noise process in the I or Q channel at a particular array element with L time samples taken for each of the I and Q channels. The noise signal data is stored in the same matrix form as the array element output electrical signal data.

The complex envelope noise data is submitted to the array processor subprogram for processing in exactly the same manner as the input signal data. The result is an array total noise output signal. Processing the noise alone in this manner provides some gain in execution speed and provides the flexibility to estimate the probability of false alarm directly, if desired. The DFT and IDFT are linear operations, and the principle of superposition holds. Therefore, the addition of the total noise and total signal at the output of the array processor is equivalent to adding noise to the signal at each element prior to passing the data to the array processor subprogram.

Correlation of the sum of the total signal and total noise with the local processing waveform is accomplished by

using the trapezoidal rule to approximate the integral of equation (2.67). The magnitude-square of the correlator output is obtained by taking the complex product

$$|\tilde{\ell}|^2 = \tilde{\ell} \cdot \tilde{\ell}^* \quad (3.1)$$

The threshold detection portion of the receiver is implemented by comparing the output of the magnitude-square operation to the decision threshold, using a simple IF-THEN-ELSE binary branch. The number of hits, or times the output exceeds the threshold, are counted and stored. The process of generating noise samples, and making a hit or miss decision continues through a large number of trials. Since the correlation is done using the  $H_1$  (signal plus noise) hypothesis,  $P_d$  can be directly estimated using the ratio

$$\hat{P}_d = \text{HITS/TRIALS} \quad (3.2)$$

The first approach taken to determine the minimum number of trials required to estimate  $P_d$  was based on equation (2.82). After rearranging terms, equation (2.82) can be written as

$$P_{fa} = P_d^{[1+SNR]} \quad (3.3)$$

The central idea was to compute an estimate of  $P_{fa}$ , using equation (3.3), from the relative frequency estimate of  $P_d$



in equation (3.2). The algorithm would then terminate when the computed estimate of Pfa differed from the Pfa input parameter by some arbitrary small amount. However, the use of equation (3.3) was found to be a poor test for establishing when the algorithm should terminate, and would not terminate the algorithm for Pd values greater than about 0.6.

A perturbation sensitivity analysis of equation (3.3) can be performed by computing the total differential of equation (3.3). That is,

$$dPfa = \frac{\partial Pfa}{\partial Pd} dPd + \frac{\partial Pfa}{\partial SNR} dSNR$$

$$dPfa = [1+SNR]Pd^{SNR}dPd + Pd^{[1+SNR]} \ln(Pd) dSNR \quad (3.4)$$

Assuming that the SNR is a constant, or equivalently, the differential dSNR is zero, dPfa becomes

$$dPfa = [1+SNR]Pd^{SNR}dPd \quad (3.5)$$

or

$$\Delta Pfa = [1+SNR]Pd^{SNR}\Delta Pd \quad (3.6)$$

where

$$dPfa \approx \Delta Pfa = |Pfa - \hat{Pfa}| \quad (3.7)$$

and

$$dPd \approx \Delta Pd = |Pd - \hat{Pd}| \quad (3.8)$$

Dividing both sides of equation (3.6) by equation (3.3) yields

$$\frac{\Delta Pfa}{Pfa} = [1+SNR] \frac{\Delta Pd}{Pd} \quad (3.9)$$

where  $\Delta Pfa/Pfa$  and  $\Delta Pd/Pd$  represent the fractional error between the actual and estimated values of  $Pfa$  and  $Pd$ , respectively.

Such an analysis indicates that the percent error in the computed estimate of  $Pfa$  is linearly related to the percent error in the estimate of  $Pd$ . The constant of proportionality relating the error in the computed estimate of  $Pfa$  to the error in  $Pd$  estimate is equal to  $(1 + SNR)$  where the SNR is taken at the output of the magnitude-square operation. Thus for SNR values greater than approximately 1, or 0 dB, a small error in the relative frequency estimate of  $Pd$  is scaled to a larger error in the estimate of  $Pfa$  found by using equation (3.3). Note that for a  $5 \times 5$  element planar array and a bandwidth of 5 times the fundamental frequency as in the CW pulse case, the array element input SNR can be found by

equation (2.92), and is roughly 24 dB less than the SNR at the output of the magnitude-square operation. That is, a 0 dB SNR at the output of the magnitude-square operation corresponds to an array element input SNR of -24 dB. The end result is an estimate of Pfa that diverges wildly from the specified Pfa parameter at SNR values over which the receiver operates. In addition, equation (3.3) was derived using certain assumptions regarding the statistics of the input noise that may not be precisely duplicated by the pseudorandom noise data generated by the computer program. If the assumptions regarding the use of zero mean, uncorrelated, Gaussian noise are not satisfied by the pseudorandom noise source, equation (3.3) does not hold, and the algorithm would not be suitable for other input noise models. For these reasons, the use of equation (3.3) was abandoned in favor of an empirically determined fixed number of trials to estimate Pd.

The number of trials needed to estimate Pd was found by assuming that the absolute minimum number of trials should be the reciprocal of the Pfa parameter. That is, if a Pfa of 0.01 is specified, at least 100 trials must be taken to allow at least one chance in one hundred of a false alarm occurring. Even though a relative frequency estimate of Pd is being computed, Pd is related implicitly to Pfa through the decision threshold, and the value of the Pfa parameter should be taken into account when attempting to fix the number of trials needed to estimate Pd.

The number of trials was empirically determined by running the receiver simulation program repeatedly with increasing multiples of the minimum number of trials, and observing the effect on the estimate of Pd. Depending upon the value of the Pfa parameter, it was found that four to eight times the minimum number of trials would produce curves that did not change appreciably as the number of trials was increased further. Therefore, the fixed number of trials used to estimate Pd was arbitrarily set at  $10 \times 1/Pfa$  for Pfa of 0.1, and to  $5 \times 1/Pfa$  for Pfa of 0.01. The smaller multiplier for the Pfa of 0.01 became necessary due to limits on computer resources.

1. Subprogram READY

The function of subprogram READY is to obtain the simulation parameters and the complex envelope output electrical signal data from a data file. The data file is generated by the ocean communications channel simulation computer program developed by Vos and Ziomek [Ref. 3]. That is, READY forms the interface between the RCVR simulation and the ocean communications channel program. A flowchart of READY is shown in Figure 10.

The simulation parameters are read in first, and are stored in the named COMMON blocks: HEADER, SIGNAL, ARRAY, and MEDIUM. The named COMMON blocks provide the mechanism for communicating simulation parameters into the various subprograms. The HEADER data documents the type of

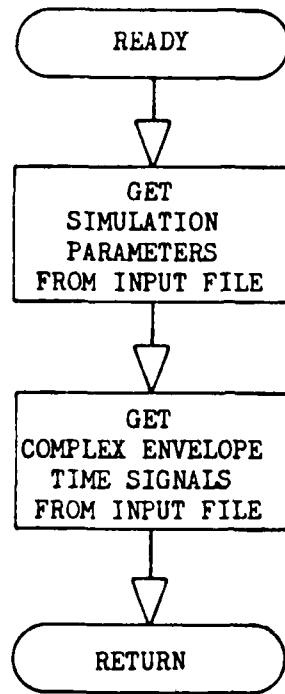


Figure 10. Subprogram READY Flowchart

communication channel, and the date the data was generated by the ocean communication channel simulation. The SIGNAL data includes: the fundamental frequency  $f_0$  and the period  $T_0$ ; the number of harmonics  $K$ ; the same rate  $f_s$  and the sample period  $T_s$ ; the number of time samples  $L$ ; the carrier frequency  $f_c$ ; and the number of zeroes padded to the input signal data, if any. The ARRAY data includes: the number array elements  $M$  and element spacing  $d_x$  in the  $x$ -direction; the number of elements  $N$  and element spacing  $d_y$  in the  $y$ -direction; the direction cosines  $u_r$  and  $v_r$ , representing the direction of the direct path from the transmit array to the

receive array; the direction cosines  $u_b$  and  $v_b$ , representing the direction the transmit array beam pattern was steered in the communication channel simulation; the depth  $y_o$  of the center element of the transmit array; and the depth  $y_r$  of the center element of the receive array. The MEDIUM data includes the speed of sound  $c_o$  at the center element of the transmit array; the sound-speed-profile gradient  $g$ ; and the speed of sound  $c_{yr}$  at the center element of the receive array.

The time-sampled, complex envelope, output electrical signal data is read in next. The data is stored in the complex matrix variable YCE with dimensions L, M and N. The maximum values of L, M, and N are limited to 33, 11 and 11, respectively.

## 2. Subprogram SGNLGN

The function of subprogram SGNLGN is to generate the time samples of the complex envelope and to compute the energy of the local processing waveform given by equation (2.64). A flowchart of Subprogram SGNLGN is shown in Figure 11.

The local processing waveform  $\tilde{g}(\ell T_s)$  is synthesized from a finite, complex Fourier series with provisions for incorporating the estimates of time delay  $\hat{\tau}$  and doppler shift  $\hat{\phi}$  in the total received signal  $\tilde{y}(\ell \tau_s)$ . Accurate estimates of  $\hat{T}$  and  $\hat{\phi}$  are necessary to achieve maximum output from the correlator/matched filter detector portion of the

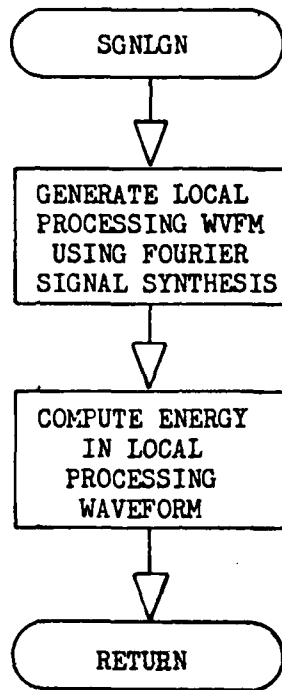


Figure 11. Subprogram SGNLGN Flowchart

receiver. That is, the maximum receiver sensitivity is obtained when  $\hat{\tau} = \tau_A$  and  $\hat{\phi} = \phi_A$  as indicated in equations (2.65) and (2.66).

For the purpose of this study, the actual doppler shift is always set to zero in the transmit signal synthesizer, and the actual time delay due to the range or distance between array is set by the system geometry under consideration and the reference speed of sound at the transmit array. Therefore, the estimate of doppler shift is set to zero in subprogram SGNLGN, and the estimate of time delay due to range is computed from the line-of-sight range between the center element of the transmit array and the

center element of the receive array, and the speed of sound  $c_0$  at the center element of the transmit array, or

$$\hat{\tau} = \sqrt{(x_0 - x_r)^2 + (y_0 - y_r)^2 + (z_0 - z_r)^2} / c_0 \quad (3.10)$$

where  $(x_0, y_0, z_0)$  are the coordinates of the center element of the transmit array, and  $(x_r, y_r, z_r)$  are the coordinates of the center element of the receive array.

The estimates of  $\hat{\tau}$  and  $\hat{\phi}$  are easily incorporated into the local processing waveform of equation (2.64) by applying well-known properties of Fourier transforms to equation (2.17) to yield

$$\tilde{x}(t - \hat{\tau}) \exp[j2\pi\hat{\phi}t] = \sum_{q=-K}^K c_q \exp[j2\pi q f_0 (t - \hat{\tau}) + j2\pi\hat{\phi}t] \quad (3.11)$$

Note that the right hand side of equation (2.64) is just the time-sampled form of equation (3.11).

The complex Fourier coefficients  $c_q$  of equation (3.11) are identical to those used in equation (2.17) to generate the transmit signal in the ocean communication channel simulation computer program. Thus, the local processing waveform is identical to the transmit signal in functional form and total energy content, but is shifted in time and frequency by the estimates of range delay and doppler shift, respectively.



Subprogram SGNLGN also computes the local processing waveform signal energy  $E_g^-$  for later use in setting the decision threshold  $\gamma$ . To compute the energy the magnitude-square of the complex Fourier coefficients are summed over all harmonics as indicated in equation (2.42) where  $c_q$  is the  $q$ -th harmonic of the local processing waveform. This sum is equivalent to the time-average power in the complex envelope of the local processing waveform. The energy can then be found by multiplying the time-average power by the fundamental period  $T_0$  of the local processing waveform.

### 3. Subprogram AMPWGT

The function of subprogram AMPWGT is to provide the real-valued, amplitude factors  $a_m$  and  $b_n$  of the separable complex weights  $c_m$  and  $d_n$  in equation (2.26). A flowchart of subprogram AMPWGT is shown in Figure 12.

To generate the rectangular amplitude window,  $a_m$  and  $b_n$  are set equal to 1.0 for all elements  $(m,n)$  in the receive planar array. A separate subprogram to generate the amplitude weights facilitates generation of other forms of amplitude windows such as triangular, Hamming, Blackman, etc. However, only the rectangular window is used in this study.

### 4. Subprogram PHSWGT

The function of subprogram PHSWGT is to generate the phase factors  $\theta_m$  and  $\phi_n$  of the separable complex weights  $c_m$  and  $d_n$  in equation (2.26). A flowchart of subprogram

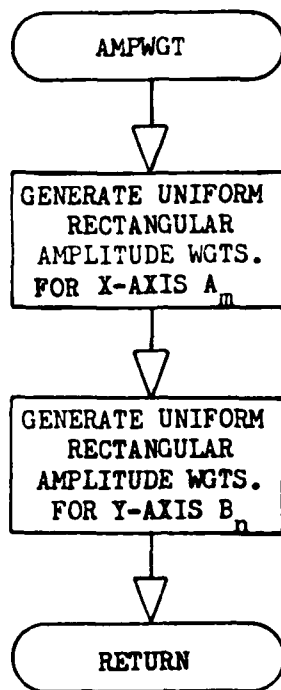


Figure 12. Subprogram AMPWGT Flowchart

PHSWGt is shown in Figures 13a and 13b. PSHWGt can be programmed to compute phase factors that compensate, or remove the effects of, system geometry and deterministic medium wave propagation effects. PHSWGt can also introduce random noise in the phase factors for study purposes.

The phase corrections for system geometry are computed using equations (2.27) and (2.28), where the direction cosines  $u$  and  $v$  are selected such that receive array beam pattern is aimed at the transmit array along the direct path from the receive array to the transmit array. That is, if  $\hat{n}_0$  in equation (2.5) represents the direction of the direct path from the transmit array to the receive array,  $u$  and  $v$

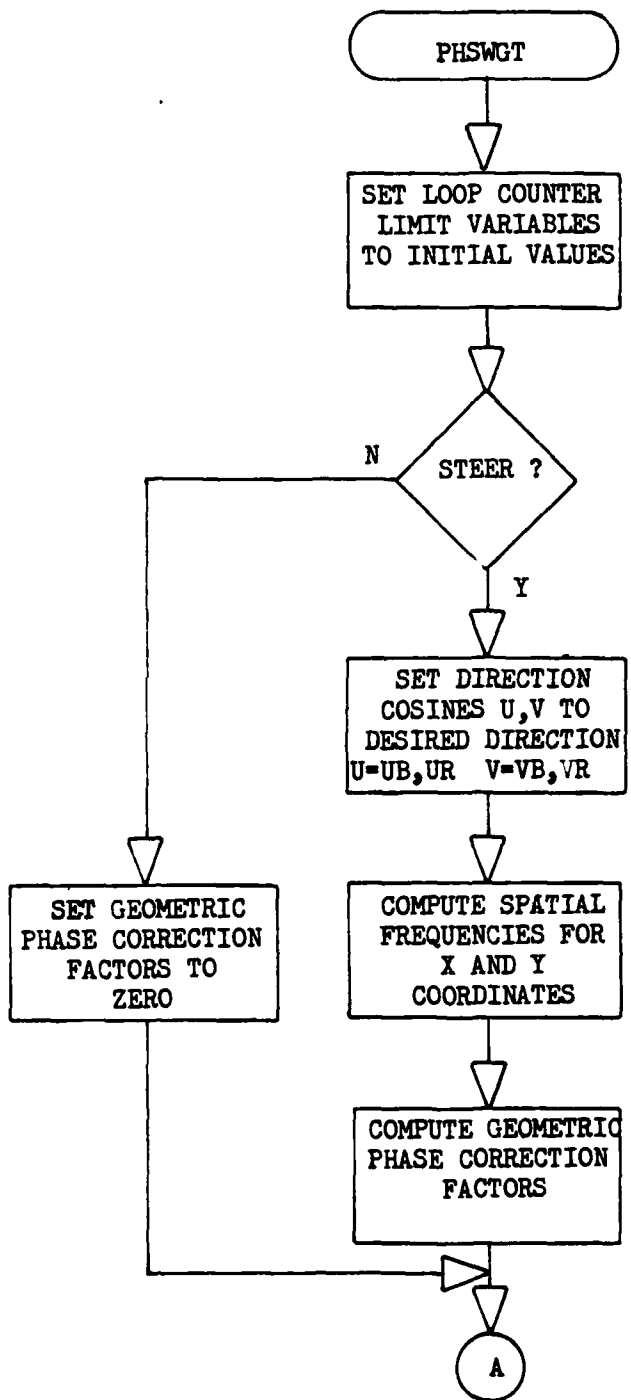


Figure 13a. Subprogram PHSWGT Flowchart

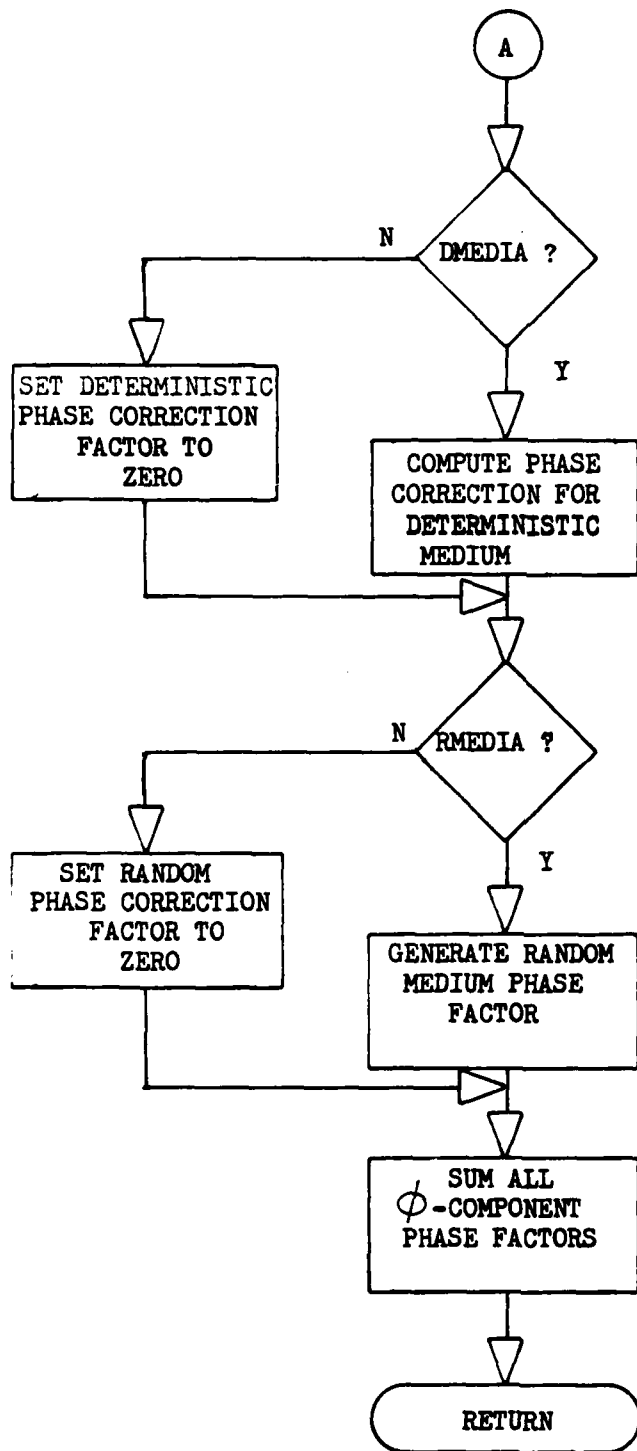


Figure 13b. Subprogram PHSWGT Flowchart

are set equal to  $-u_0$  and  $-v_0$  so that the receive array beam pattern points in the  $-\hat{n}_0$  direction.

The deterministic medium phase correction factor is found by using equation (2.32) to compute the phase shift of the signal due to propagation through an inhomogeneous medium, and then negating the result. The random medium effect can also be computed from a closed form expression, but its use in generating phase correction factors is not the subject of this study, and will not be discussed. The total phase correction factor for the  $y$ -direction is obtained by adding the system geometry and deterministic correction factors.

#### 5. Subprogram ARYPRO

The array processor subprogram ARYPRO uses DFT and IDFT algorithms to:

- generate the spectrum of the input electrical signal data at each element,
- correct the phase of the spectral components to co-phase the signals at all array elements, and
- inverse transform the signal spectrum at each array element to recover the cophased signal data.

A block diagram of the subprogram ARYPRO is shown in Figures 14a and 14b.

The output of the array processor is a time-sampled, complex envelope signal representing the sum over all array elements of the signals at each element. The defining equation for the DFT is used instead of a fast Fourier transform algorithm because the maximum number of time

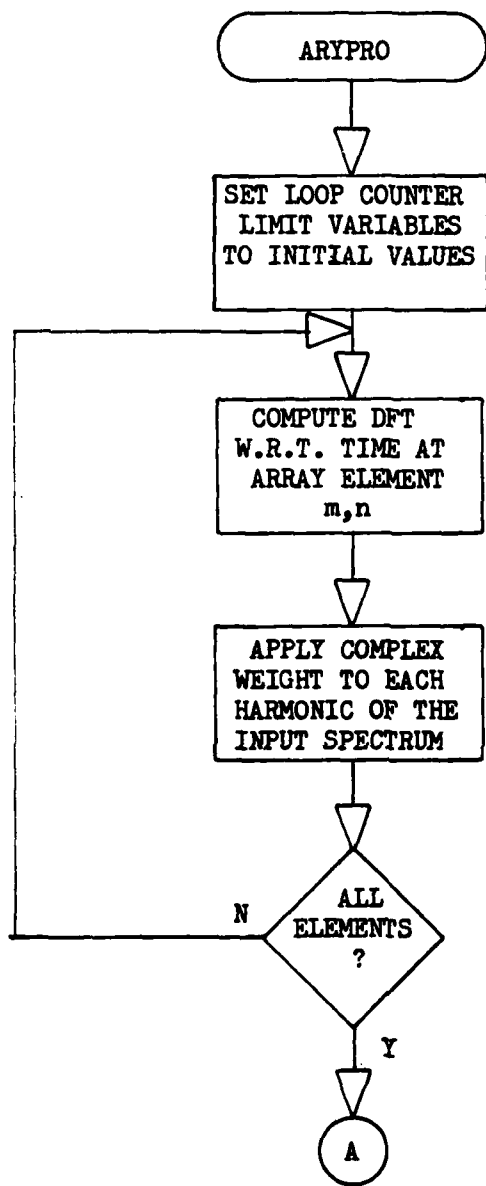


Figure 14a. Subprogram ARYPRO Flowchart

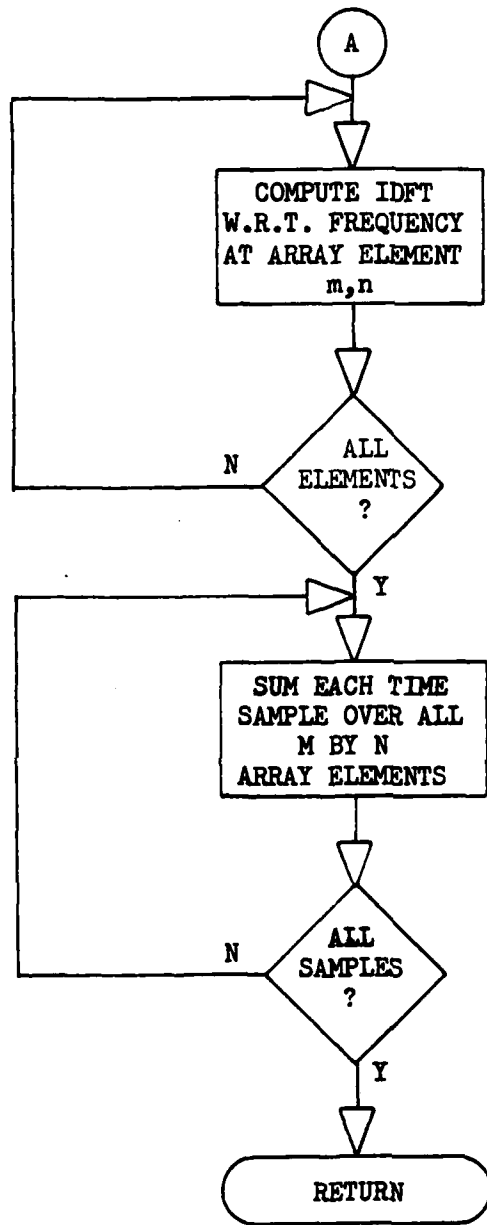


Figure 14b. Subprogram ARYPRO Flowchart

samples permitted (33) is insufficient to achieve a measurable improvement in speed of execution [Ref. 6:pp. 151-152]. Additionally, use of the DFT equation relates the structure of the program directly to previous work by Ziomek [Ref. 2] and Vos [Ref. 3].

#### 6. Subprogram AWGN

The function of subprogram AWGN is to generate one sample of an uncorrelated, Gaussian process with arbitrary mean and variance. A flowchart of AWGN is shown in Figure 15.

AWGN is based on the International Mathematical Subroutine Library (IMSL) FORTRAN pseudorandom number generator routine GGNQF. GGNQF is a function subprogram that returns one zero mean, unit variance, Gaussian, or  $N(0,1)$ , pseudorandom number with each call to the function subprogram. The zero mean, unit variance pseudorandom number  $x_n$  is then scaled with the desired mean  $\mu_x$  and the desired standard deviation  $\sigma_x$  using the relation

$$X = \sigma_x X_n + \mu_x \quad (3.12)$$

where the standard deviation is computed from the variance as

$$\sigma_x = \sqrt{\sigma_x^2} \quad (3.13)$$

The desired mean and standard deviation are passed to AWGN as arguments from the main program. The mean is



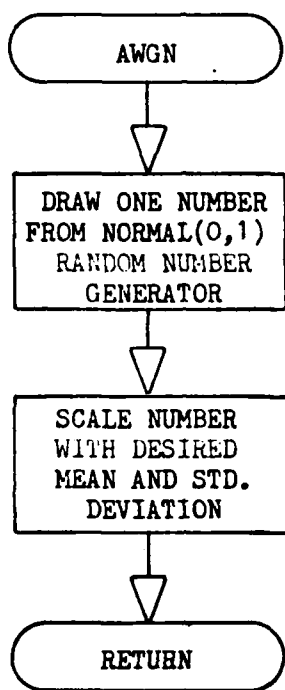


Figure 15. Subprogram AWGN Flowchart

always set to zero for the purposes of this study and the standard deviation is found from equation (3.13) where the variance represents the desired power level in either the I or Q channel noise signal.

The function subprogram GGNQF internally recomputes a new seed value for subsequent calls from a seed provided on the first call to the function. Since the first seed value is set as a parameter in the top level program, and is passed as an argument through AWGN to GGNQF, the pseudo-random sequence always follows the same pattern each time

the receiver simulation is run. Using the same pseudo-random sequence for each simulation run is essential if comparisons between different runs are to be made from the receiver simulation output plots.

7. Subprogram INTGRT

The function of subprogram INTGRT is to compute, using equation (2.68), the approximation of the correlation integral given in equation (2.67). A flowchart of subprogram INTGRT is shown in Figure 16. The complex product of the

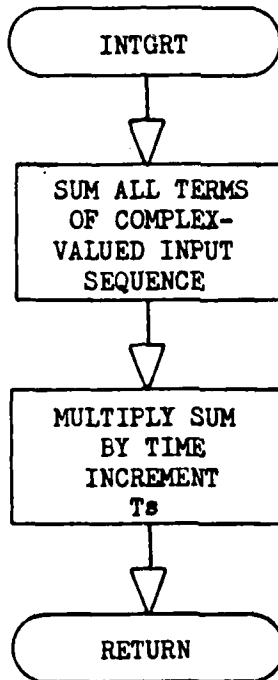


Figure 16. Subprogram INTGRT Flowchart

total signal and noise, and the local processing waveform is computed in the top level program. The resulting

complex-valued sequence is passed to INTGRT which computes the correlator output  $\tilde{l}$  by using a trapezoidal integration algorithm to approximate the integral of equation (2.67). A separate subprogram allows easy implementation of other numerical integration algorithms, if desired.

#### 8. Subprogram WRITBL

The function of subprogram WRITBL is to simply provide tabular output of the simulation parameters and selected information generated during the execution of the program. A flowchart of subprogram WRITBL is shown in Figure 17.

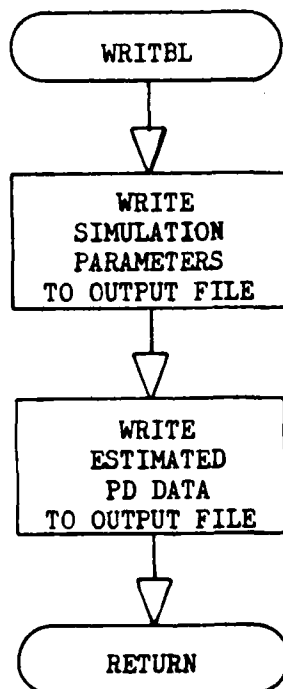


Figure 17. Subprogram WRITBL Flowchart

Besides the data read into the COMMON storage blocks by subprogram READY, the information output to the data file

in table form includes the array element input SNR at which the  $P_d$  is estimated, the estimate of  $P_d$ , an estimate of  $P_{fa}$  obtained using equation (2.82), the SNR at the output of the array processor, the array gain and the SNR at the output of the magnitude-square operation. The tabular output is intended primarily to provide a convenient means of testing program modifications. It is not intended to be the primary simulation output, and will not be discussed further.

#### 9. Subprogram PDPLOT

The function of subprogram PDPLOT is to convert the numeric data generated by the receiver simulation into graphic form. A flowchart of the subprogram PDPLOT is shown in Figure 18. The plots generated from the numeric data are obtained through the use of standard DISSPLA graphics library subroutines.

The primary output of the receiver simulation is a plot of the estimate of  $P_d$  versus the array element input SNR with a fixed value of  $P_{fa}$  as a parameter. PDPLOT also computes a theoretical value of  $P_d$  using the equation (2.82) where the SNR at the output of the magnitude-square operation is related to the array element input SNR through equation (2.91).

The curve representing the estimated  $P_d$  is plotted through the estimated  $P_d$  data using the DISSPLA least squares, cubic spline, curve fitting plot routine SMOOTH. The value of  $P_d$  obtained from equation (2.82) is plotted using the

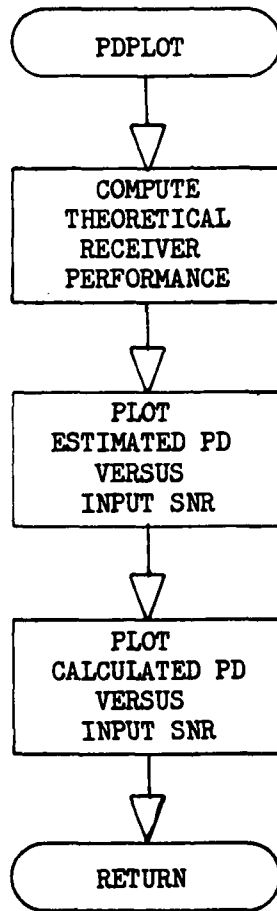


Figure 18. Subprogram PDPLOT Flowchart

DISSPLA cubic spline, interpolating polynomial routine SPLINE, and appears as a dashed line on all plots generated by the receiver simulation. That is, the curve for the calculated value of  $P_d$  is an interpolating polynomial that passes through the calculated  $P_d$  data points, while the curve for the estimated value of  $P_d$  is allowed to pass within some arbitrary, small offset of the estimated  $P_d$  data point. For the purpose of this study, the maximum offset allowed was 10 percent of the data point value. This value of offset provided a reasonable compromise between obtaining a relatively smooth fit of the plotted curve without diverging excessively from the data points. Both the estimated and calculated  $P_d$  data points are plotted at the same array element input SNR.

#### B. MODEL VERIFICATION

Verification of the receiver model involved two tasks, characterization of the pseudorandom number generator noise source, and a comparison of the data generated by the receiver simulation program with the results predicted by the theoretical development discussed in Section II. Why simulate a test case for which a theoretical model exists? The main reason is to gain some confidence in the results generated by the simulation when the inputs are such that a theoretical model does not exist or is mathematically intractable.

## 1. Characterization of the Noise Source

The capability to generate noise samples consistent with the noise description used in developing the receiver equations is central to verification and usefulness of the computer simulation. Thus, the first step is to ascertain the statistical properties of the noise source used in the computer program. Recall that the assumption required in developing the relations between  $P_d$ ,  $P_{fa}$ , decision threshold and SNR of the magnitude-square of the correlator output involved the use of zero mean, Gaussian noise which is uncorrelated in both spatial and temporal coordinates. The noise source was tested by taking a sequence of noise samples for both I and Q channels in manner identical to that used in the receiver simulation. That is, the subprogram AWGN was embedded in a test program to ascertain the statistical properties of the complex envelope of the noise signal. The following tests were applied to the I and Q channel sample sequences to verify agreement with the noise process assumptions:

- sample mean
- sample variance
- histogram
- autocovariance, and
- estimated power spectral density.

The test algorithms were obtained from standard IMSL procedures.

Figures 19 and 20 show the results of the sample mean, variance and histogram calculations for the noise processes in the I and Q channels, respectively. The sample mean and variance calculations approximate the zero mean, unit variance assumptions quite well. The histogram calculations indicate the distribution of the samples is roughly Gaussian. The smooth curve plotted through the histogram represents the exact Gaussian distribution for the size of the sample window used. The greatest deviation from Gaussian appears near the mean value which unfortunately is where most of the sample values lie. Thus, some difficulty in achieving a perfect correlation between simulated performance and theoretical results was anticipated, and in fact some deviation from theory at large values of  $P_d$  did occur.

The space-time correlation properties of the sample sequence was measured by computing the autocovariance function of 2000 samples over a total time (or space) displacement (lag) of 1000 samples. The autocovariance was computed using the IMSL routine FTAUTO. The correlation of adjacent samples, whether one or two or 1000 samples apart, was found to be remarkably small. The autocovariance function of the I and Q channel noise is shown in Figures 21 and 22, respectively. Because of the manner in which the samples are drawn in the simulation, the distinction of a sample being assigned to a particular channel at a particular



HISTOGRAM OF I CHANNEL NOISE

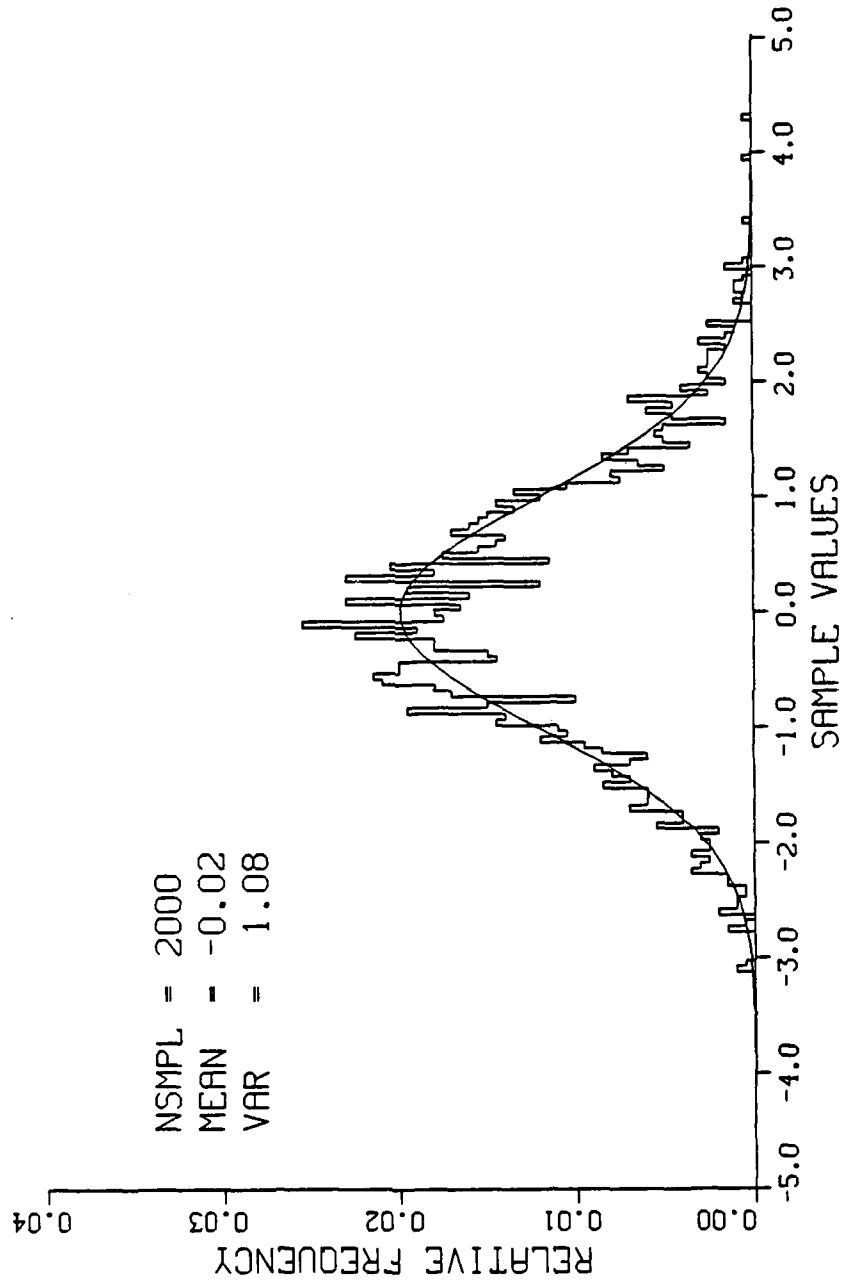


Figure 19. Histogram of I-Channel Noise

# HISTOGRAM OF Q CHANNEL NOISE

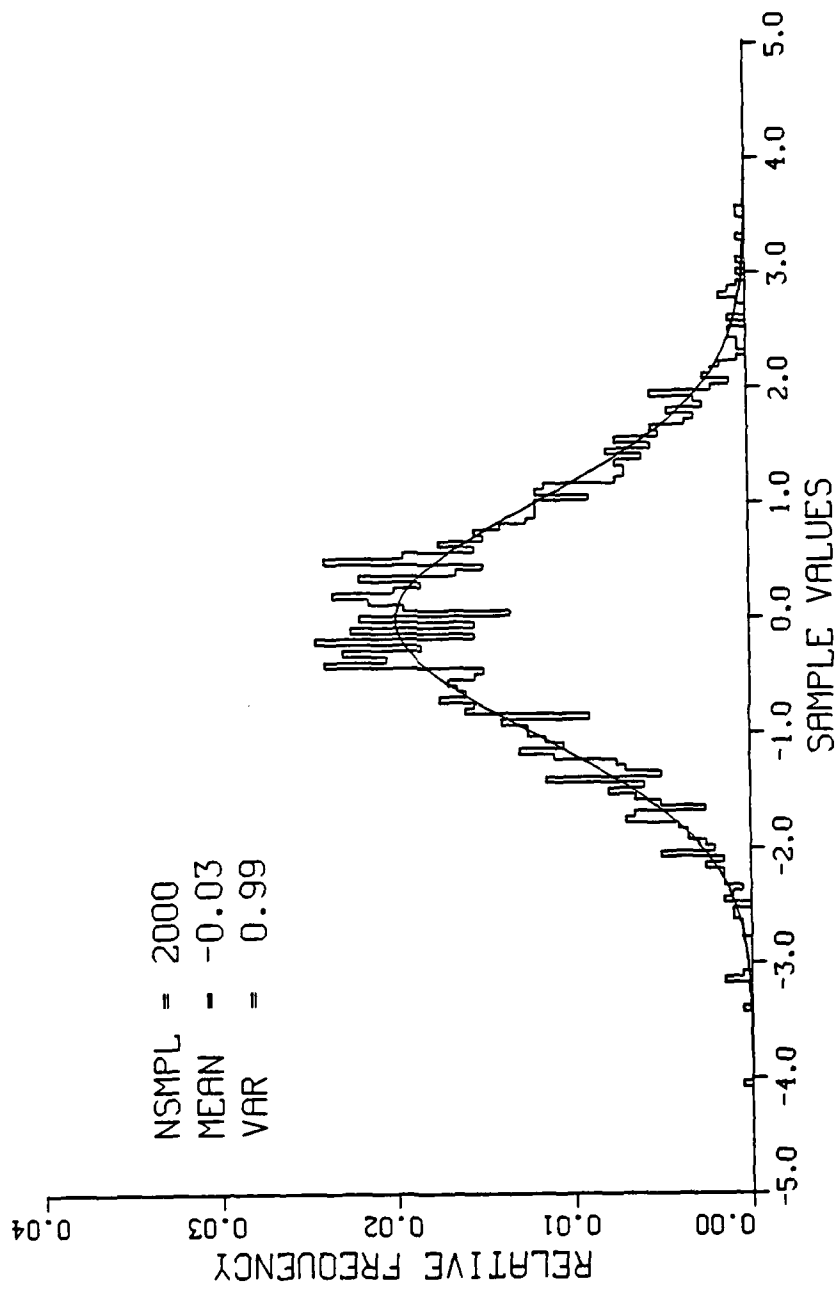


Figure 20. Histogram of Q-Channel Noise

AUTOVARIANCE OF I CHANNEL NOISE

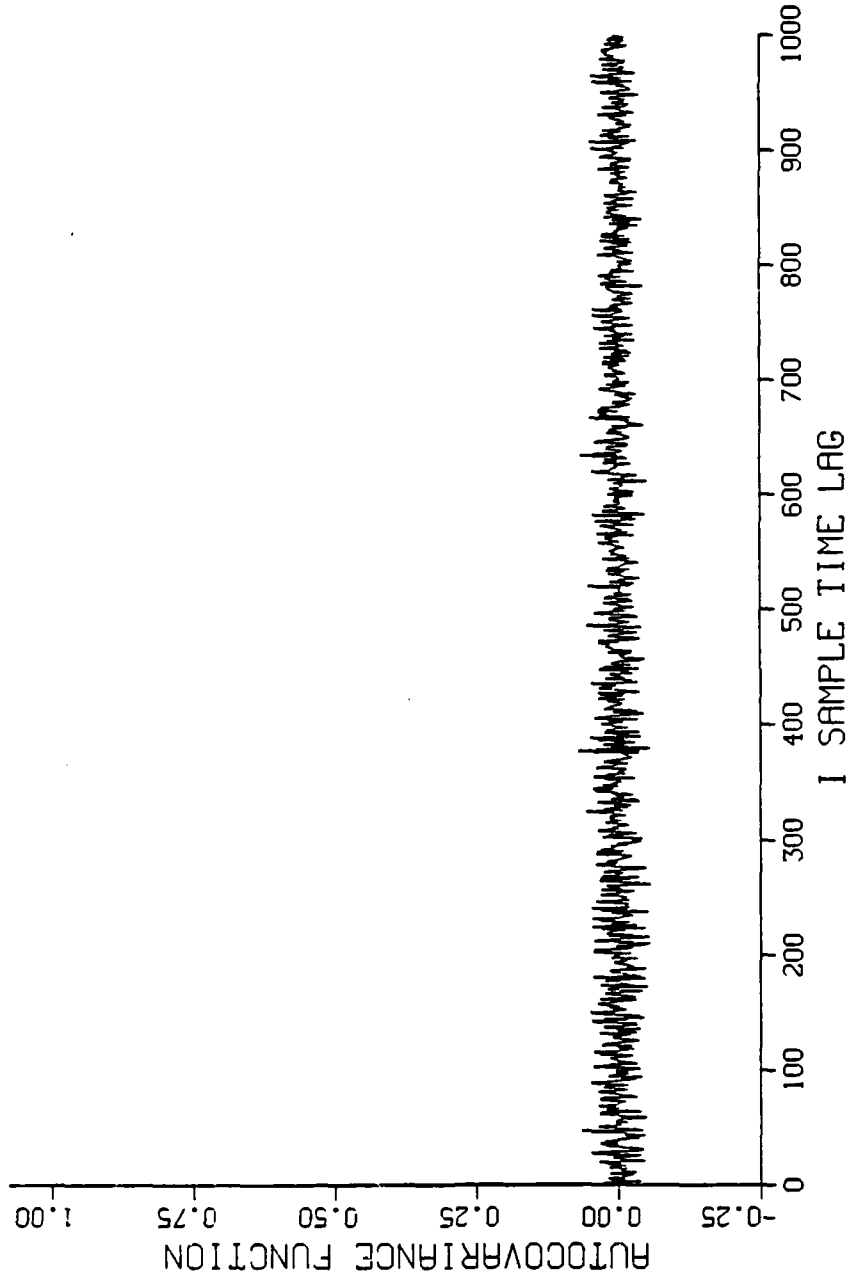


Figure 21. Autocovariance Function of I-Channel Noise

AUTOVARIANCE OF Q CHANNEL NOISE

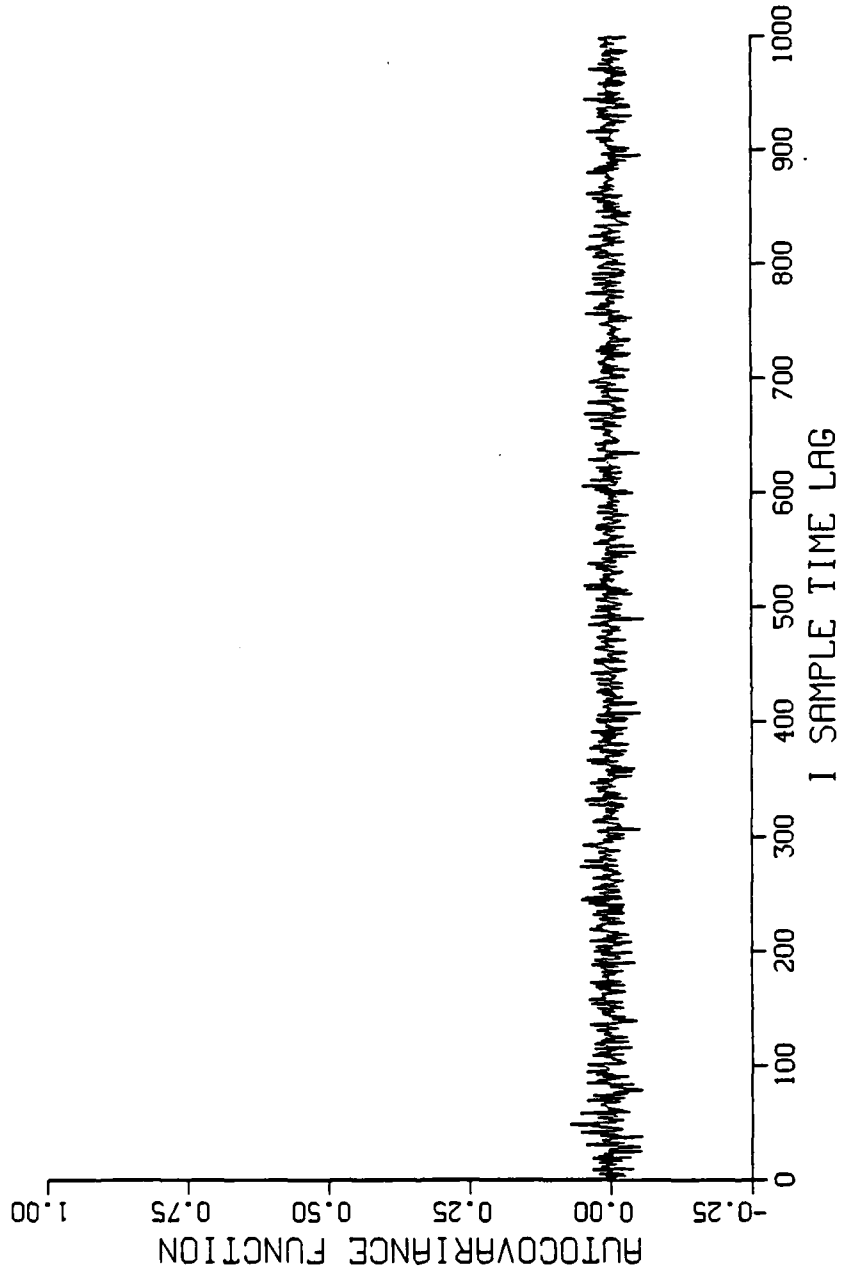


Figure 22. Autocovariance Function of Q-Channel Noise

element at a particular time is immaterial. The autocovariance of the samples indicates that noise samples can be generated which are independent of sample time, array element location, and receiver channel.

The estimated PSD was computed primarily to reinforce the results obtained from the autocovariance computation. The IMSL routine, FTFPS, used to compute the PSD of the sample sequence implements an algorithm similar to that due to Welch [Ref. 7:pp. 553-554] in which the total sample record is partitioned into contiguous subrecords. Each subrecord is amplitude weighted with a triangle window function. Then, a periodogram of each amplitude weighted sample subrecord is computed. The resulting subrecord periodograms are averaged over all subrecords in an effort to reduce the variance of the estimate of the PSD. The estimate of PSD for the I and Q channel noise is shown in Figures 23 and 24, respectively. The estimated PSD is approximately flat for both the I and Q channels over the sampled frequency range of 0 to  $\pi$  radians, or one sample frequency period. This tends to support the results obtained from the autocovariance computation that the noise samples are indeed uncorrelated.

## 2. Verification of the Output Data

The primary output data from the receiver simulation is a plot of an estimate of  $P_d$  for various values of input SNR at a given  $P_{fa}$ . As shown in equation (2.82), a closed

ESTIMATED POWER SPECTRAL DENSITY  
I CHANNEL NOISE

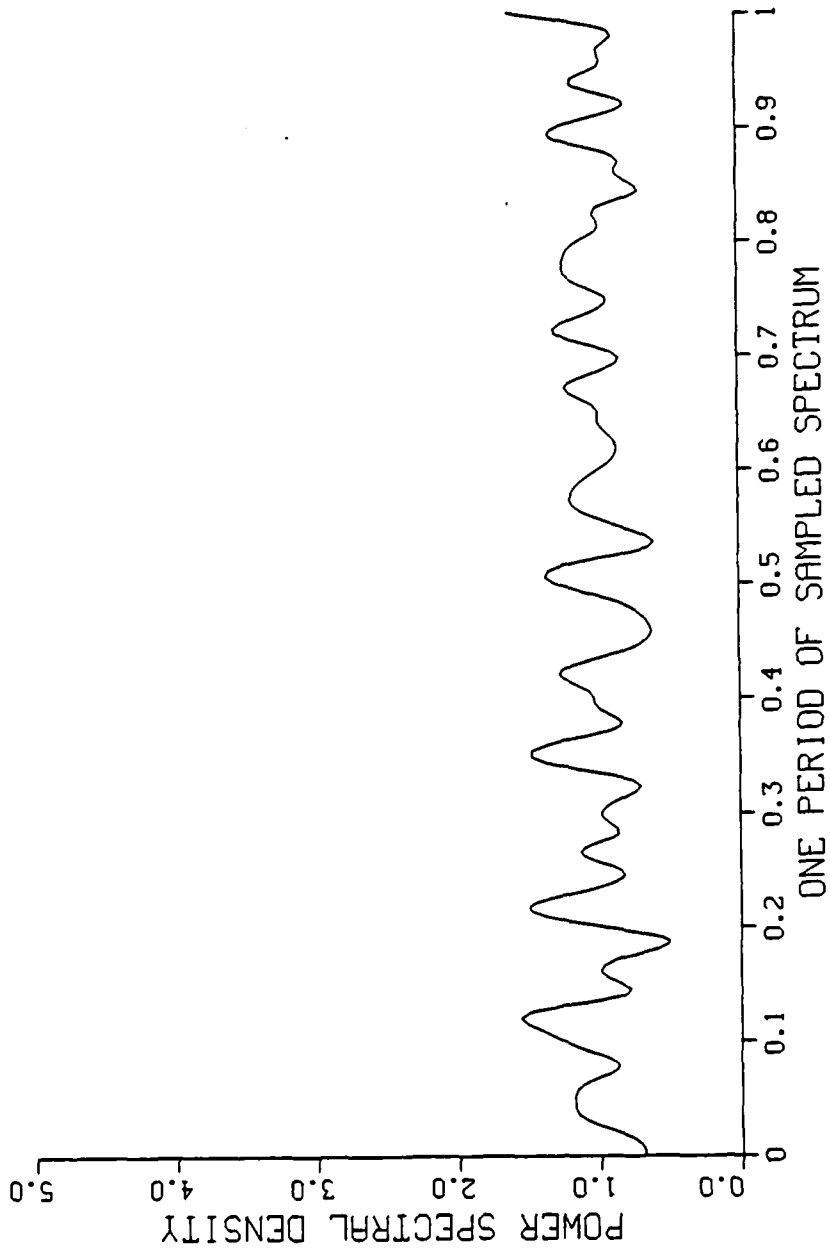


Figure 23. Estimated Power Spectral Density of I-Channel Noise

ESTIMATED POWER SPECTRAL DENSITY  
Q CHANNEL NOISE

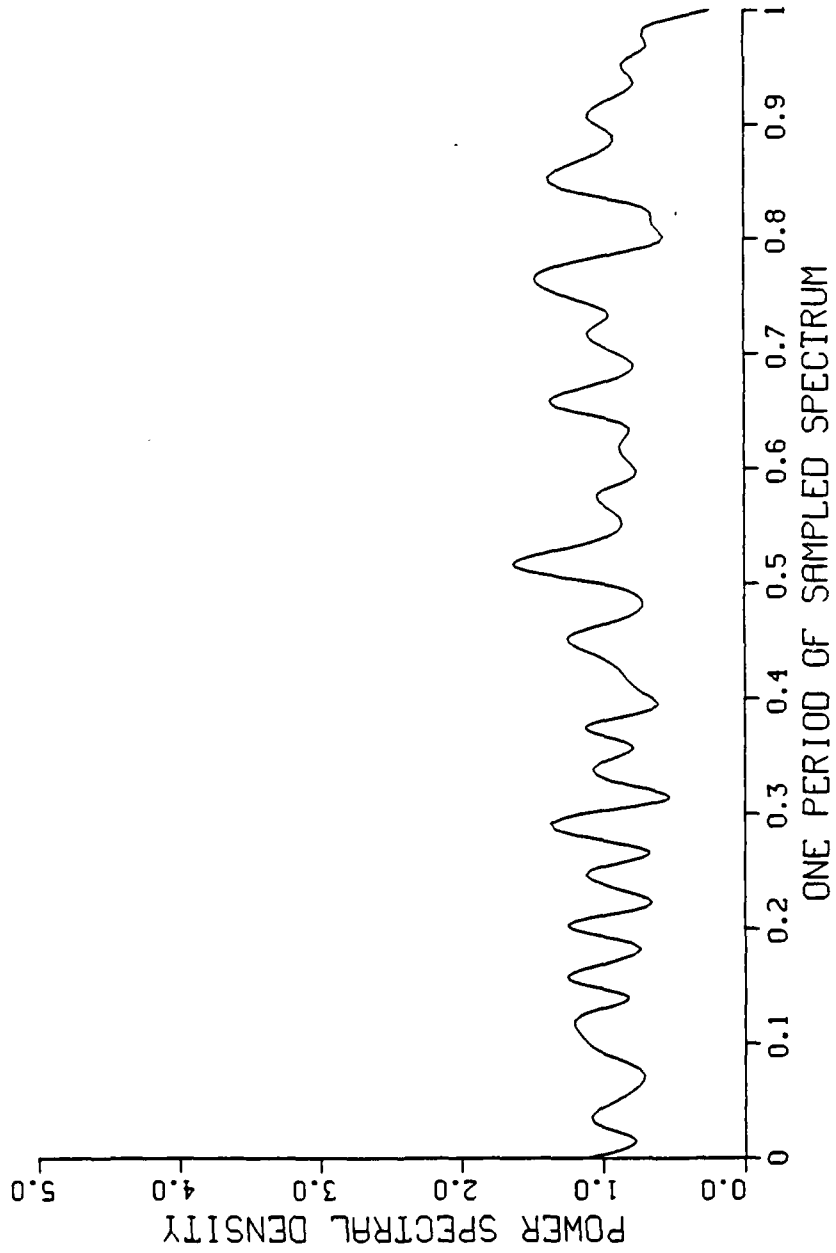


Figure 24. Estimated Power Spectral Density of Q-Channel Noise

form relation exists between the  $P_d$ ,  $P_{fa}$  and correlator output SNR. Furthermore, the correlator output SNR can be related to the array input SNR when the signals at all array elements are precisely cophased by equation (2.91). Therefore, a plot of the theoretical performance computed using equations (2.82) and (2.91) can be superimposed on the plot of the receiver simulated performance. The curve representing theoretical performance provides verification of the simulated performance when input signal parameters and phase weighting allow precise signal cophasing to occur. The computed performance curve also provides a baseline to evaluate simulated performance when the input noise or receiver operating conditions differ from the assumptions used in formulating the receiver model. In all the plots, the theoretical performance is shown as a dashed curve.



#### IV. PRESENTATION OF RESULTS

This section presents the results of three receiver simulation case studies and analyzes the simulation output in each case. The three cases considered are:

- Case TEST, in which the output electrical signal data at each array element is produced by a test signal generator computer program, and is free of communication channel effects such as attenuation, phase shifts due to wave front refraction, time delay due to range separation, and the transmit array beam pattern.
- Case HMGl, in which the output electrical signal data at each array element is produced by the ocean communication channel simulation computer program, and includes the effects of path attenuation, phase shifts due to system geometry, time delay due to range separation, and the transmit array beam pattern.
- Case INHMGl, in which the output electrical signal data at each array element is produced by the ocean communication channel simulation computer program, and includes not only the effects given in case HMGl, but also contains phase shifts due to refraction of the wavefront along the propagation path.

The results of these case studies will be analyzed by providing a brief description of the transmit signal waveforms used to generate the array element output electrical signal data, by listing the system parameters that distinguish the test cases, and finally, by interpreting the plots of  $P_d$  versus array element input SNR for each case study.

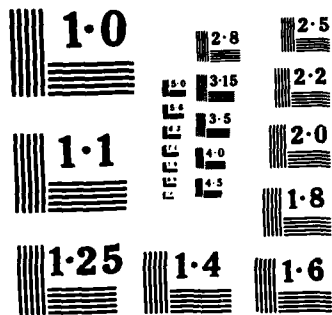
##### A. TRANSMIT WAVEFORMS

The analysis and theoretical development of the receiver simulation in Section II makes no assumption regarding the

functional form of the transmit signal. The receiver should perform equally well regardless of the type of transmit signal provided that the correlator/matched filter uses a replica of the transmit signal as the local processing waveform. To verify this hypothesis, and thereby test the integrity of the receiver simulation and the validity of the assumptions used in generating the model, more than one type of transmit signal was used to test receiver simulation performance. The use of multiple transmit signal waveforms also provides a broader base from which to draw conclusions regarding the concept of model-based signal processing. For the purpose of this research, two types of transmit waveforms were used in producing the Pd versus array element input SNR plots in each of the three case studies.

A rectangular envelope CW pulse and a rectangular envelope LFM pulse were selected as transmit signals. These two particular forms were chosen for several reasons. First, the CW pulse and LFM pulse waveforms were considered to be typical transmit signals used in SONAR and acoustic signaling systems. Second, the CW pulse provides a simple case of amplitude modulation while the LFM pulse provides an example of an amplitude and angle modulated waveform with considerably different spectral characteristics. Finally, either signal can be readily synthesized from a finite, complex, Fourier series whose coefficients  $c_q$  may be calculated





NATIONAL BUREAU OF STANDARDS  
MICROCOPY RESOLUTION TEST CHART

from a closed form expression for the frequency spectrum of the time domain pulse characteristics.

The rectangular envelope CW pulse is discussed first. The pulse repetition frequency is the same as the fundamental frequency  $f_0$  of the finite frequency spectrum from which the pulse is synthesized. The pulse duty cycle was arbitrarily taken to be 0.5 yielding a pulse width of  $T_0/2$  seconds where  $T_0 = 1/f_0$ . The complex, Fourier series coefficients used to synthesize the complex envelope of the CW pulse are obtained from a closed form expression for the complex-valued continuous spectrum. To obtain the Fourier coefficients, the closed form expression for the continuous spectrum is evaluated at the discrete frequencies  $qf_0$ , and the resulting complex value is divided by the fundamental pulse period  $T_0$ . The index  $q$  takes on integer values between  $-K$  to  $K$  where  $K$  is the maximum number of harmonics in the finite Fourier series used to synthesize the CW pulse. The continuous spectrum of the CW pulse is the familiar  $\sin(x)/x$  form obtained by taking the Fourier transform of the rectangular pulse shape where the pulse width is one-half the pulse period. The following specific transmit signal parameters were used in all CW pulse simulations:

- Amplitude,  $A = 40.0$
- Duty Cycle,  $D = 0.5$
- Fundamental Frequency,  $f_0 = 200 \text{ Hz}$

- Number of harmonics,  $KMAX = 5$
- Harmonic values.
  - $c_0 = 20.00000 \exp[j0^\circ]$
  - $c_{-1} = c_1 = 12.33240 \exp[j0^\circ]$
  - $c_{-2} = c_2 = 0.000000 \exp[j0^\circ]$
  - $c_{-3} = c_3 = 4.244132 \exp[j180^\circ]$
  - $c_{-4} = c_4 = 0.000000 \exp[j0^\circ]$
  - $c_{-5} = c_5 = 2.546479 \exp[j0^\circ]$

The LFM pulse, or linear frequency modulated pulsed carrier waveform, is discussed next. The complex Fourier coefficients used to synthesize the LFM pulse are found using a procedure similar to that used for the CW pulse except the closed form expression for the complex-valued continuous spectrum of the LFM pulse was found by using the method of stationary phase. Officer [Ref. 8:pp. 67-68] describes the method of stationary phase as does Papoulis [Ref. 9:pp. 267-273] who also provides a complete description of the LFM waveform. The following transmit signal parameters are used in all LFM pulse simulations:

- Amplitude,  $A = 40.0$
- Duty Cycle,  $D = 0.8$
- Phase Deviation Constant  $B = 2356.2$  radians/volt
- Fundamental Frequency,  $f_0 = 10$  Hz
- Number of harmonics,  $KMAX = 3$
- Harmonic values,
  - $c_0 = 14.60593 \exp[j45^\circ]$
  - $c_{-1} = c_1 = 14.60593 \exp[j21^\circ]$
  - $c_{-2} = c_2 = 14.60593 \exp[j309^\circ]$
  - $c_{-3} = c_3 = 14.60593 \exp[j189^\circ]$

It should be emphasized that these complex, Fourier series coefficients which are used in the ocean communication channel simulation computer program to synthesize the complex envelope CW and LFM pulse transmit waveforms are also used in subprogram SGNLGN to produce the local processing waveform for the correlator/matched filter detector section of the receiver simulation computer program RCVR.

#### B. CASE TEST

The input signal data for case TEST is obtained from a separate computer program written to synthesize array element output electrical test signals from a finite Fourier series expansion of the test signal waveform. The technique is similar to that used in generating the receiver simulation local processing waveform in subprogram SGNLGN. However, appropriate phase shifts are added to the Fourier coefficients to vary the direction of arrival of the plane wave incident on the receive array, and to incorporate the time delays due to spatial separation,  $d_x$  and  $d_y$ , of the array elements. Furthermore, the time delay due to range and the doppler shift of the test signals are both set to zero to prevent signal loss in the correlator/matched filter due to a mismatch between the total array output signal and the local processing waveform. In this way, array element output electrical signals are obtained that exclude effects due to propagation of the sound wave through the ocean medium, or spatial modulation of the signals due to the

transmit array beam pattern. Since the medium effects are excluded from the case TEST array element signals, the carrier frequency  $f_c$  is set to zero, and the array element spacing is increased to keep the interelement spacing  $d_x$  and  $d_y$  equal to one-half the shortest wavelength in the transmit signal. Note that this produces different interelement spacings for the CW and LFM pulse situations.

Signals generated in this fashion allow the receiver output to be analyzed separately from the communication channel. Essentially, it is equivalent to having a signal generator that provides a test signal to measure receiver performance. The results obtained from case TEST, when combined with the plot of theoretically predicted performance, provides a baseline with which to analyze the receiver output when the ocean communication channel simulation data is processed.

The system parameters defining case TEST are as follows:

- Array Parameters

|                           |                                |
|---------------------------|--------------------------------|
| Number of array elements, | $M = N = 5$                    |
| Array Element Spacing,    | CW $d_x = d_y = 0.7375$ meters |
|                           | LFM $d_x = d_y = 24.58$ meters |

- Medium Parameters

|                      |                            |
|----------------------|----------------------------|
| Speed of Sound,      | $c_o = 1475$ meters/second |
| Actual time delay    | $\tau_A = 0.0$ seconds     |
| Actual doppler shift | $\phi_A = 0.0$ Hertz       |

Four plots representing receiver performance were generated for case TEST. Phase weighting is done to



compensate for the direction of arrival of an acoustic plane wave incident upon the array elements. The direction of arrival can be set to any arbitrary direction by the test signal generator computer program. However, the direction was chosen to be the same as that due to the system geometry used in the case studies HMG1 and INHMG1. Phase weighting for geometry is indicated by the state of the logical variable STEER. The estimates of time delay due to range and doppler shift were both set to zero in subprogram SGNLGN to maximize the output of the correlator/matched filter detector. Two of the plots, Figures 25 and 26, show receiver performance for a rectangular envelope CW pulse. Figure 25 was produced using a Pfa of 0.1, and Figure 26 shows the effect of a Pfa of 0.01. The remaining two plots generated for case TEST, Figures 27 and 28, show receiver performance for a rectangular envelope LFM pulse at a Pfa of 0.1 and 0.01, respectively. Since the input electrical signal data does not incorporate channel effects, phase weighting for deterministic and random medium effects was not done for case TEST.

Several observations regarding model performance can be made by analyzing the plots. Generally for all plots, the measured performance of the simulation (solid curve) follows the predicted theoretical performance (dashed curve), but the agreement is not exact. That is, the estimate of  $P_d$  follows the same trend as the predicted  $P_d$ , but the

SIMULATED RECEIVER PERFORMANCE  
AS A FUNCTION OF  
SNR AT A SINGLE ARRAY ELEMENT

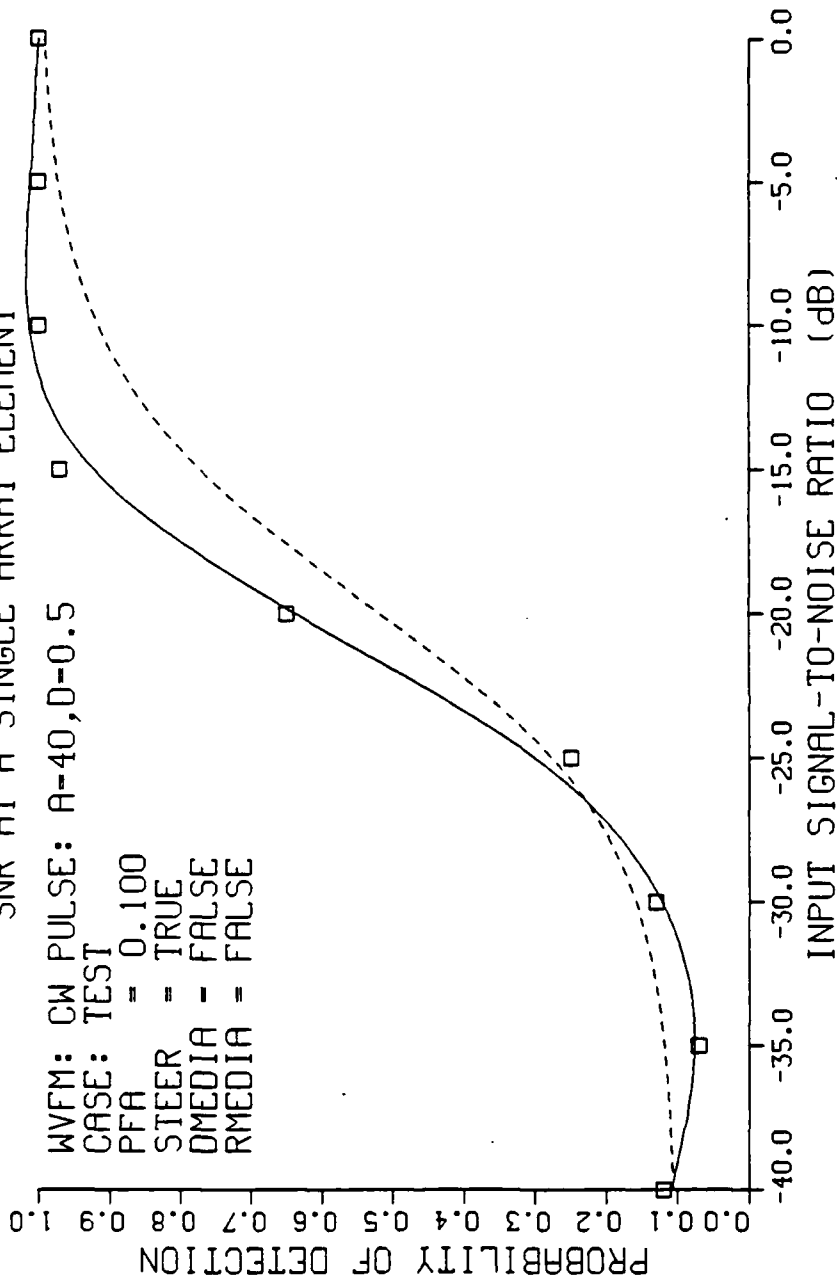


Figure 25. Receiver Performance for case TEST, CW Pulse,  
Pfa = 0.1, Geometry Phase Weighting

SIMULATED RECEIVER PERFORMANCE  
 AS A FUNCTION OF  
 SNR AT A SINGLE ARRAY ELEMENT

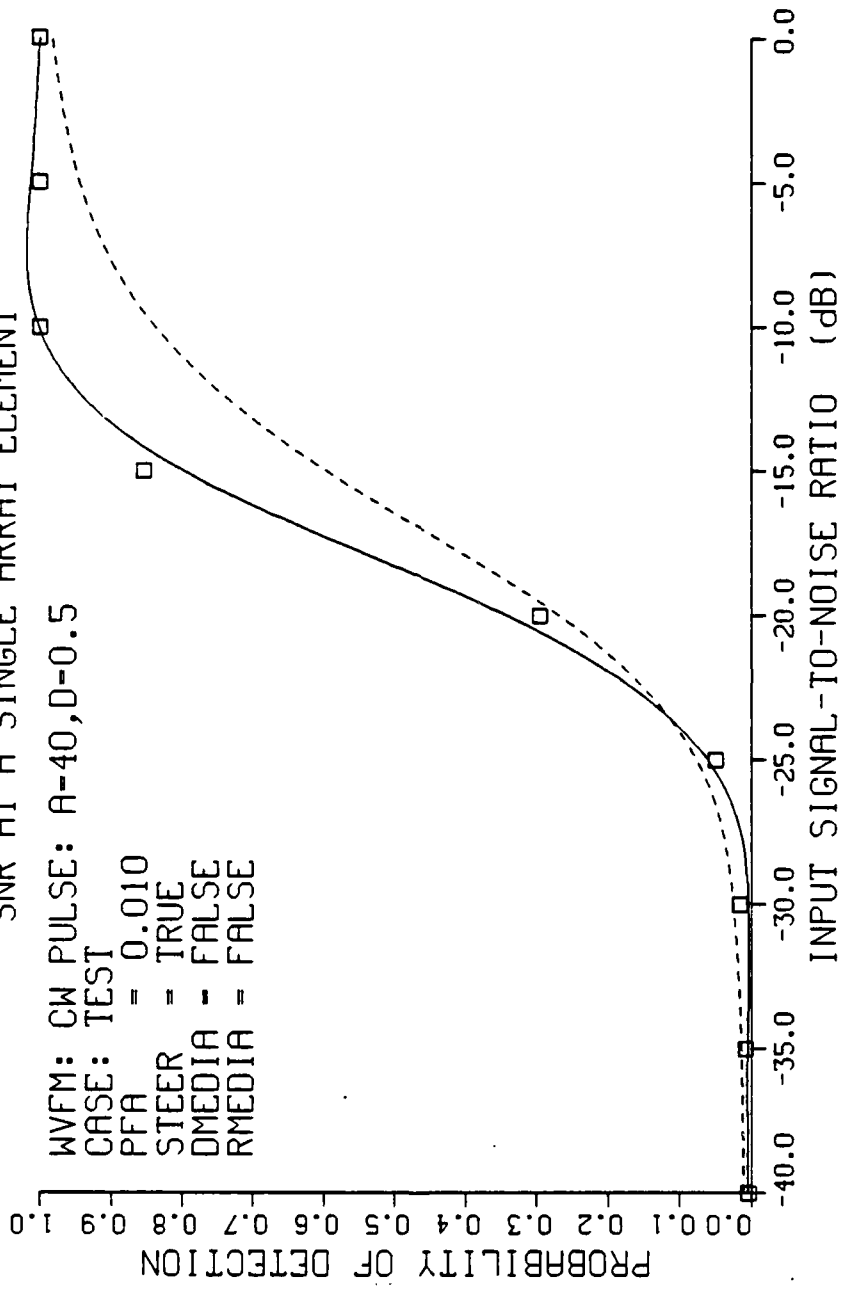


Figure 26. Receiver Performance for case TEST, CW Pulse,  
 Pfa = 0.01, Geometry Phase Weighting

SIMULATED RECEIVER PERFORMANCE  
AS A FUNCTION OF  
SNR AT A SINGLE ARRAY ELEMENT

WVFM: LFM PULSE: A-40, D-0.8, B-2356.2  
CASE: TEST  
PFA = 0.100  
STEER = TRUE  
OMEDIA = FALSE  
RMEDIA = FALSE

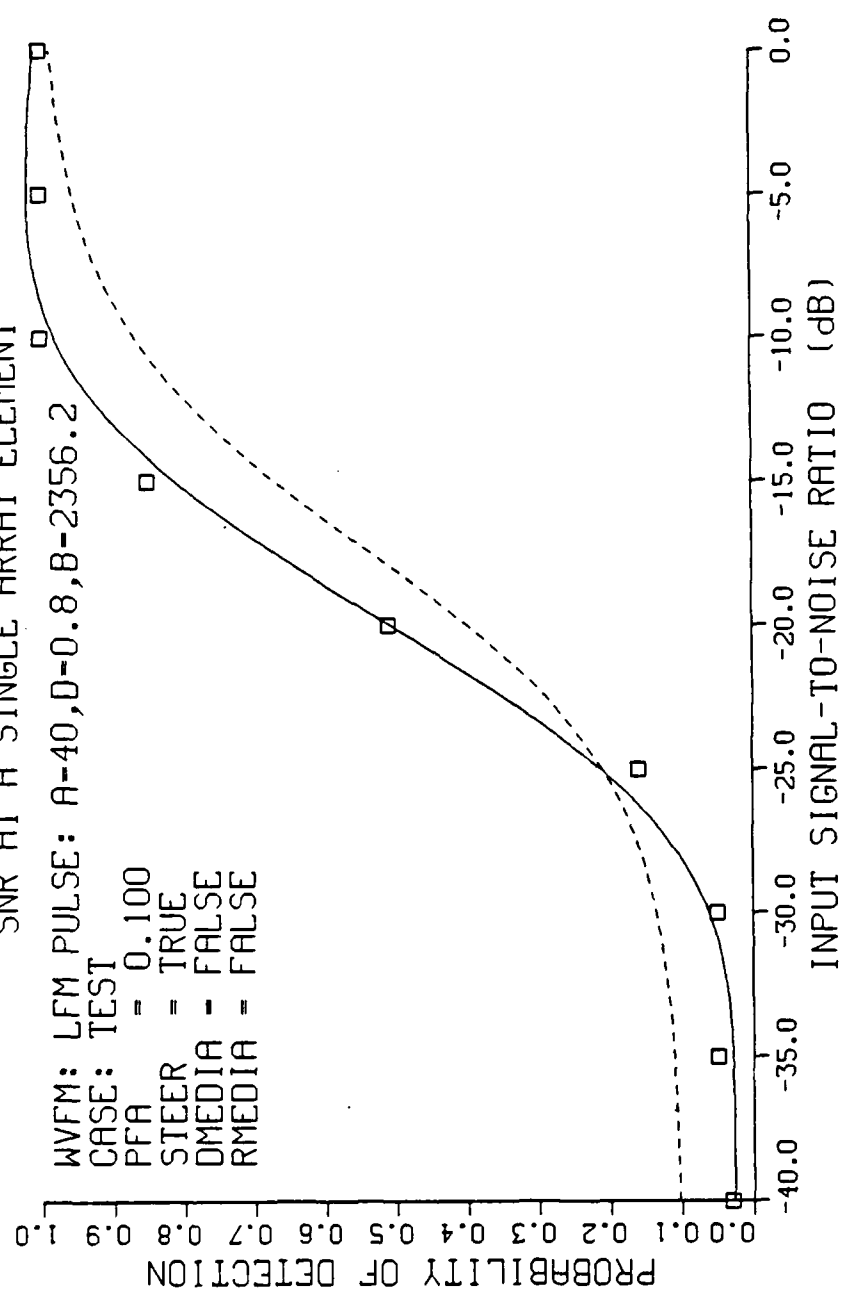


Figure 27. Receiver Performance for case TEST, LFM Pulse,  
Pfa = 0.1, Geometry Phase Weighting

SIMULATED RECEIVER PERFORMANCE  
AS A FUNCTION OF  
SNR AT A SINGLE ARRAY ELEMENT

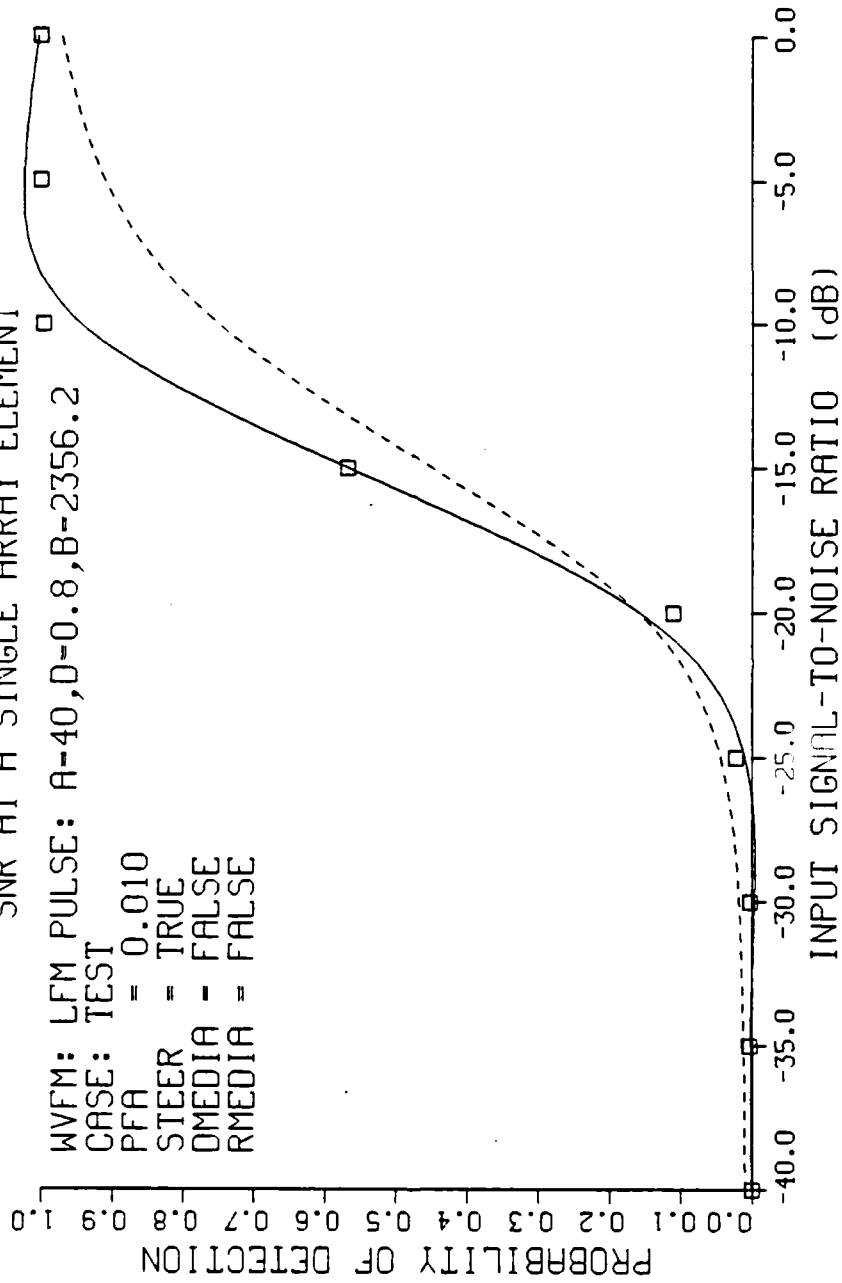


Figure 28. Receiver Performance for case TEST, LFM Pulse,  
Pfa = 0.01, Geometry Phase Weighting

transition from a low  $P_d$  to a  $P_d$  of 1 is more sensitive to changes in the array element input SNR. A comparison between the plots shows the  $P_d$  to be a function of the  $P_{fa}$  as predicted by equation (2.82), and for small values of SNR, the estimated  $P_d$  approaches the  $P_{fa}$  parameter used by the simulation in generating the plots. This effect is also predicted by equation (2.82) since at SNR values much less than one, the input signal is essentially off, and only the noise is producing signal detections. A comparison between the plots for the CW pulse and LFM pulse does show some minor difference in receiver performance, but the same general trends seem to hold regardless of the functional form of the transmit signal.

The differences in the measured performance between the CW pulse and the LFM pulse simulations can be attributed in part to the difference in the maximum number of harmonics used to synthesize the transmit signals. As shown by equation (2.22), the number of time samples  $L$  is related to the maximum number of harmonics  $K$  used to synthesize the transmit signal. The difference in the number of time samples causes different subsequences of noise samples to be drawn from the noise generator subprogram AWGN. The different noise sample subsequences will cause small variations in the relative frequency estimate of  $P_d$ . Thus, an exact comparison of the noise performance cannot be made across different types of transmit signals when the number

of harmonics used to create the transmit signal are not the same. However, the real significance of this effect is that even with different noise sample subsequences in the I and Q receiver channels at the array elements, the measured performance conforms closely to the performance predicted by theory under the very ideal assumptions of precise signal cophasing, and zero-mean, white, Gaussian input noise.

For these reasons, it can be inferred that the basic receiver model is valid, but some difficulty may exist in generating precisely white, zero-mean, Gaussian noise within the simulation program. Indeed as indicated in Section III.B.1, the noise source used in the receiver simulation does not generate precisely zero-mean, white, Gaussian noise. Furthermore, the measured  $P_d$  is a relative frequency estimate of the actual receiver performance, and may also contribute some error in the simulation results.

Considering these approximations to the assumptions used in the receiver model development of Section II, exact agreement should not be expected even in the case where the communication channel effects are excluded. However if only relative changes or effects are to be observed, moderate disagreement between the theory and simulated receiver performance can be negated by comparing only differences in the estimate of  $P_d$  for each of the case studies. A comparison of the differences in the measured receiver performance will indicate if, and to what degree, the effects due

to the physics of acoustic wave propagation can be compensated for by model-based signal processing. The results of case TEST then can be viewed as a validation of the receiver model and the applied programming used to implement the model.

### C. CASE HMGL

The input signal data for case HMGL and case INHMGL is produced by the ocean communication channel simulation program due to Vos and Ziomek [Ref. 3]. For case HMGL, the ocean is considered to be a homogeneous medium with respect to the speed of sound propagation through the water. That is, the speed of sound is identical at the transmit and receive arrays, and at all points inbetween. In this model of the ocean medium, refraction or ray bending of the sound wave does not occur. Thus, only phase weighting for geometry is required, and only those results will be presented. The homogeneous case provides a needed baseline with which to judge the effects of model-based signal processing when inhomogeneous case data is studied.

Since case HMGL includes the effects of the ocean communication channel, a carrier frequency is used to convey the modulation through the channel. In case HMGL and case INHMGL the carrier frequency was set to 5.0 kHz. The array interelement spacing was adjusted accordingly to maintain the one-half wavelength spacing needed to prevent grating



lobes in the array beam patterns. Note that the interelement spacing was set using the highest frequency expected for either the CW pulse or the LFM pulse waveforms, and was kept constant for both the HMGL and INHMGL case studies. The highest frequency occurred for the CW pulse case, and was equal to 6000 Hz. The estimates of the time delay and Doppler shift in subprogram SGNLGN were set equal to the actual values to maximize the correlator output.

The system parameters defining case HMGL are as follows:

- Array Parameters

|                           |                             |
|---------------------------|-----------------------------|
| Number of array elements, | $M = N = 5$                 |
| Array Element Spacing,    | $d_x = d_y = 0.1229$ meters |

- Medium Parameters

|                                 |                             |
|---------------------------------|-----------------------------|
| Speed of Sound,                 | $c_o = 1475$ meters/second  |
| Actual line of sight time delay | $\tau_A = 2.033898$ seconds |
| Actual Doppler shift            | $\phi_A = 0.0$ Hertz        |

- System Geometry (See Figure 1)

|                         |                             |
|-------------------------|-----------------------------|
| Depth of Transmit Array | $y_o = 1000.0$ meters       |
| Depth of Receive Array  | $y_r = 2500.0$ meters       |
| Cross Range             | $x_r - x_o = 500.0$ meters  |
| Line of sight range     | $ r - r_o  = 3000.0$ meters |

Eight plots were generated for case HMGL. The first four plots, Figures 29 through 32, were produced using the rectangular envelope CW pulse transmit signal. The remaining four plots, Figures 33 through 36 were produced by the rectangular envelope LFM pulse transmit signal. Figures

SIMULATED RECEIVER PERFORMANCE  
AS A FUNCTION OF  
SNR AT A SINGLE ARRAY ELEMENT

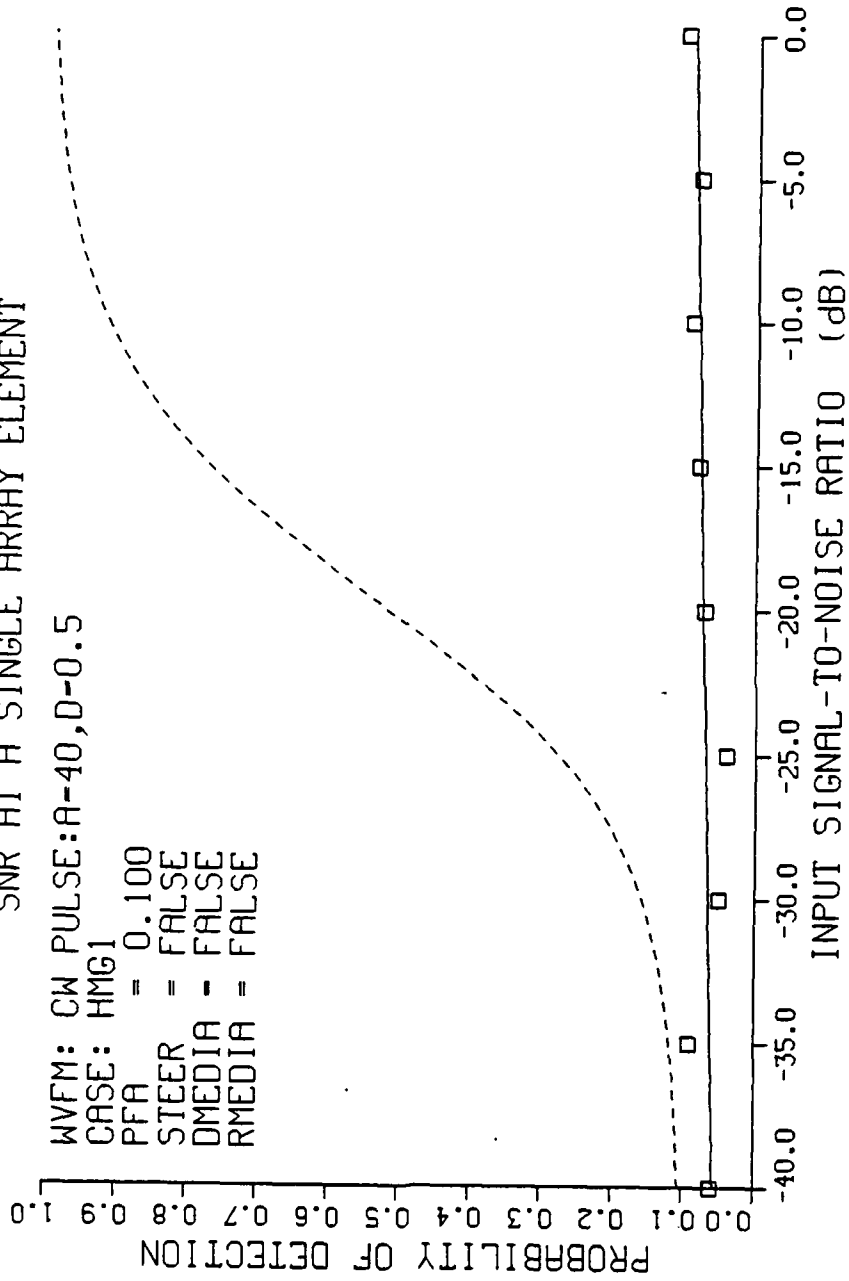


Figure 29. Receiver Performance for case HMG1, CW Pulse,  
Pfa = 0.01, No Phase Weighting

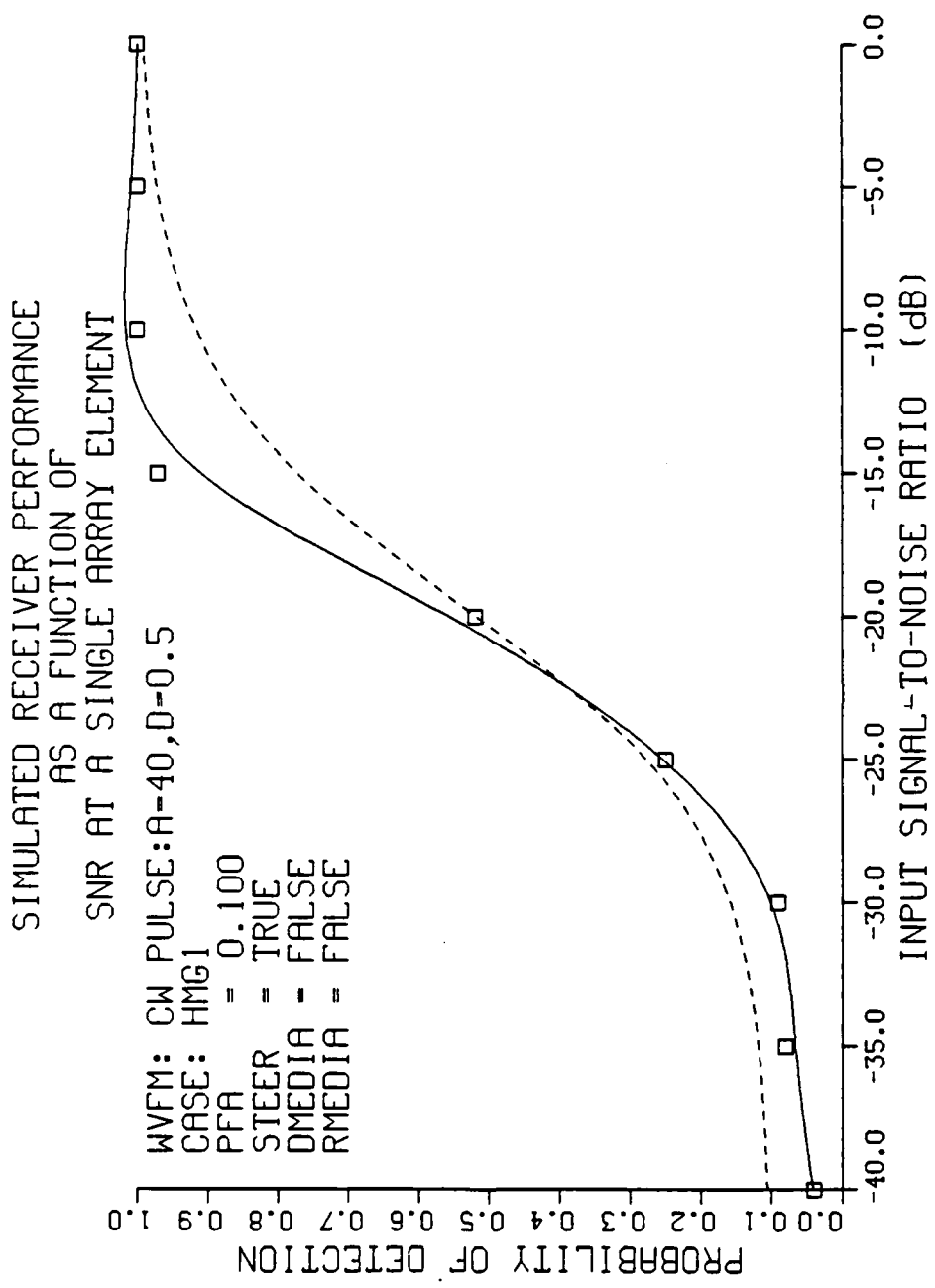


Figure 30. Receiver Performance for case HMG1, CW Pulse, Pfa = 0.1, Geometry Phase Weighting

SIMULATED RECEIVER PERFORMANCE  
 AS A FUNCTION OF  
 SNR AT A SINGLE ARRAY ELEMENT

WVFM: CW PULSE:A-40,D-0.5  
 CASE: HMG1  
 PFA = 0.010  
 STEER = FALSE  
 DMEDIA = FALSE  
 RMEDIA = FALSE

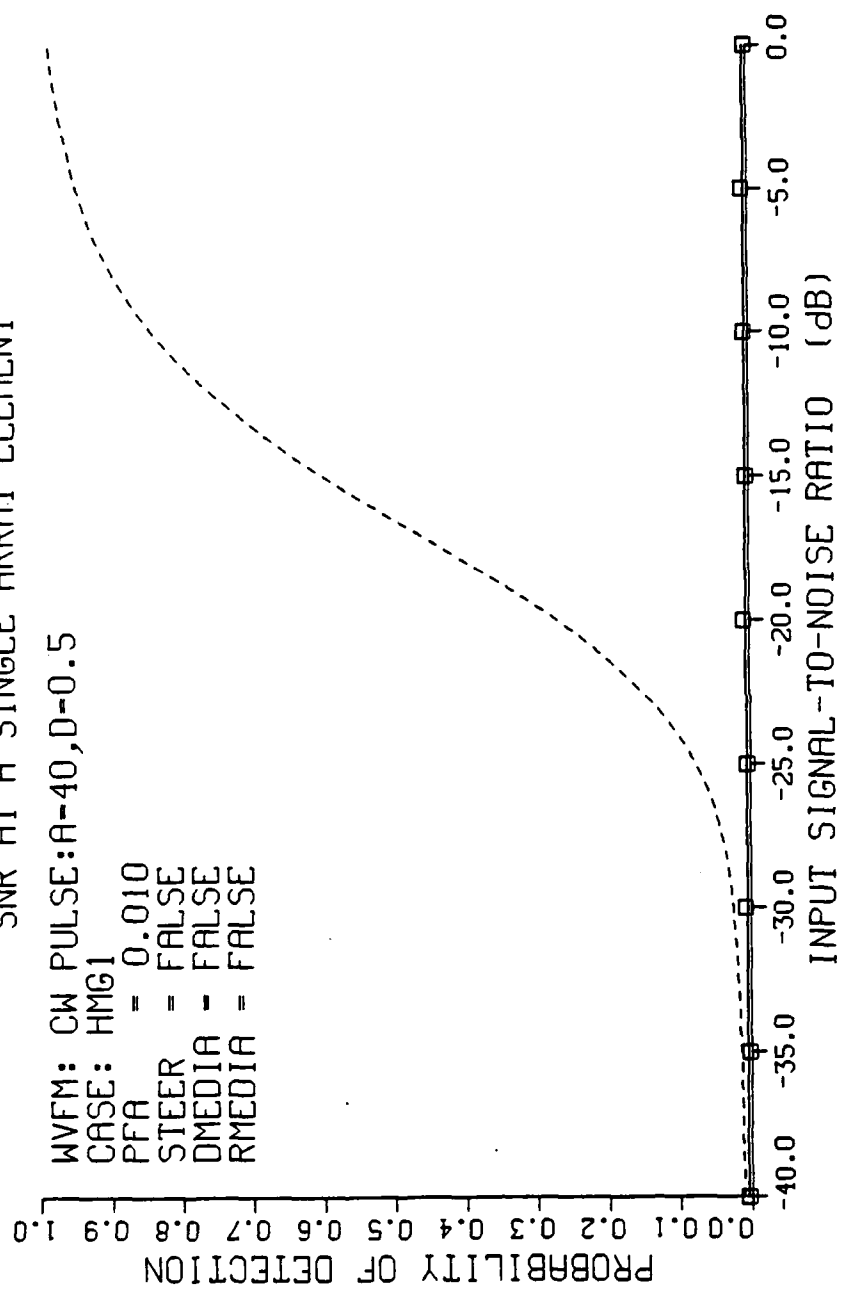


Figure 31. Receiver Performance for case HMG1, CW Pulse, Pfa = 0.01, No Phase Weighting

SIMULATED RECEIVER PERFORMANCE  
AS A FUNCTION OF  
SNR AT A SINGLE ARRAY ELEMENT

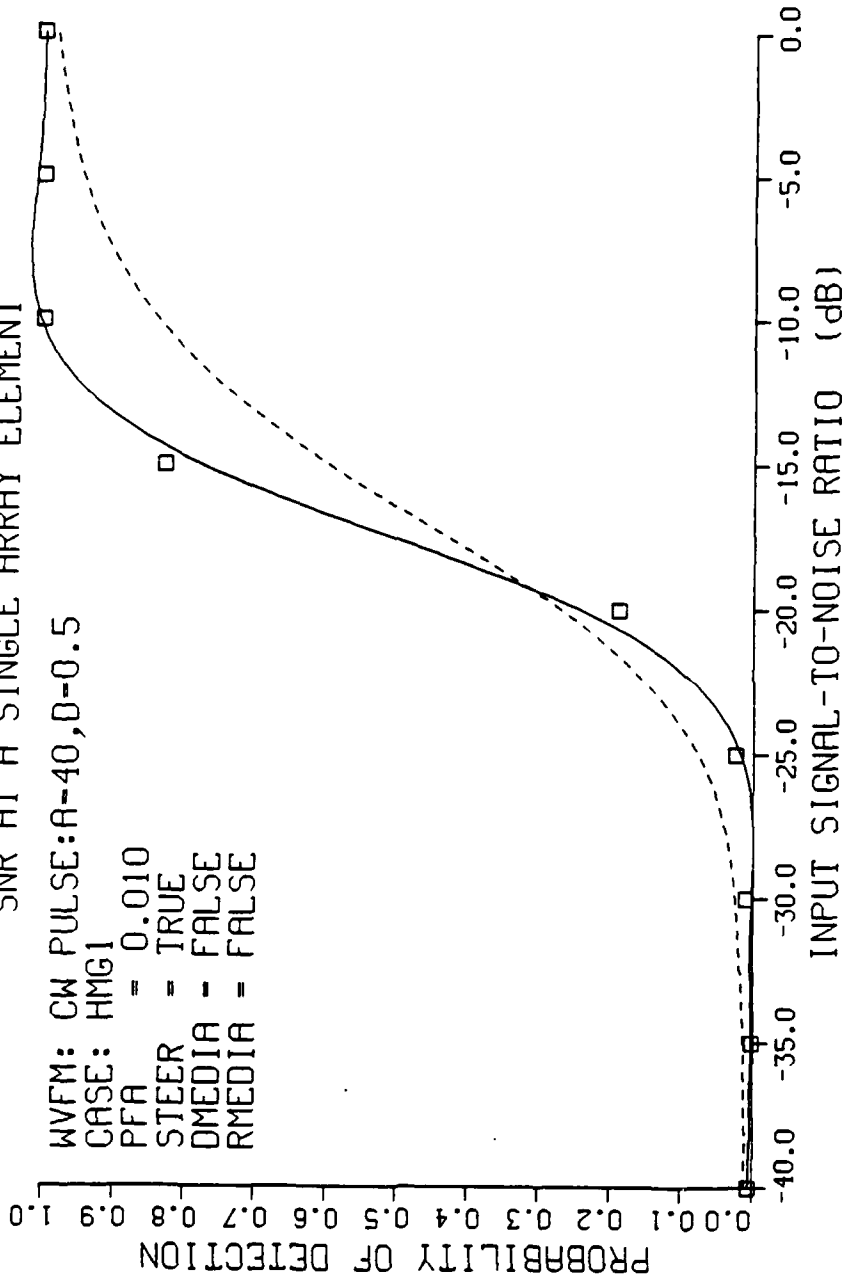


Figure 32. Receiver Performance for case HMG1, CW Pulse, Pfa = 0.01, Geometry Phase Weighting

SIMULATED RECEIVER PERFORMANCE  
AS A FUNCTION OF  
SNR AT A SINGLE ARRAY ELEMENT

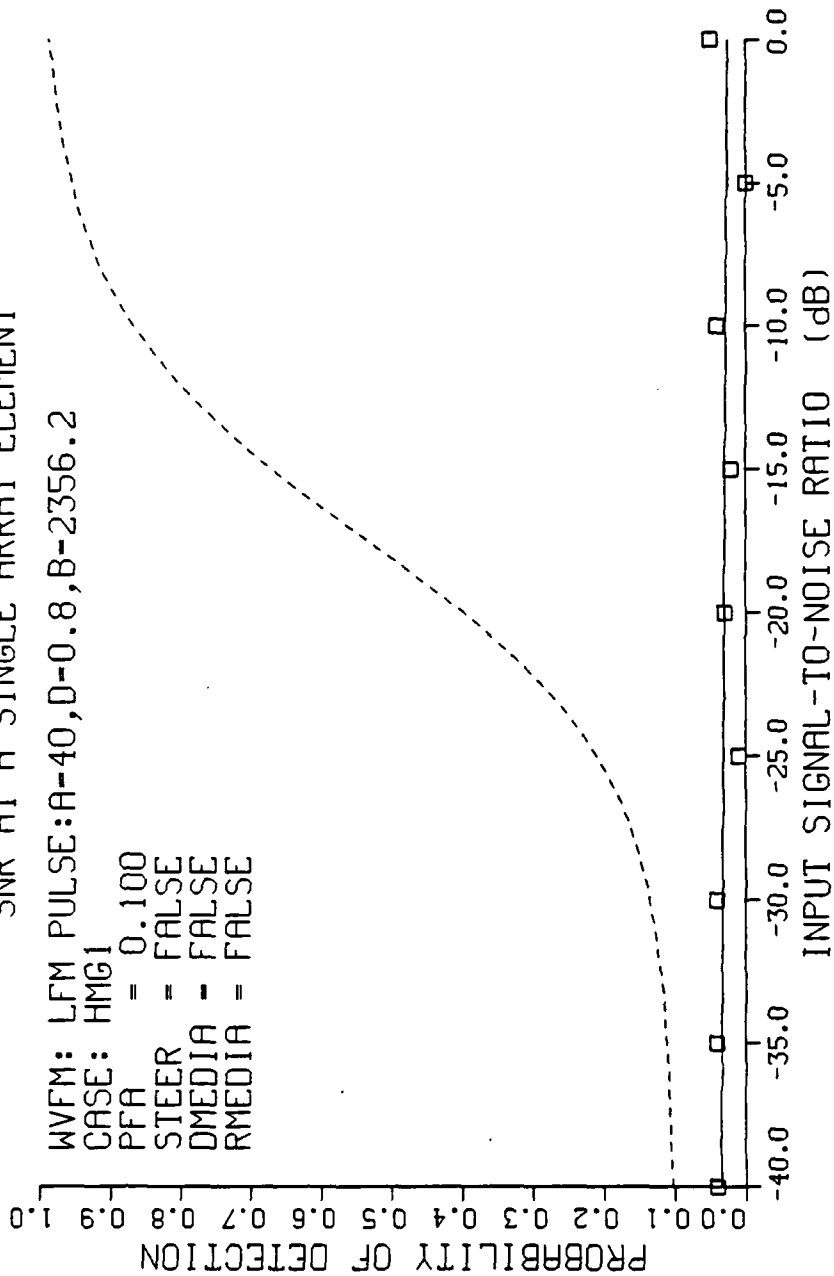


Figure 33. Receiver Performance for case HMGL, LFM Pulse,  
Pfa = 0.1, No Phase Weighting

SIMULATED RECEIVER PERFORMANCE  
AS A FUNCTION OF  
SNR AT A SINGLE ARRAY ELEMENT

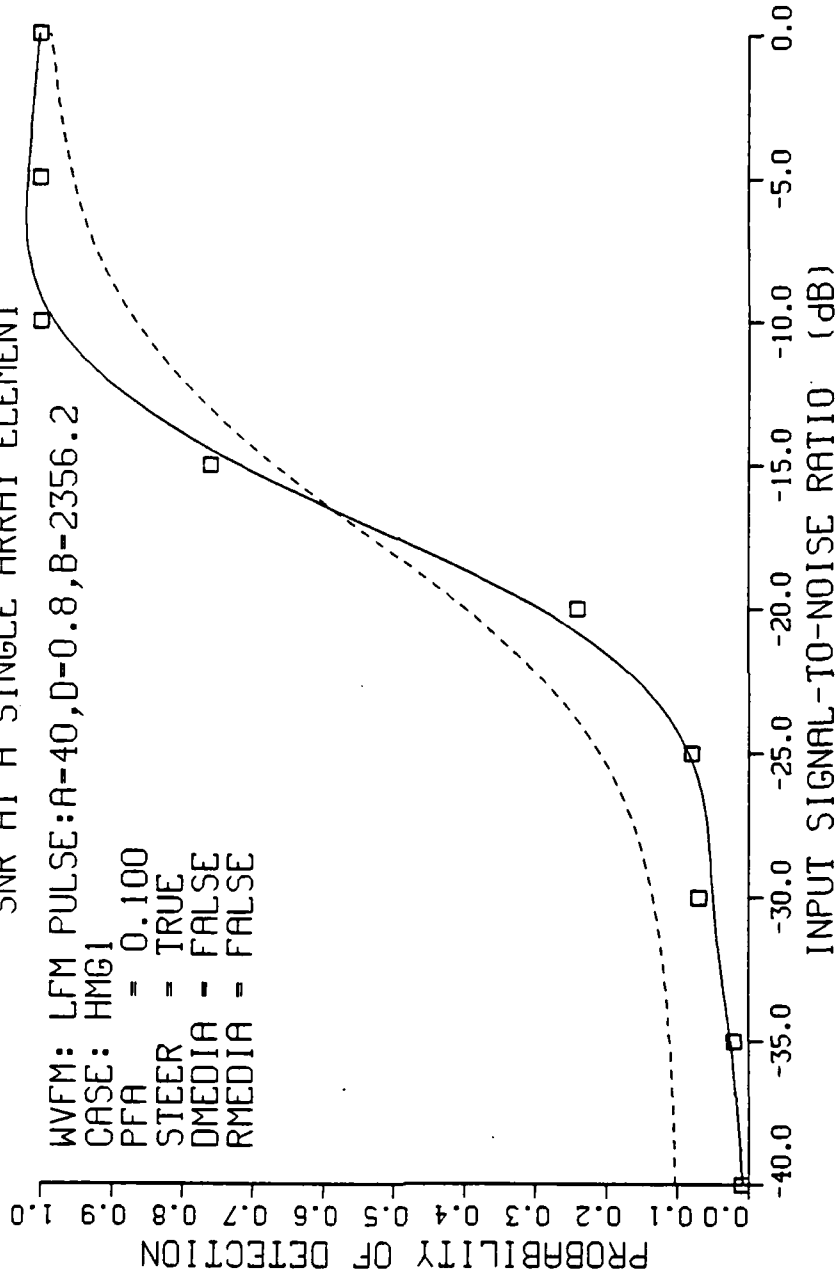


Figure 34. Receiver Performance for case HMG1, LFM Pulse,  
Pfa = 0.1, Geometry Phase Weighting

SIMULATED RECEIVER PERFORMANCE  
 AS A FUNCTION OF  
 SNR AT A SINGLE ARRAY ELEMENT

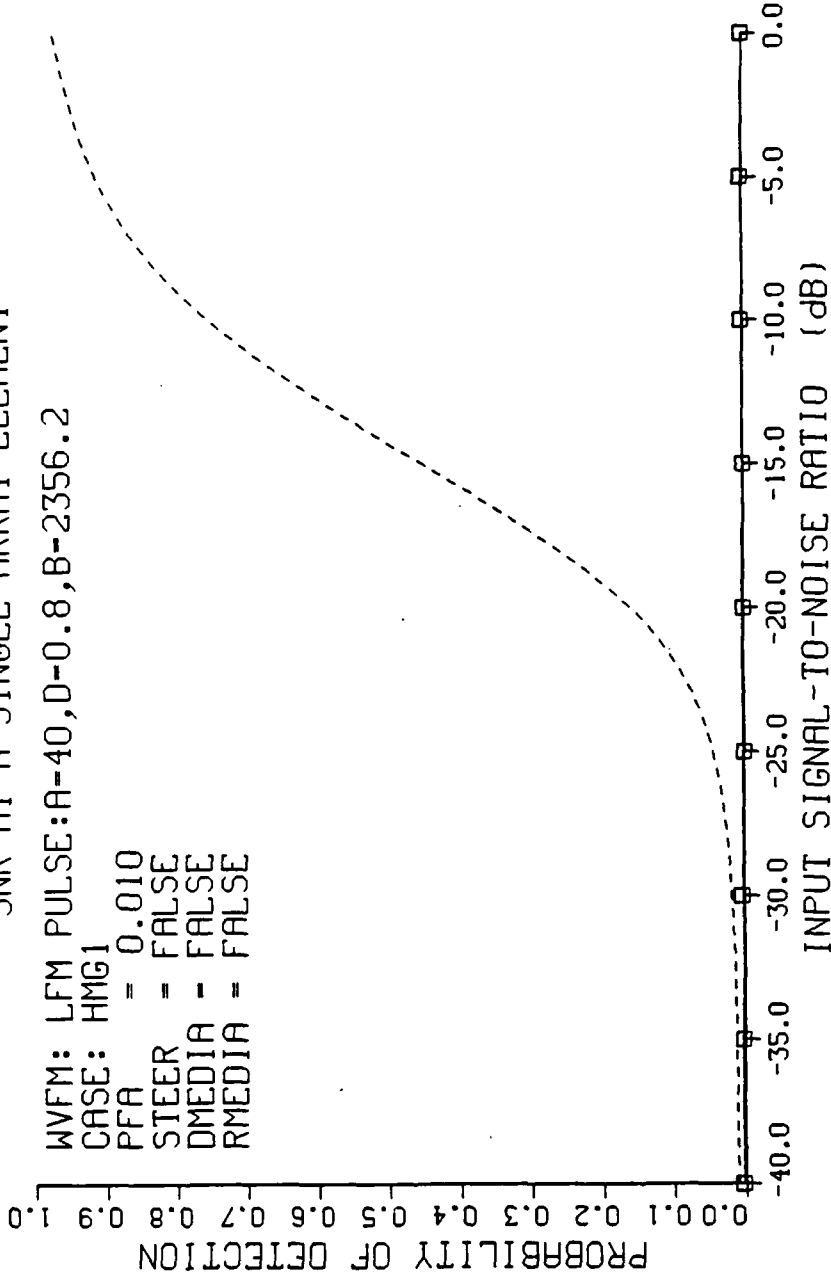


Figure 35. Receiver Performance for case HMG1, LFM Pulse,  
 Pfa = 0.01, No Phase Weighting



SIMULATED RECEIVER PERFORMANCE  
AS A FUNCTION OF  
SNR AT A SINGLE ARRAY ELEMENT

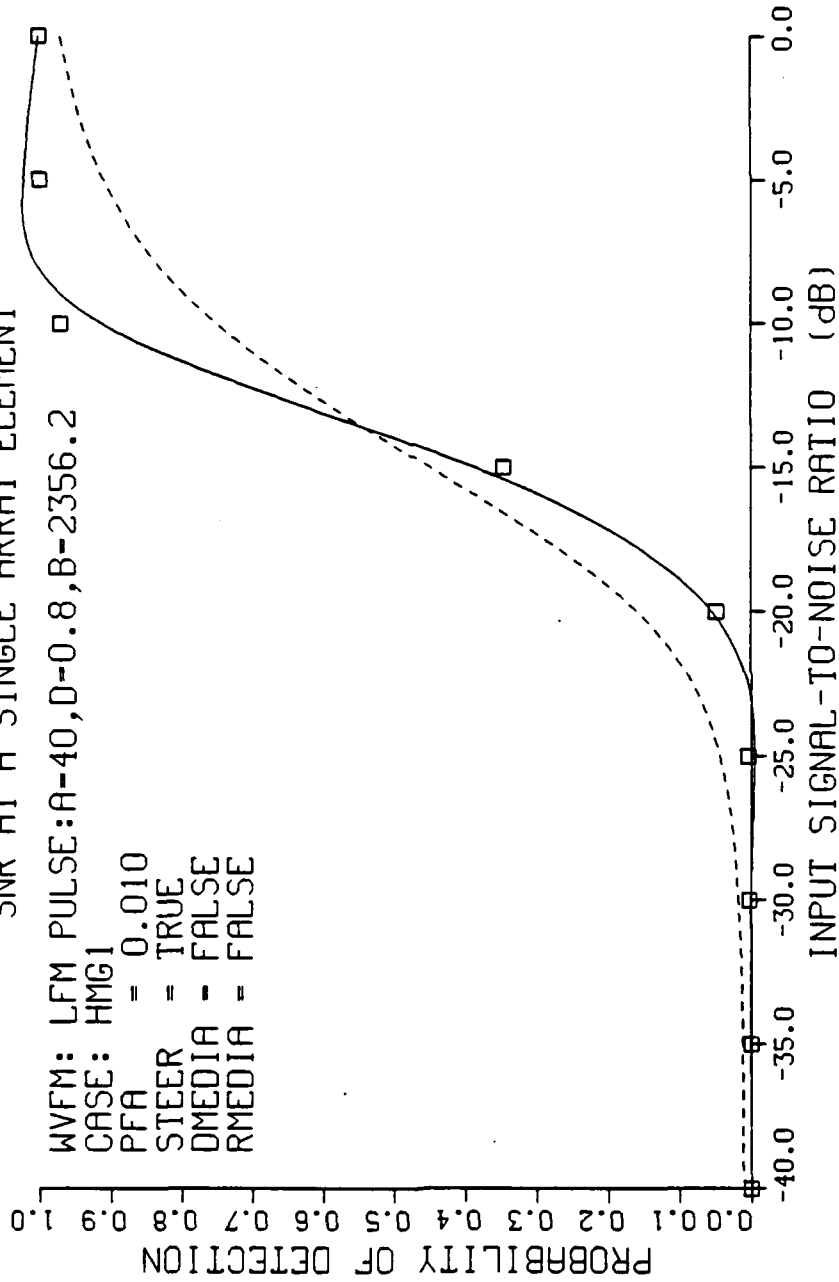


Figure 36. Receiver Performance for case HMG1, LFM Pulse,  
Pfa = 0.01, Geometry Phase Weighting

29, 31, 33 and 35 show receiver performance when no phase weighting is done. These plots indicate that performance will be very poor when the output signals from the array elements are not cophased. Again, it is significant that the Pd in this case is approximately equal to the value of the Pfa parameter used in obtaining the plot. That is, the total array output signal must be very small because of destructive interference of the array element signals, and the only detections appear to be due to the noise.

Figures 30, 32, 34 and 36 show performance when phase weighting is done to compensate for system geometry. These plots indicate receiver performance can be made to approximate the theoretical predicted performance if the individual array element signals can be cophased to provide constructive interference at the output of the array processor.

Figures 29, 30, 33 and 34 show receiver performance at a Pfa of 0.1. Figures 31, 32, 35 and 36 show the effect of decreasing the Pfa to 0.01. The effect of decreasing the Pfa on the simulated performance follows the theoretically predicted performance and provides further confirmation that the computer implementation of the model is accurate.

The important conclusion from case HMGI is dramatic improvement in receiver performance is possible provided that enough information about system geometry exists to generate phase weights that will properly cophase the array element output signals.

#### D. CASE INHMGL

The input signal data for case INHMGL is produced in the same manner as case HMGL. The transmit signal waveforms, system geometry, and transmit and receive arrays are identical. The only difference between the two cases is the model of the ocean medium. For case INHMGL, the ocean is considered to be an inhomogeneous medium with respect to the speed of sound propagation through the water. The speed of sound is assumed to vary linearly with depth (or y-coordinate) only. That is, the speed of sound is not identical at the transmit and receive arrays. In this space-variant model of the ocean medium, refraction or ray bending of the sound wave does occur, and the model of the ocean medium due to Ziomek [Ref. 2] predicts what the phase shifts in array element output electrical signals will be. Using this knowledge of the physics of acoustic wave propagation, phase weights are generated that attempt to compensate for the refraction of the acoustic wave along the ray path, and the system geometry. To determine the effect of this model-based signal processing algorithm, the inhomogeneous data was also processed using phase weights that compensate just for system geometry. The difference in simulated receiver performance between these two situations will graphically show the effectiveness of the model-based signal processing approach.

The system parameters defining case INHMGL are as follows:

- Array Parameters

Number of array elements,  $M = N = 5$   
Array Element Spacing,  $d_x = d_y = 0.1229$  meters

- Medium Parameters

Speed of Sound,  $c_o = 1475$  meters/second  
Gradient  $g = .017$

Actual line of sight  
time delay  $\tau_A = 2.033898$  seconds

Actual Doppler shift  $\phi_A = 0.0$  Hertz

- System Geometry (See Figure 1)

Depth of Transmit Array  $y_o = 1000.0$  meters

Depth of Receiver Array  $y_r = 2500.0$  meters

Cross Range  $x_r - x_o = 500.0$  meters

Line of sight range  $|r - r_o| = 3000.0$  meters

Twelve plots were generated for case INHMGl. The first six plots, Figures 37 through 42 show receiver performance for a rectangular envelope CW pulse. The remaining six plots, Figures 43 through 48, are the result of a rectangular envelope LFM pulse transmit signal. Differences in receiver performance due to the form of the transmit signal are measurable, but not significant.

Figures 37, 40, 43 and 46 were generated when no phase weighting is applied to the array output electrical signals. Again, these figures indicate that the array element output electrical signals must be cophased to provide any useful detection capability in the receiver.

SIMULATED RECEIVER PERFORMANCE  
AS A FUNCTION OF  
SNR AT A SINGLE ARRAY ELEMENT

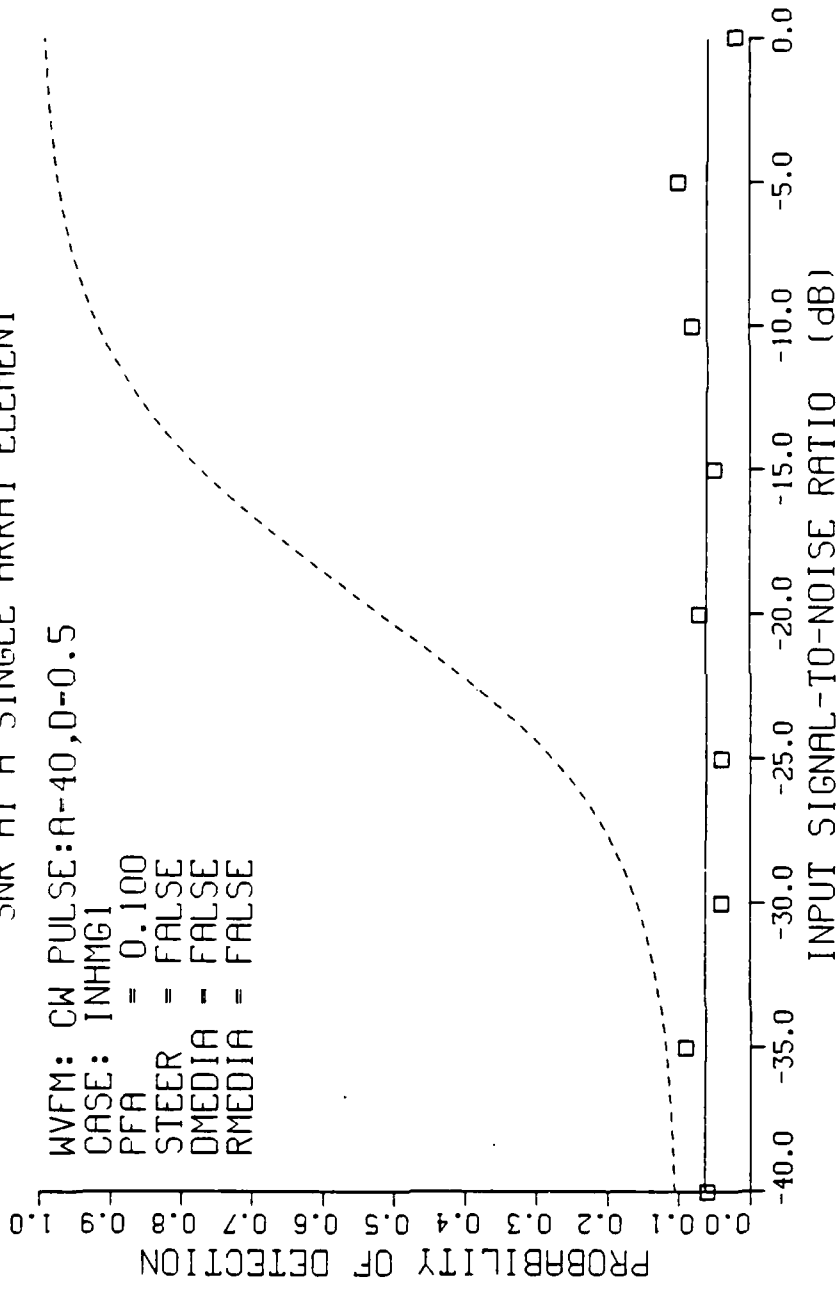


Figure 37. Receiver Performance for case INHMG1, CW Pulse,  
Pfa = 0.1, No Phase Weighting

SIMULATED RECEIVER PERFORMANCE  
 AS A FUNCTION OF  
 SNR AT A SINGLE ARRAY ELEMENT

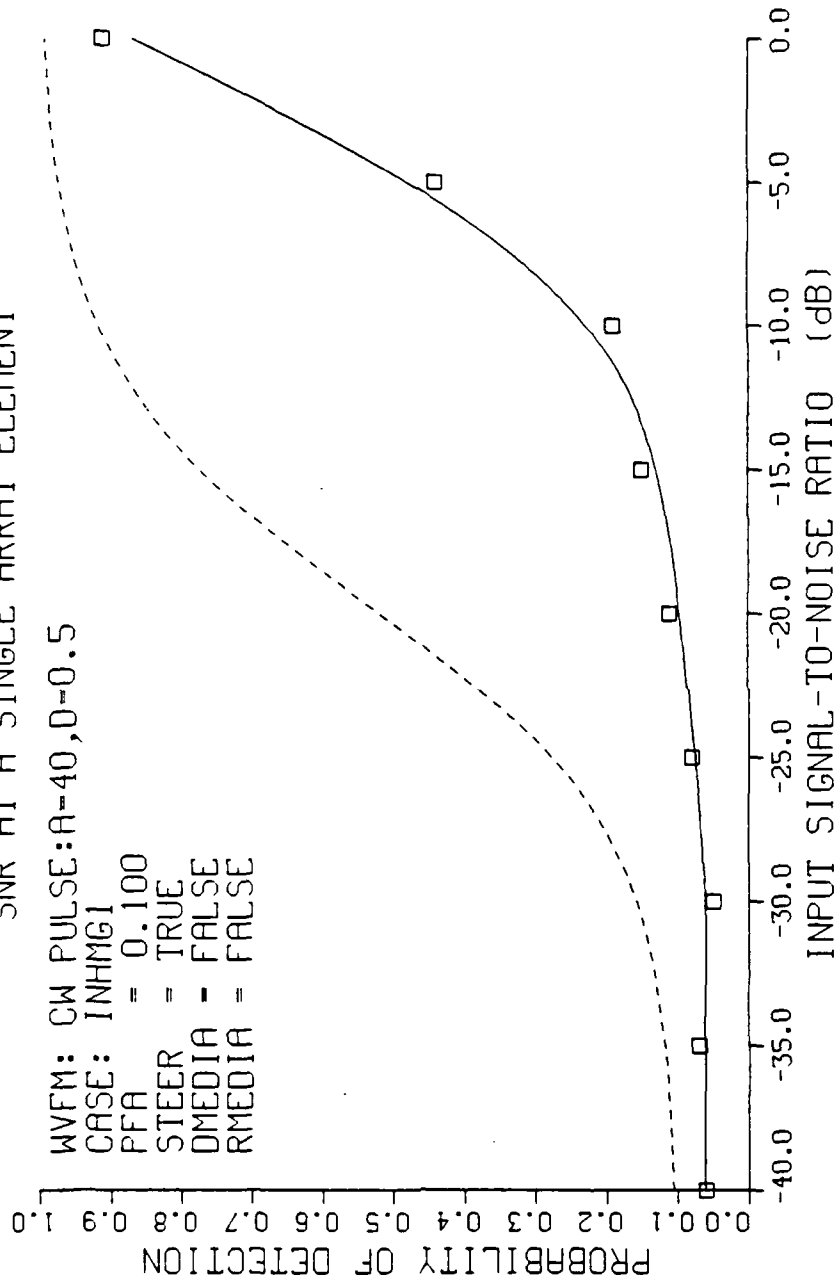


Figure 38. Receiver Performance for case INHMG1, CW Pulse, Pfa = 0.1, Geometry Phase Weighting

SIMULATED RECEIVER PERFORMANCE  
AS A FUNCTION OF  
SNR AT A SINGLE ARRAY ELEMENT

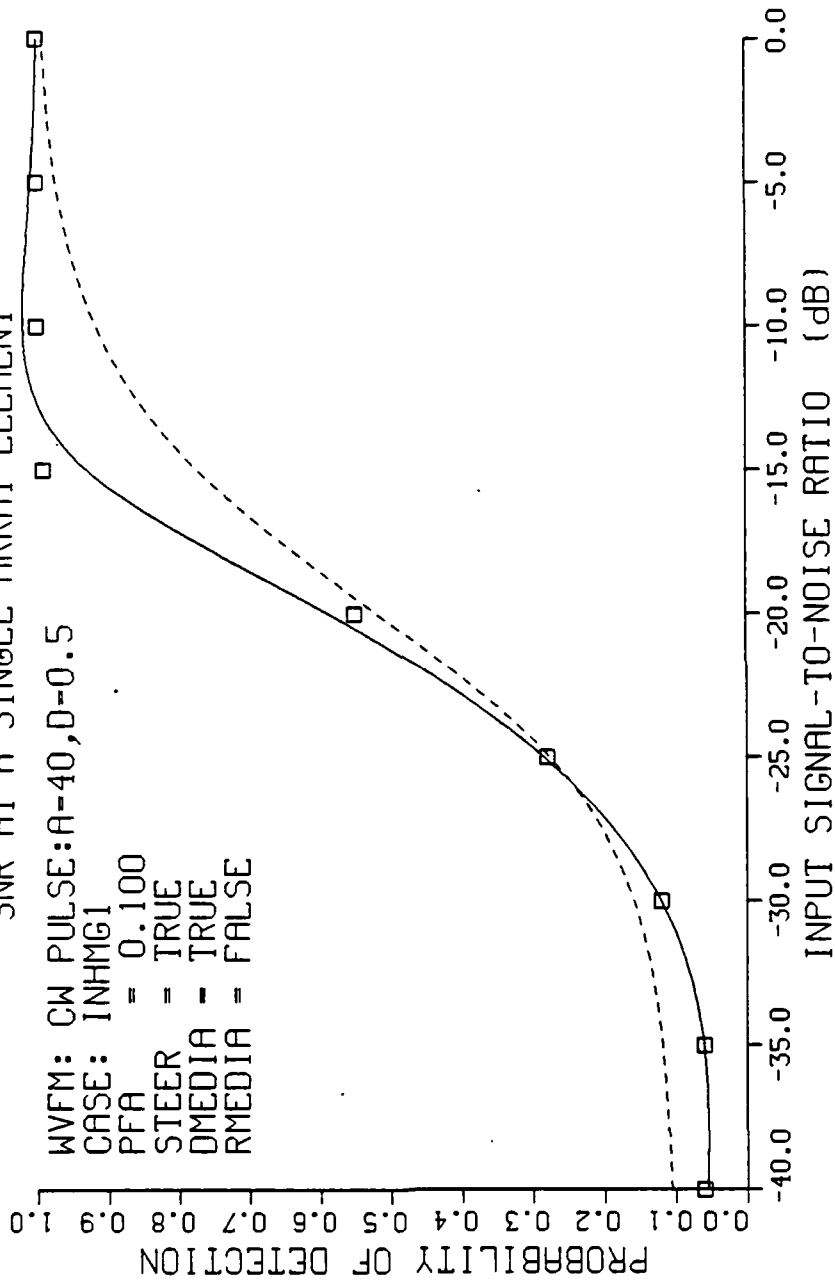


Figure 39. Receiver Performance for case INHMGI, CW Pulse,  
Pfa = 0.1, Medium Phase Weighting

SIMULATED RECEIVER PERFORMANCE  
AS A FUNCTION OF  
SNR AT A SINGLE ARRAY ELEMENT

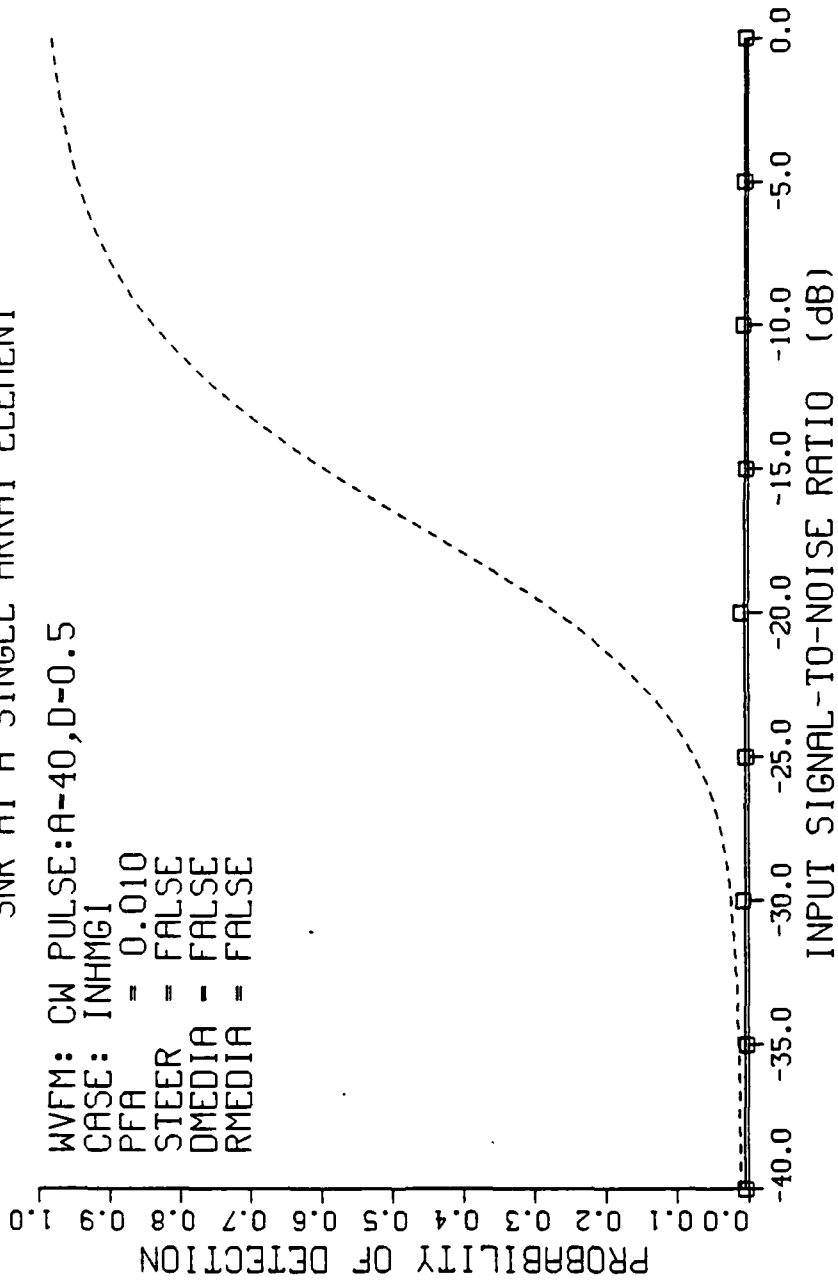


Figure 40. Receiver Performance for case INHMG1, CW Pulse,  
Pfa = 0.01, No Phase Weighting



SIMULATED RECEIVER PERFORMANCE  
AS A FUNCTION OF  
SNR AT A SINGLE ARRAY ELEMENT

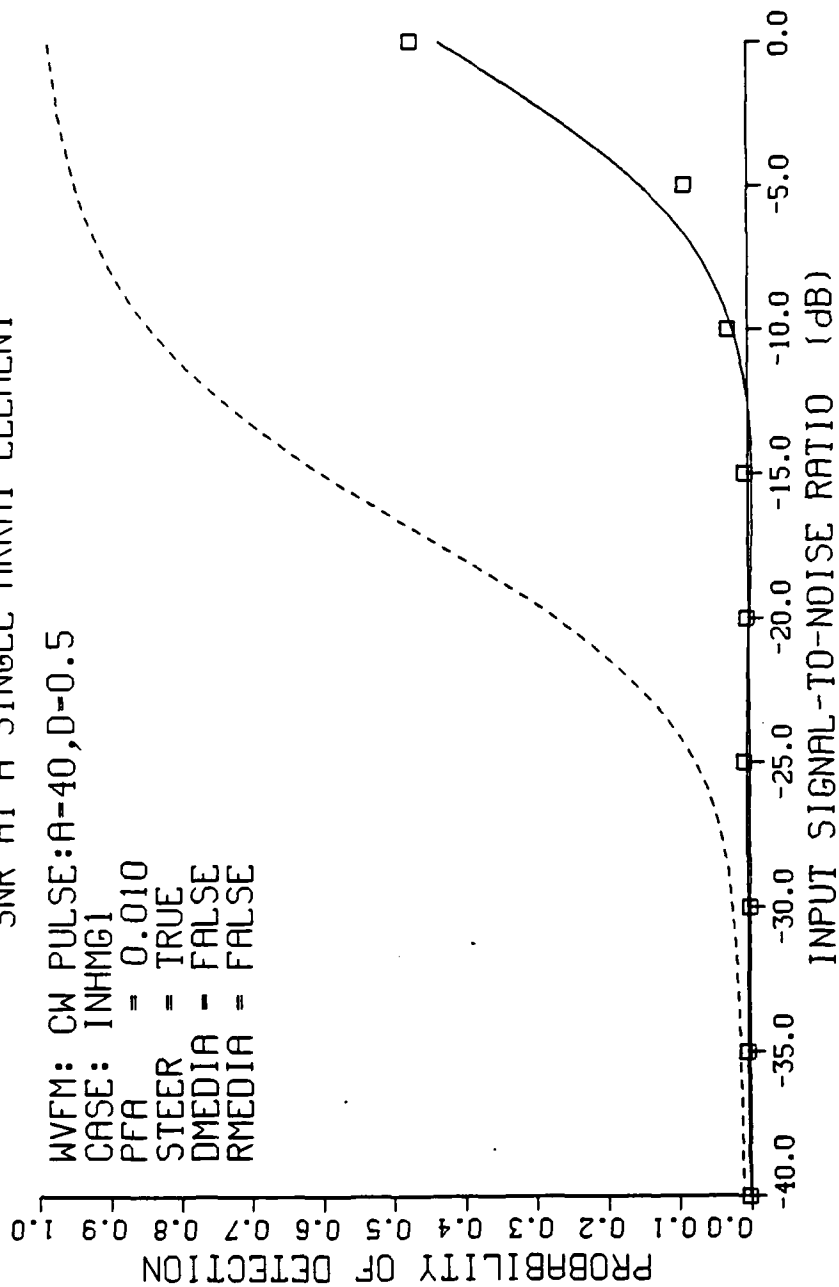


Figure 41. Receiver Performance for case INHMGI, CW Pulse,  
Pfa = 0.01, Geometry Phase Weighting

SIMULATED RECEIVER PERFORMANCE  
AS A FUNCTION OF  
SNR AT A SINGLE ARRAY ELEMENT

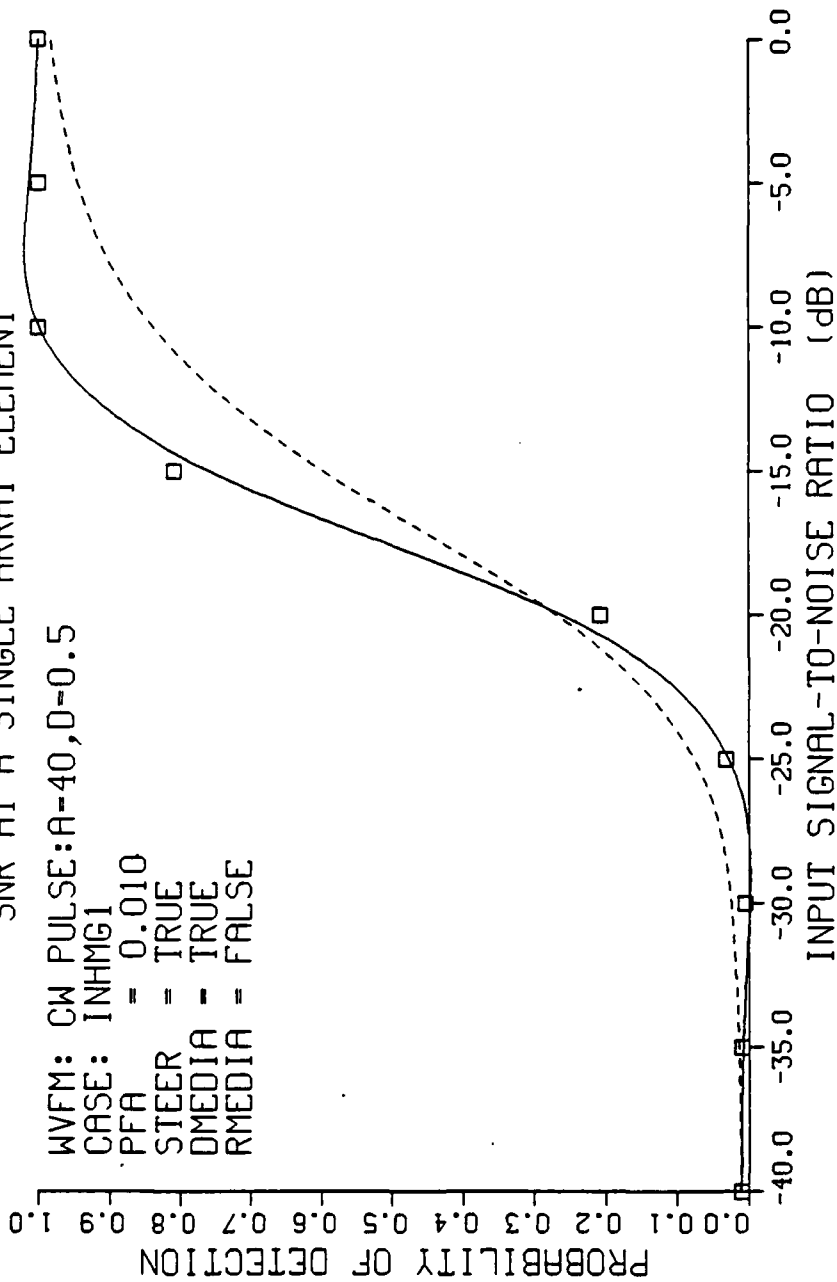


Figure 42. Receiver Performance for case INHMG1, CW Pulse, Pfa = 0.01, Medium Phase Weighting

SIMULATED RECEIVER PERFORMANCE  
AS A FUNCTION OF  
SNR AT A SINGLE ARRAY ELEMENT

WVFM: LFM PULSE:A-40,D-0.8,B-2356.2

CASE: INHMG1

PFA = 0.100

STEER = FALSE

DMEDIA = FALSE

RMEDIA = FALSE

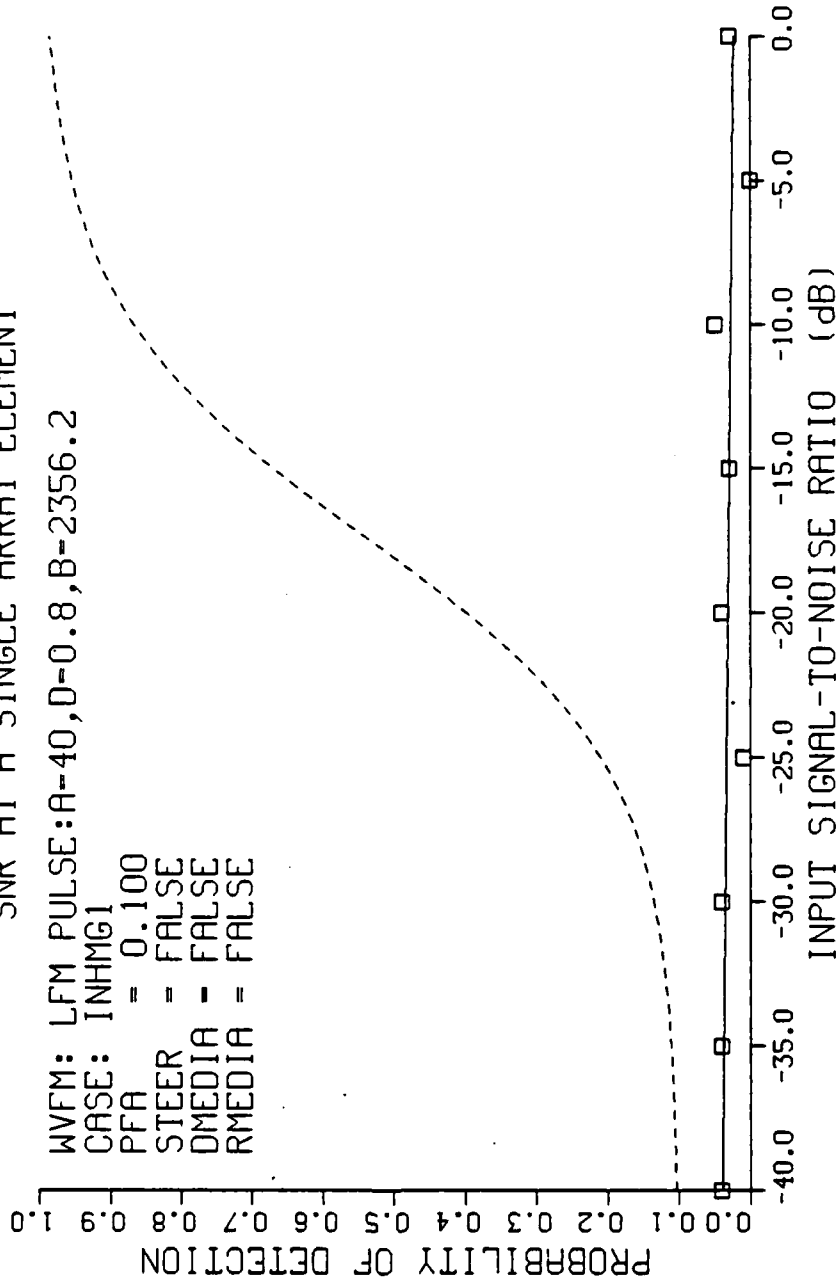


Figure 43. Receiver Performance for case INHMG1, LFM Pulse,  
Pfa = 0.1, No Phase Weighting

SIMULATED RECEIVER PERFORMANCE  
AS A FUNCTION OF  
SNR AT A SINGLE ARRAY ELEMENT

WVFM: LFM PULSE:A-40,D-0.8,B-2356.2

CASE: INHMG1

PFA = 0.100

STEER = TRUE

DMEDIA = FALSE

RMEDIA = FALSE

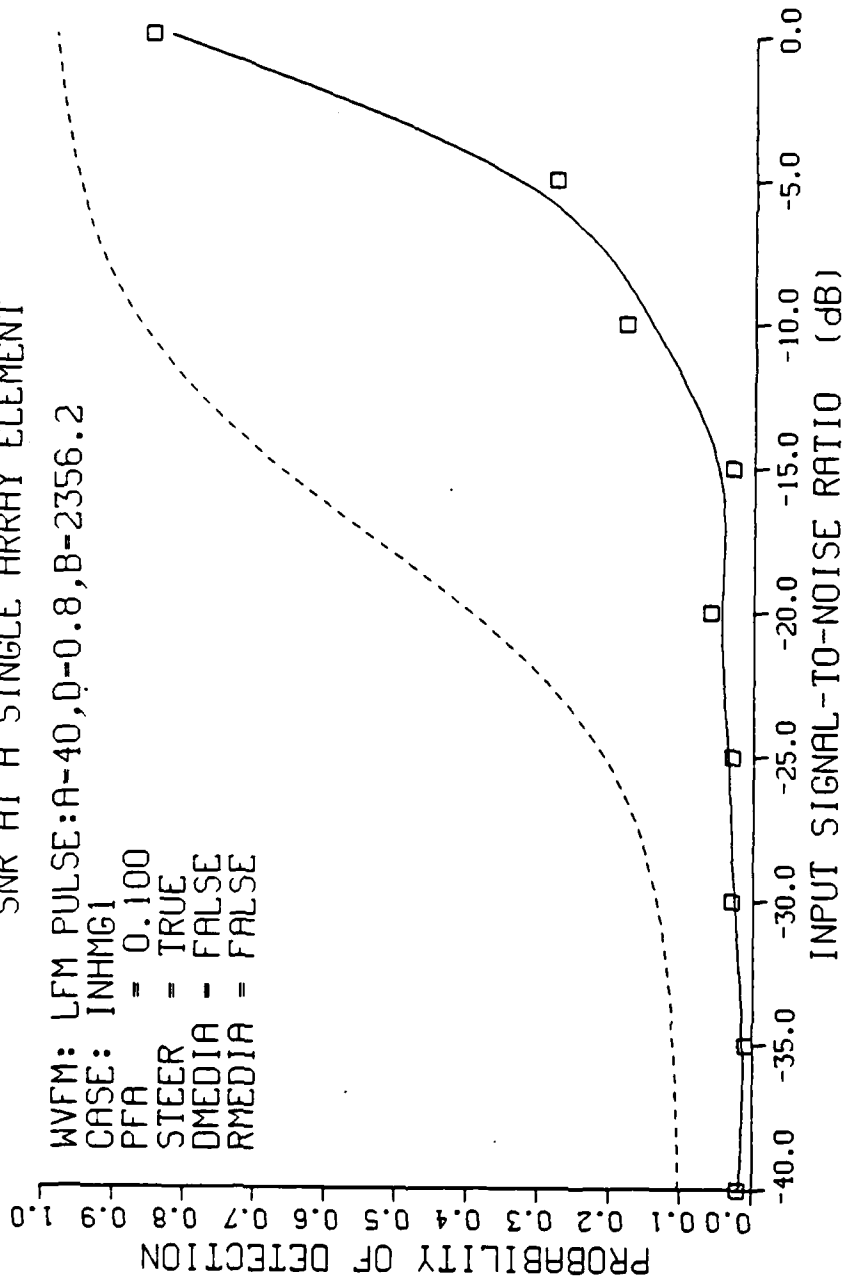


Figure 44. Receiver Performance for case INHMG1, LFM Pulse,  
Pfa = 0.1, Geometry Phase Weighting

SIMULATED RECEIVER PERFORMANCE  
AS A FUNCTION OF  
SNR AT A SINGLE ARRAY ELEMENT

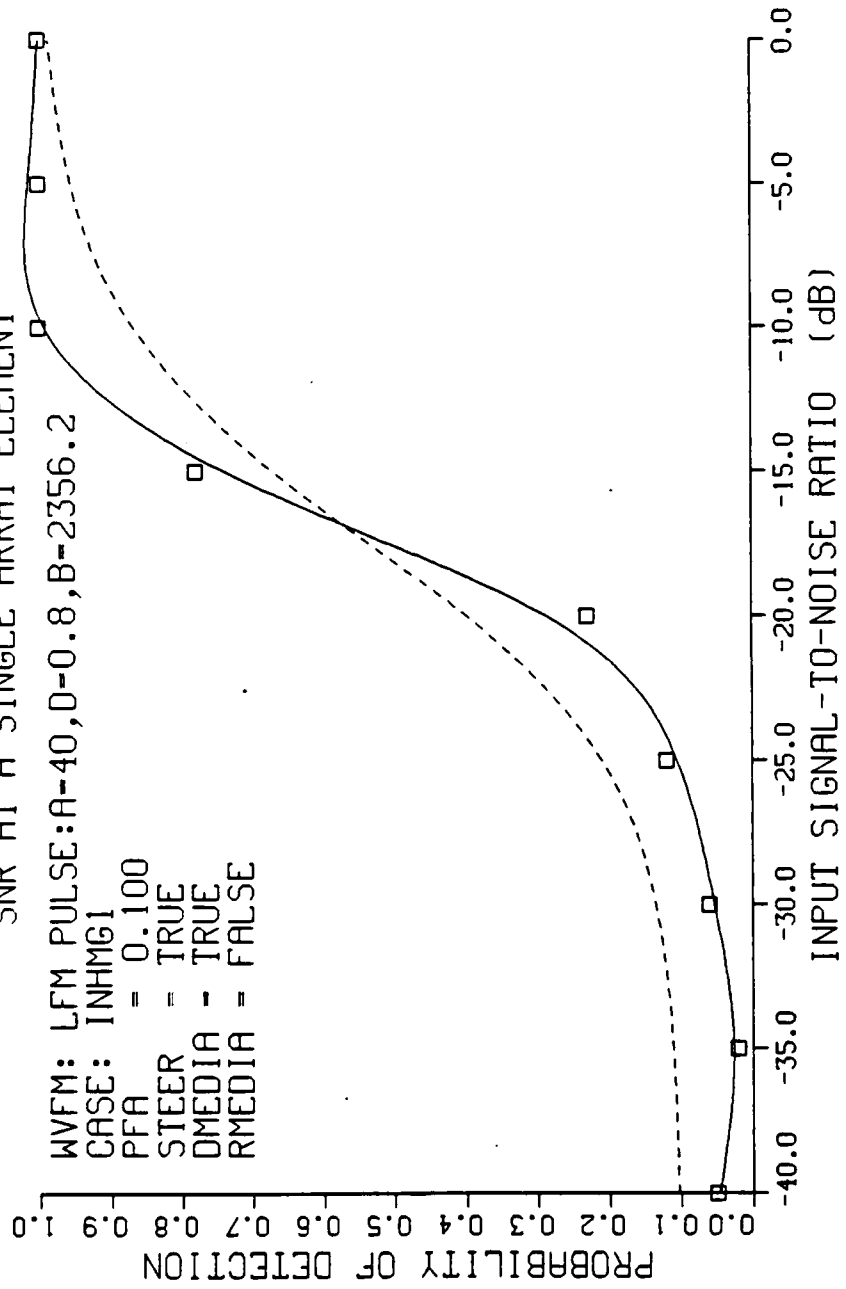


Figure 45. Receiver Performance for case INHMGI, LFM Pulse,  
Pfa = 0.1, Medium Phase Weighting

SIMULATED RECEIVER PERFORMANCE  
AS A FUNCTION OF  
SNR AT A SINGLE ARRAY ELEMENT

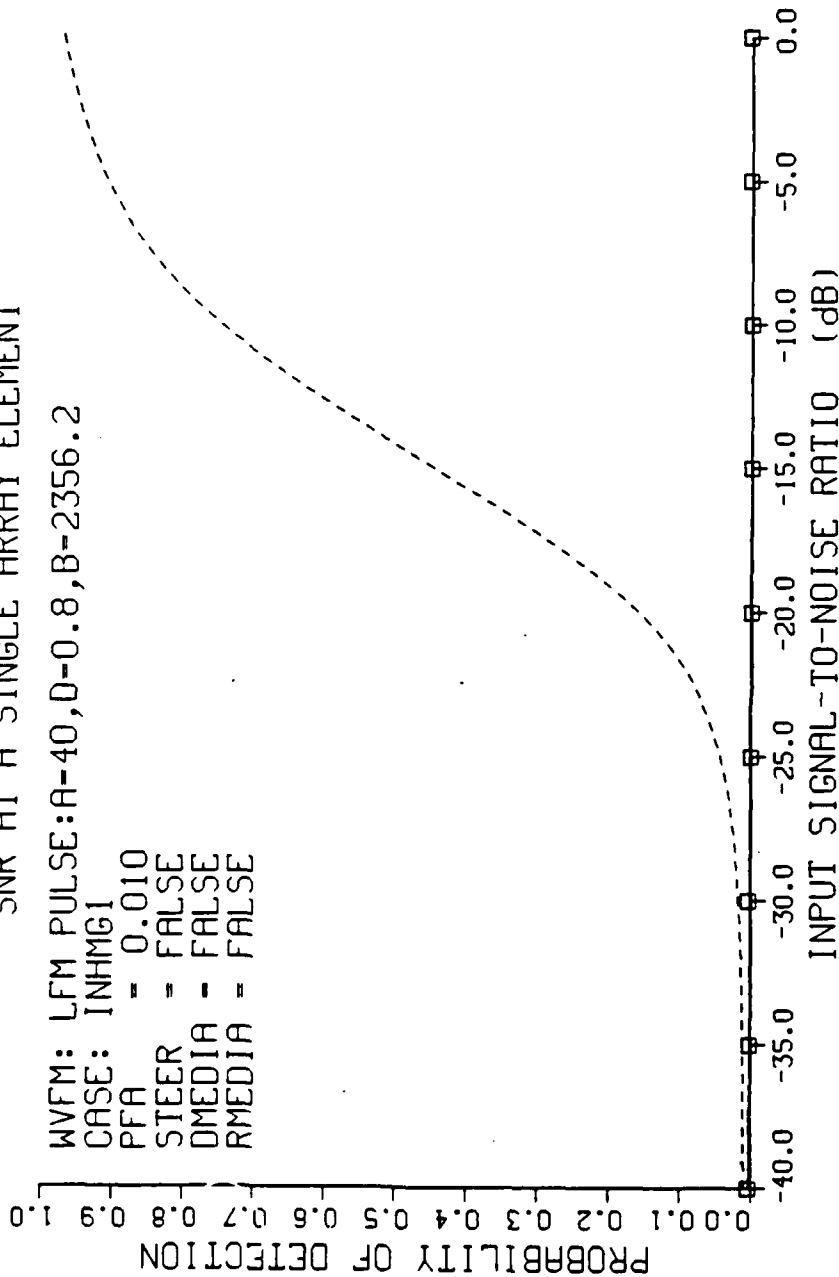


Figure 46. Receiver Performance for case INHMG1, LFM Pulse,  
Pfa = 0.01, No Phase Weighting

SIMULATED RECEIVER PERFORMANCE  
AS A FUNCTION OF  
SNR AT A SINGLE ARRAY ELEMENT

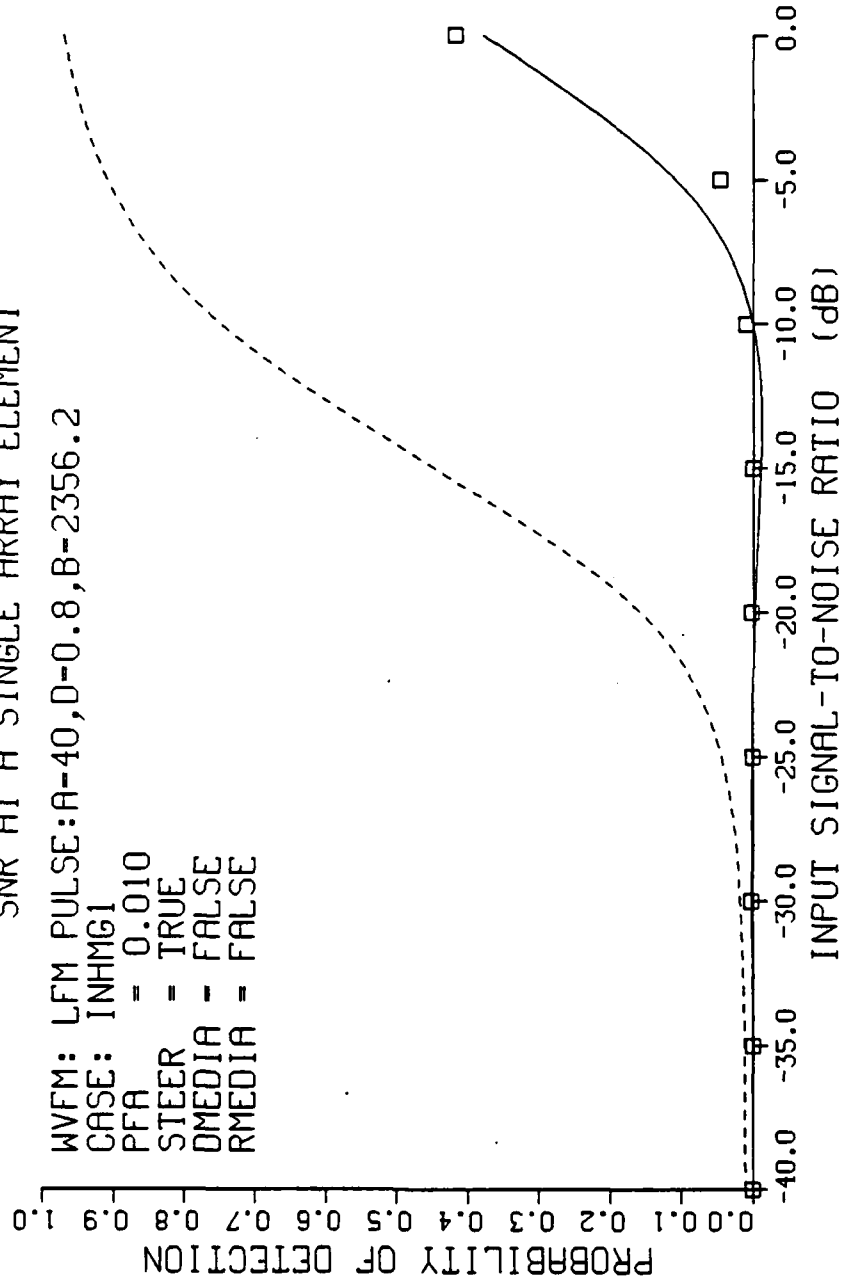


Figure 47. Receiver Performance for case INHMG1, LFM Pulse,  
Pfa = 0.01, Geometry Phase Weighting

SIMULATED RECEIVER PERFORMANCE  
AS A FUNCTION OF  
SNR AT A SINGLE ARRAY ELEMENT

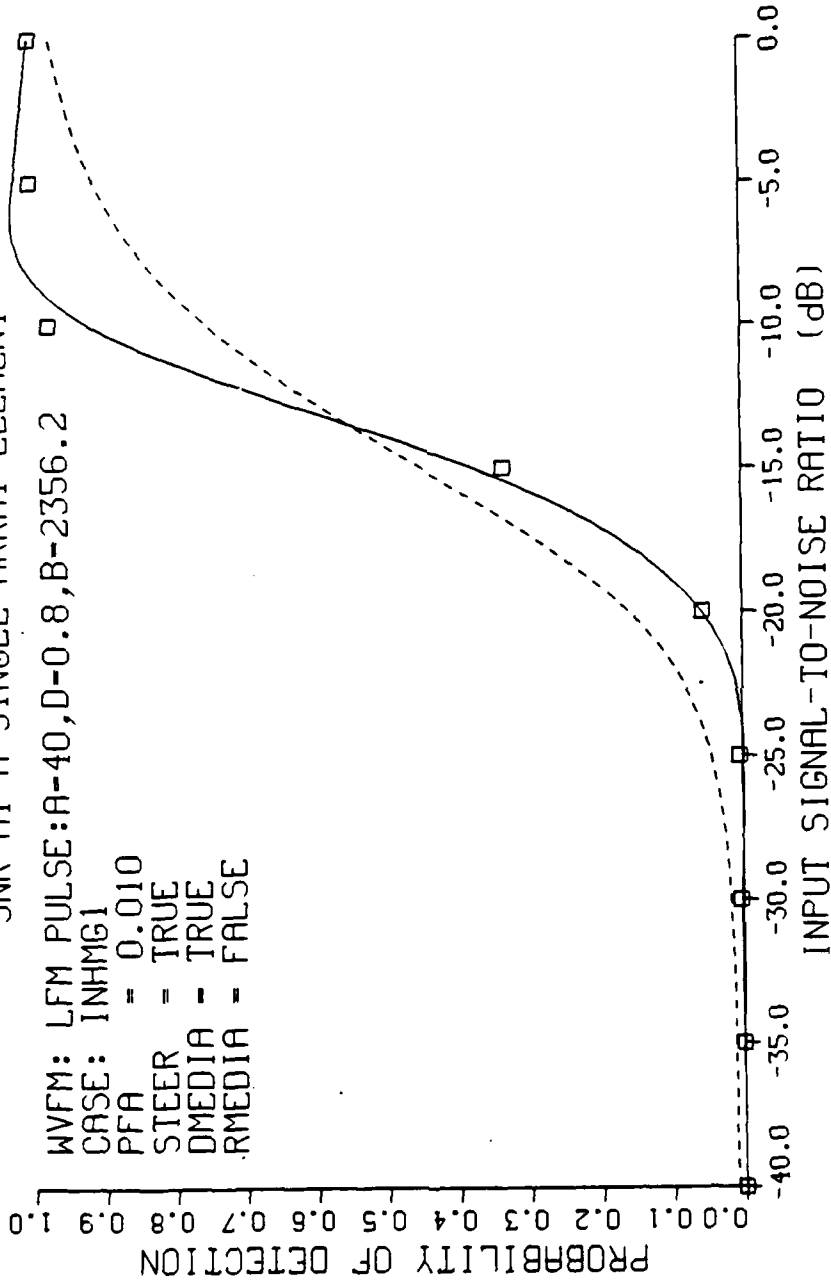


Figure 48. Receiver Performance for case INHMG1, LFM Pulse,  
Ffa = 0.01, Medium Phase Weighting



Figures 38, 41, 44 and 47 show the receiver performance when only the system geometry is compensated for by the phase weights used in the array processor. These figures indicate that in the presence of the inhomogeneous ocean medium, phase weighting to compensate for system geometry will not achieve the receiver performance predicted by theory. That is, traditional beam steering is not sufficient for maximum receiver performance, and a large margin for improved performance exists when the effects of the ocean medium on the received signal can be predicted. Note also that the degradation in performance is consistent for the different transmit waveforms and values of  $P_{fa}$ .

Figures 39, 42, 45 and 48 show the effect on receiver performance when phase weights are computed based on both the system geometry and the refraction of the acoustic wave in the ocean medium. The state of the logical variable DMEDIA indicates if the phase weights contain the correction for deterministic, inhomogeneous medium wave propagation effects. As expected, the simulated receiver performance conforms to the performance predicted by theory, and is nearly identical to that of case TEST when all medium effects have been corrected for.

However, the really significant result is seen by comparing Figures 38, 41, 44 and 47 with Figures 39, 42, 45 and 48. The only difference between these plots is in use of phase weights that compensate for the phase shifts due to

propagation through an inhomogeneous ocean medium, and the model of the inhomogeneous ocean medium is based on the physics of acoustic wave propagation. If one assumes a marginal detection probability of 50% ( $P_d = 0.5$ ), the improvement in receiver performance due to the application of a model-based signal processing approach for this particular simulation geometry and ocean medium characteristic varies from 14 dB to 18 dB depending on the type of transmit waveform or value of  $P_{fa}$ . The conclusion is that the physics of wave propagation can be used to develop signal processing algorithms having significant impact on the performance of a receiver designed to process complex envelope, electrical signals from an array of point source elements.

## V. CONCLUSIONS AND RECOMMENDATIONS

The original objectives of this research have been accomplished. The computer simulation of a correlator/matched filter receiver to process data from an array of electroacoustic transducers has been developed and validated. The concept of model-based signal processing was applied to the development of an array signal processing algorithm, and was shown to have a marked impact on the capability of the receiver to detect the presence of a signal in zero-mean, additive, white Gaussian noise.

The computer simulation of the receiver was validated by a direct comparison between the measured performance of the simulation and the performance predicted by theory when all array element output electrical signals are precisely cophased. The agreement between predicted and measured performance was close but not exact since the noise assumptions made in developing the theoretical performance could not be precisely duplicated by the computer simulation. However, the close agreement with theoretical performance was considered to be a validation of the receiver simulation computer program.

Test cases were designed and run that permitted relative changes in receiver performance to be measured. In this way, the effectiveness of the model-based signal processing approach could be quantified. For the simulation parameters

and transmit signals used in this study, compensating for the refraction of the acoustic field in the ocean medium was found to improve receiver performance over traditional beam steering by at least 14 dB when measured at the point of 50% probability of detection.

Suggestions for further study of the receiver model include:

- Obtain, or develop, a pseudorandom noise generator that more closely approximates the noise model assumptions implicit in the derivation of the theoretical receiver performance, and revalidate the computer simulation.
- Simulate more realistic noise processes, such as colored noise, and determine the impact on receiver performance.
- Try decision rules other than Neyman-Pearson, such as the minimum average probability of error criterion to measure probability of error performance for an underwater, acoustic data communication system.
- Experiment with other functional forms for the transmit signal, and measure the effect on performance when errors in the estimate of time delay and Doppler shift exist.

### LIST OF REFERENCES

1. Mendel, J., "Model-Based Signal Processing," Trends & Perspectives in Signal Processing, pp. 9-11, December 1983.
2. Ziomek, L.J., Underwater Acoustics--A Linear Systems Theory Approach, Academic Press, 1985.
3. Vos, J., Linear Time-Invariant, Space-Variant Filters and the WKB Approximation with Applications to Underwater Acoustic Signal Processing, Master's Thesis, Naval Postgraduate School, Monterey, California, December 1984.
4. Van Trees, H.L., Detection, Estimation, and Modulation Theory, v. III, John Wiley & Sons, Inc., 1971.
5. Couch, L.W., Digital and Analog Communications Systems, Macmillan Publishing Co., 1983.
6. Brigham, O.E., The Fast Fourier Transform, Prentice Hall, Inc., 1974.
7. Oppenheim, A.V., and Schafer, R.W., Digital Signal Processing, Prentice Hall, Inc., 1975.
8. Officer, C.B., Introduction to the Theory of Sound Transmission, McGraw-Hill Book Co., 1958.
9. Papoulis, A., Signal Analysis, McGraw-Hill Book Co., 1977.

INITIAL DISTRIBUTION LIST

|   | No. Copies |
|---|------------|
| 1. Defense Technical Information Center<br>Cameron Station<br>Alexandria, Virginia 22304-6145   | 2          |
| 2. Library, Code 0142<br>Naval Postgraduate School<br>Monterey, California 93943-5100   | 2          |
| 3. Assistant Professor L.J. Ziomek, Code 62Zm<br>Department of Electrical and<br>Computer Engineering<br>Naval Postgraduate School<br>Monterey, California 93943-5100 | 15         |
| 4. Commandant (G-TPP/HRP)<br>U.S. Coast Guard Headquarters<br>2100 Second St. S.W.<br>Washington, D.C. 20593  | 2          |
| 5. LT R.J. Blount<br>c/o Commanding Officer (MW)<br>U.S. Coast Guard<br>Electronics Engineering Center<br>Wildwood, New Jersey 08260                                  | 2          |
| 6. Mr. Charles Stuart<br>DARPA<br>1400 Wilson Blvd.<br>Arlington, Virginia 22209  | 1          |

**END**

**FILMED**

**2-86**

**DTIC**